

FIRE RISK, BURN SEVERITY, AND VEGETATION RECOVERY FOR THE BERRY
FIRE, GRAND TETON NATIONAL PARK

by

David M. Szpakowski, M.S.

A dissertation submitted to the Graduate Council of
Texas State University in partial fulfillment
of the requirements for the degree of
Doctor of Philosophy
with a Major in Geography
August 2020

Committee Members:

Jennifer L.R. Jensen, Chair

Edwin T.E. Chow

David R. Butler

Michael J. Falkowski

COPYRIGHT

by

David M. Szpakowski

2020

FAIR USE AND AUTHOR'S PERMISSION STATEMENT

Fair Use

This work is protected by the Copyright Laws of the United States (Public Law 94-553, section 107). Consistent with fair use as defined in the Copyright Laws, brief quotations from this material are allowed with proper acknowledgement. Use of this material for financial gain without the author's express written permission is not allowed.

Duplication Permission

As the copyright holder of this work I, David M. Szpakowski, authorize duplication of this work, in whole or in part, for educational or scholarly purposes only.

DEDICATION

I would like to dedicate this work to my Sally A. Szpakowski and Jim Szpakowski. I could never have accomplished this without their support and encouragement. Thank you, mom and dad.

ACKNOWLEDGEMENTS

I would like to acknowledge Dr. Jennifer Jensen for mentoring me and helping me organize and conduct my research; Brandon Rose and Lucas Chavez for traveling to Wyoming to conduct fieldwork with me; Dr. Butler, Dr. Chow, and Dr. Falkowski for serving on my committee and providing helpful feedback and advice; and the staff and faculty of the Geography Department for all their help and encouragement along the way.

TABLE OF CONTENTS

	Page
ACKNOWLEDGEMENTS.....	v
LIST OF TABLES.....	vii
LIST OF FIGURES.....	ix
LIST OF ABBREVIATIONS.....	xi
ABSTRACT.....	xii
CHAPTER	
I. INTRODUCTION.....	1
II. GRAND TETON FIRE HAZARD AND BURN SEVERITY.....	20
III. ASSESSING FIRE EFFECTS IN THE GREATER YELLOWSTONE ECOSYSTEM USING BURN RATIOS AND RED-EDGE SPECTRAL INDICES.....	59
IV. BERRY FIRE VEGETATION RECOVERY.....	90
V. CONCLUSION.....	115
REFERENCES.....	121

LIST OF TABLES

Table	Page
1. Burn category characteristics.....	3
2. Relationship between CBI score and Burn Severity.....	4
3. Sensors used for various wildfire data collection.	8
4. Sentinel-2A spectral and spatial resolutions.....	27
5. Hazard rankings for 40FBFM fuel categories.	30
6. Hazard rankings for canopy cover.....	30
7. Hazard rankings for NDMI.....	31
8. Hazard rankings for elevation.....	31
9. Hazard rankings for slope.....	32
10. Hazard rankings for aspect.....	32
11. Hazard rankings for roads, trails, and structures.....	33
12. Correlation matrix for model input variables.....	39
13. First sensitivity analysis for proposed model input variables based on the assumption of variable.....	40
14. Second sensitivity analysis for model inputs based on the assumption of variable independence.....	41
15. Descriptive statistics for the fire hazard model output.....	43
16. Summary of logistic regression results for each run.....	44
17. Multinomial logistic regression with unburned as reference group.....	50
18. Field measurement definitions and units of measurement.....	68

19. List of indices generated for estimating burn severity.....	71
20. Descriptive statistics for Berry Fire indices.....	75
21. Descriptive statistics for Maple Fire indices.....	76
22. Correlations between field measurements and spectral indices.....	79
23. Results from all-possible-models regression	81
24. Plots broken down by category.....	98
25. List of indices generated for estimating fractional vegetation cover	102
26. Descriptive statistics of <i>in situ</i> FVC based on CAN-EYE processing.....	105
27. Significant models from subset regression analysis	106
28. Validation plots regression results from calibration regression fit	108
29. Field measured FVC by burn severity category	111

LIST OF FIGURES

Figure	Page
1. The study area for Grand Teton National Park and J.D. Rockefeller Parkway.....	18
2. Grand Teton National Park and John D. Rockefeller Parkway	26
3. Fire hazard output	42
4. Logistic regression plots of fire hazard and burn severity	45
5. ROC curves of fire hazard and burn severity.....	47
6. Moderate to high burn severity logistic regression results	50
7. Unburned logistic regression results.....	51
8. Fire hazards for initial Berry Fire perimeter	53
9. Proportion of pixels belonging to each fire hazard category	54
10. Study area within Greater Yellowstone Ecosystem including Yellowstone National Park and Grand Teton National Park	65
11. Locations of the twenty-seven field plots collected by Turner et al. (2019)	68
12. The dNBR index	72
13. Standard least squares for models with best predictive capabilities	84
14. Example of a mixed pixel consisting of vegetation and bare earth.	94
15. Study area and plot locations	97
16. Example plot layout	99
17. NDVIre1n derived fractional vegetation cover for the Berry Fire	107
18. Standard least squares output for NDVIre1n FVC	108

19. MESMA output.....	109
20. Standard least squares output for the MESMA FVC.....	110

LIST OF ABBREVIATIONS

Abbreviation	Description
AUC	Area Under the Curve
ASTER	Advanced Spaceborne Thermal Emission and Reflection Radiometer
AVIRIS	Airborne Visible/Infrared Imaging Spectroradiometer
BAER	Burned Area Emergency Response
BARC	Burned Area Reflectance Classification
BLM	Bureau of Land Management
CBI	Composite Burn Index
Clre	Chlorophyll Index re-edge
CLre_PF	Chlorophyll Index re-edge Post-fire
CO2	Carbon di-oxide
DEM	Digital Elevation Model
dCLre	delta Chlorophyll Index re-edge
dGNDVI	delta Green Normalized Difference Vegetation Index
dMSRren	delta Modified Simple Ratio red-edge narrow
dNBR	delta Normalized Burn Ratio
dNDre1	delta Normalized Difference re-edge 1
dNDre2	delta Normalized Difference re-edge 2

dNDVI	delta Normalized Difference Vegetation Index
dNDVIre1n	delta Normalized Difference Vegetation Index red-edge 1 narrow
dNDVIre2n	delta Normalized Difference Vegetation Index red-edge 2 narrow
dNDVIre3n	delta Normalized Difference Vegetation Index red-edge 1 narrow
dPSRI	delta Plant Senescence Reflectance Index
ERS-1	European Remote-Sensing Satellite
FBFM13	Thirteen Anderson Fire Behavior Fuel Model
FFDRS	Forest Fire Danger Rating System
FLM	Fuel Loading Model
FRI	Fire Risk Index
FWI	Fire Weather Index
GIS	Geographic Information System
GNDVI	Green Normalized Difference Vegetation Index
GOES	Geostationary Operational Environmental Satellite
HFI	Hybrid Fire Index
JERS-1	Japanese Earth Resource Satellite
LAI	Leaf Area Index
Lidar	Light Detection and Ranging

LST	Land Surface Temperature
MESMA	Multiple-endmember Spectral Mixture Analysis
MODIS	Moderate Resolution Imaging Spectroradiometer
MSRren MSS	Modified Simple Ratio red-edge narrow Multispectral Scanner
NASA	National Aeronautics and Space Administration
NBR	Normalized Burn Ratio
NBR_B5	Normalized Burn Ratio Band 5 version
NBR_B6	Normalized Burn Ratio Band 6 version
NBR_B7	Normalized Burn Ratio Band 7 version
NDre1	Normalized Difference re-edge 1
NDre2	Normalized Difference red-edge 2
NDVI	Normalized Difference Vegetation Index
NDVIre1n	Normalized Difference Vegetation Index red-edge 1 narrow
NDVIre2n	Normalized Difference Vegetation Index red-edge 2 narrow
NDVIre3n	Normalized Difference Vegetation Index red-edge 3 narrow
NDWI	Normalized Difference Water Index
NIR	Near Infrared

NPS	National Park Service
NSF	National Science Foundation
OLI	Operational Land Imager
PSRI	Plant Senescence Reflectance Index
Radar	Radio Detection and Ranging
RBR	Revitalized Burn Ratio
RBR_B5	Revitalized Burn Ratio Band 5 version
RBR_B6	Revitalized Burn Ratio Band 6 version
RBR_B7	Revitalized Burn Ratio Band 7 version
RdNBR	Relative difference Normalized Burn Ratio
RdNBR_B5	Relative difference Normalized Burn Ratio Band 5 version
RdNBR_B6	Relative difference Normalized Burn Ratio Band 6 version
RdNBR_B7	Relative difference Normalized Burn Ratio Band 7 version
ROC	Receiver Operating Characteristic
SMA	Spectral Mixture Analysis
SFI	Structural Fire Index
STRM	Shuttle Radar Topography Mission
SWIR	Short-Wave Infrared
TIR	Thermal Infrared

TM	Thematic Mapper
ETM+	Enhanced Thematic Mapper
USBR	United States Bureau of Reclamation
USFS	United States Forest Service
VI	Vegetation Index
VRAF	Vegetation Resilience After Fire
WFAS	Wildland Fire Assessment System

ABSTRACT

Wildfires considerably impact environments and communities around the world. Wildfires can alter ecosystems, damage property and infrastructure, and harm the wellbeing of at-risk populations. In the summer of 2016, several wildfires occurred in the Greater Yellowstone Ecosystem, one of which was named the Berry Fire. The Berry Fire consumed over 8,000 ha making it the largest fire on record for Grand Teton National Park. This study explores the fire ecology of the Berry Fire by modeling pre-fire risk, estimating field measured fire effects using Sentinel-2 imagery and assessing vegetation recovery via regression fitted spectral indices and multiple-endmember spectral mixture analysis (MESMA). For pre-fire risk assessment, multicriteria evaluation based on fuel type, canopy cover, relative moisture content, slope, elevation, aspect and distance to roads, trails and structures was implemented. The resulting risks were then compared to burn severity levels using logistic regression. The relationship between risk and burn severity was found to be generally weak, with only two burn severity categories (unburned and moderate to high) possessing moderately strong relationships to the pre-fire risk.

The next analysis examined the ability for spectral indices to estimate field measured fire effects related to burn severity. Currently, most burn severity research attempts to associate spectral indices with the field measured composite burn index (CBI), however this approach is limited due to CBI being optically assessed and therefore subjective. Studies which have attempted to measure fire effects using Landsat imagery

have not found strong correlations between tested spectral indices and fire effects. The recent availability of red-edge bands at a moderate spatial resolution, thanks to the launch of the Sentinel-2 constellation, allows for the calculation of spectral indices not available to the Landsat satellites. Using all-possible-models multivariate regression, a total of thirty different spectral indices were calculated and compared to field measured fire effects collected by Turner et al. 2019. Six of the fire effects possessed models that possessed coefficients of determination and variance inflation factors that passed the criteria for a suitable model. The best models for each of these fire effects were then further explored. All six of these models included red-edge indices based on Sentinel-2 band five, which strengthens other research findings indicating the usefulness of this band for burn severity assessments.

Finally, vegetation recovery was assessed using fractional vegetation cover (FVC) derived from a combination of field plots, regression fitted spectral indices and MESMA. A total of sixty field plots were collected in the summer of 2019 in each of which eight downward and eight upward hemispherical photographs were taken. The FVC was then calculated for each photograph belonging to a plot within CAN-EYE and the average FVC was calculated. Thirty-one of these plots were then used to derive the regression fits for the spectral indices, which were implemented using raster algebra. The resulting regression fit values were then compared to the remaining plots via linear regression to determine how accurately FVC was mapped. The MESMA, derived using three forest and three herbaceous endmembers, was compared to all sixty plots using linear

regression. The results indicate that a red-edge index (NDVI_{re1n}) outperformed all other methods for estimating FVC.

The objective of this research was to examine three temporal stages of fire ecology for the Berry Fire: pre-fire risk, immediate post-fire fire effects (burn severity) and vegetation recovery three years post-fire. This was accomplished using geographic information systems and remote sensing analyses based on current research trends and newly available datasets. As each of these dynamics influence and impact the following dynamic, they combine to create a holistic view of the conditions and effects of the Berry Fire.

I. INTRODUCTION

I. Background

1.1 Fire risk Mapping

Wildfires significantly impact environments and communities around the world. Wildfires can alter the composition of vegetation (Abrahamson, 1984), alter soil characteristics lasting years after the fire (Smith, 1970; Lewis, Wu and Robichaud, 2006), and modify hydrologic regimes by increasing runoff and decreasing soil infiltration (Scott, 1993; Pierson et al., 2008). While some of these changes to local environments are desirable, the destructive and harmful consequences of wildfires are undesirable and require mitigation.

A number of studies have documented and forecast increases in the number of ignition events and the total area burned (Hurteau et al., 2014; Rocca et al., 2014; Riley and Loehma, 2016). This is primarily attributed to climate change and the land management method of fire suppression. Fire suppression practices have been documented to decrease the frequency of ignition events at the cost of increasing wildfire intensity when the events do occur (Wimberly and Liu, 2013; Loudermilk et al., 2014). Climate change is affected by wildfires due to these fires being contributors of CO₂, soot and aerosols during combustion, and through the removal of vegetation which would otherwise have acted as a filter to CO₂. This has contributed to the global trend of increasing temperatures which increases the likelihood of wildfires, especially in areas which possess favorable environmental and climactic conditions for wildfire ignition and spread.

Fire risk mapping is used to improve prediction of where ignition events will

occur as well as how the resulting wildfire will propagate (Keane, Burgan and Van Wagtendonk 2001; Jaiswal et al., 2002; Chuvieco et al., 2010). This is accomplished through two primary methods; (i) point-wise meteorological data-based operating systems; and (ii) the use of remote sensing technologies and Geographic Information Systems (GIS). The former method has four main operating systems used around the world: Wildland Fire Assessment system (WFAS), Fire Weather Index (FWI), McArthur's Forest Fire Danger Rating System (FFDRS), and the Russian Nesterov Index. These systems use meteorological data such as temperature, precipitation, humidity, and wind speed. However, these systems suffer from several limitations including input data being limited to the point distribution of data collection stations and the need for interpolation to generate fire risk maps. Due to the ability to obtain continuous data for an area, the remote sensing/GIS approach has become increasingly viewed as an effective alternative for the creation of fire risk maps (Chuvieco and Salas, 1996; Arroyo, Pascual and Manzanera 2008; Yu et al., 2017).

Fire risk maps use measurements of environmental factors, such as fuel conditions, topography, climatic conditions, and may also include proximity to human settlement/activity to identify areas at varying risk of fire occurrence (Chuvieco and Congalton, 1989; Chuvieco, Salas and Vega, 1997; Pradhan, Ergen and Akinic 2007; Adab, Kanniah and Solaimani 2013). The result is a map which displays areas with varying degrees of fire risk ranging from very low to very high risk. These maps can be used by land managers to better prepare landscapes for eventual fire events through the use of controlled burns and mechanical thinning, preparation of evacuation routes, and placement of fire watch towers. They also provide a basis for studies into the relationship

between fuel/climate conditions and fire/burn severity.

1.2 Burn Severity

Fires vary in their intensity due to a number of factors commonly implemented in the creation of fire risk maps, such as fuel load, vegetation moisture content, and vegetation type. Fire/burn severity is the impact on the landscape that results from fire intensity and duration. The two terms have been used interchangeably in the literature, with burn severity being more widely used in the remote sensing literature (Keeley, 2009). From here forward fire/burn severity will strictly be referred to as burn severity. Burn severity is often measured through vegetation loss and ranges from unburned to deep burning/crown fire (Table 1) (Keeley, 2009).

Table 1. Burn category characteristics.

Burn Category	Characteristics
Unburned	No signs of alteration by fire
Scorched	Vegetation was not directly burned but experienced leaf loss from radiated heat
Light burns	Burned or scorched understory plants, and a largely intact soil organic layer
Moderate to severe surface burns	Trees with some damage to canopy cover, all understory plants charred or consumed, and the soil organic layer largely consumed
Deep burning/crown fire	Burned canopy with dead trees, all understory plants consumed, ash deposition and charred organic matter up to several cm in depth

The burn severity experienced by areas affected by wildfires is an important measure of fire impacts on the landscape. Burn severity impacts vegetation mortality, soil hydrophobicity, soil nutrient composition, and increased runoff due to decreased infiltration (Benavides-Solorio and MacDonald, 2001; Moody and Martin, 2001; Turner et al., 2007; Robichaud et al., 2008). Burn severity is commonly measured in the field

using the composite burn index (CBI), which involves an optical assessment of burned areas to determine the fire impacts on ecological conditions. Due to the need for a systematic approach to estimate burn severity across different environments, the CBI was created to allow for visual estimations to be conducted by rating the degree of damage done by the fire, as well as the estimated vegetation recovery for the area, on a 0 to 3 scale (Kasischke et al., 2008) (Table 2). CBI estimates are time dependent and require physically visiting the burned areas to perform the assessments.

Table 2. Relationship between CBI score and Burn Severity.

CBI Score	Severity of Burning
0	Unburnt
1	Low
2	Moderate
3	High

More recently, the normalized burn ratio (NBR) has been widely used as a means for approximating the burn severity using satellite imagery (Epting, Verbyla and Sorbel 2005; Verbyla and Lord, 2008; Veraverbeke et al., 2010). NBR has shown mixed results in its effectiveness in estimating burn severity when compared CBI estimations, with forest being the environment in which it performs best, while grasslands and other less vegetated environments exhibiting less than optimal performances (Epting, Verbyla and Sorbel, 2005; Roy, Keane and Trigg, 2006; Murphy, Reynolds and Koltun, 2008). Due to these suboptimal results, modifications to NBR are being researched with the aim of

improving the ability to estimate burn severity remotely (Miller and Thode, 2007; Miller et al., 2009).

1.3 Vegetation Recovery

Vegetation recovery after a fire event is an important metric to better determine the long-term impact a fire had on an ecosystem. Gitas et al. (2012) identified four sequential stages for post-fire vegetation recovery: (i) Stand initiation/regeneration; (ii) Thinning/stem exclusion; (iii) Transition/understory regeneration; and (iv) Steady-state/old-growth. Vegetation will fall into one of these four stages depending on the degree of recovery although it can be difficult to determine precisely which stage of recovery a stand is currently in due to the complexity of the processes. A multitude of factors determine the rate of recovery including climate, initial plant mortality, soil characteristics, degree of soil disturbance, topographic influences, and vegetation composition (Johnstone and Chapin, 2006; Díaz-Delgado, Lloret and Pons, 2003).

Post-fire monitoring of vegetation recovery can be conducted through both field data collection and the use of remote sensing technologies. Field methods involve establishing plots or transects to measure seedling germination, plant survival and restoration, and vegetation characteristics (Abrahamson, 1984; Ne'eman, Lahav and Izhaki, 1995; Pausas 1997; Pausas, Ribeiro and Vallejo, 2004). These measurements are conducted from within the first-year post-fire to several years post-fire. Because of the amount of time needed to collect the field data as well as the need for repeat visits over a span of years, field data collection is considered to be costly and time-consuming (Gitas et al., 2012). Remote sensing offers an alternative means for estimating vegetation recovery over large areas in a more time efficient and less costly manner (White et al.,

1996; Gouveia et al., 2010). Most research on this topic has focused on the use of vegetation indices (VI) and spectral mixture analysis (SMA) using sensor data such as Landsat and the Moderate Resolution Imaging Spectroradiometer (MODIS) to monitor recovery (Caetano et al., 1996; Gouveia et al., 2010; Veraverbeke et al., 2010; Gitas et al., 2012). Studies have been conducted in environments ranging from arid to subarctic (Goetz, Fiske and Bunn, 2006; Hope, Tague and Clark, 2007; Van Leeuwen, 2008). Further research in identifying optimal methods for monitoring vegetation recovery is needed to improve the capabilities of remote sensing in this area of study.

1.4 Relationships between Fire risk, Burn Severity, and Vegetation Recovery

An enhanced understanding of the relationship between fire risk potential, burn severity, and vegetation recovery would allow for an improved assessment of the processes and natural evolution of fire events. This can be accomplished by first relating fire risk potential to post-fire burn severity. The literature has identified that a relationship does exist between fuel, climatic conditions, and the eventual severity of a fire (Flannigan, Stocks and Wotton, 2000; McKenzie et al., 2004; Schoennagel, Veblen and Romme, 2004; Epting, Verbyla and Sorbel 2005). The core finding is that fuel which is drier and more abundant (higher fire risk potential) causes more severe fires when ignited, resulting in more acute burn severity. Additionally, fire suppression practices lead to a greater accumulation of fuel, which enables wildfires to increase in intensity. Next, a relationship between burn severity and vegetation recovery must be established. Literature related to the topic suggests that areas that experience more severe burns take longer to recover (Racine, Johnson and Viereck, 1987; White et al., 1996). This is due to dramatic changes in soil characteristics, vegetation cover, and post-fire hydrologic

regimes.

Finally, relating fire risk potential to vegetation regeneration post-fire can be accomplished with the establishment of the previous two relationships. This would allow for better preemptive planning by land managers for post-fire recovery work, increased ability to identify at risk forest types which may be endangered or require extended periods of recovery and allow for climate change models to better assess the impacts of increased fire frequency and severity on future species richness and abundance.

II. Remote Sensing and Wildfires

2.1 Sensors and techniques

Various remote sensing platforms have been used to map fire risk, monitor active fires, estimate post-fire burn severity, and monitor vegetation regrowth (Arroyo, Pascual and Manzanera 2008; Froking et al., 2009; Gitas et al., 2012; Yebra et al., 2013). These sensors include Landsat MSS/TM/ETM+/OLI, MODIS, IKONOS, AVIRIS, GOES, Lidar, ERS-1, JERS-1, and RADARSAT. The sensors vary in resolutions and type of data collected, allowing for studies that vary in size and purpose (Table 3). The abundance of sensors and data types also allows for hybrid analyses which combine multiple sensor/data types (Arroyo, Pascual and Manzanera 2008).

Table 3. Sensors used for various wildfire data collection.

Sensor(s)	Data Type Acquired	Spatial Resolution	Spectral Resolution by Use	Advantages	Disadvantages	Studies
Landsat MSS, TM, ETM+, OLI	Imagery	15 - 30 m (Thermal infrared bands are collected at a coarser spatial resolution and resampled down)	Ultra-blue – 1 Visible – 3 NIR – 1 SWIR – 2 Thermal – 2 Panchromatic – 1 Cirrus – 1 (For Landsat 8)	Free and easily accessible	Lack of canopy penetration, low temporal resolution	Chuvieco and Congalton (1989), Lozano, Suárez-Seoane and de Luis (2007), Brandis and Jacobson (2003), Van Wagtendonk, Root and Key (2004), White et al. (1996)
Sentinel-2	Imagery	10 - 60m	Ultra-blue – 1 Visible – 3 Red Edge - 3 NIR – 2 SWIR – 2 Water Vapor - 1 Cirrus -1	Free, relatively high spatial and temporal resolution, multiple NIR bands	Lack of canopy penetration	Fernández-Manso, Quintano and Roberts (2016)
MODIS	Imagery	250m - 1km	Land/cloud/aerosols/ boundaries – 2 Land/cloud/aerosols/ properties – 5 Ocean color/ phytoplankton/ biogeochemistry – 9 Atmospheric water vapor – 3 Surface/cloud temperature – 4 Atmospheric temperature – 2 Cirrus clouds water vapor – 3 Cloud properties – 1 Ozone – 1 Surface/cloud temperature – 2 Cloud top altitude - 4	Free and easily accessible, hyperspectral sensor, high temporal resolution, large area analysis	Lack of canopy penetration, coarse spatial resolution limits analysis of smaller areas	Veraverbeke et al. (2011), Loboda and Csiszar (2007), Van Leeuwen (2008), Hope, Albers and Bart (2012), Yebra, Chuvieco and Riaño (2008), Maeda et al. (2011)
ASTER	Imagery	15 – 90m	Visible – 4 SWIR – 6 Thermal - 5	Free and easily accessible, several SWIR	Lack of canopy penetration, low temporal resolution	Peng et al. (2007), Fallowski et al. (2005),

Table 3. Continued

				bands		
IKONOS	Imagery	0.8 - 4m	Visible – 3 NIR – 1 Panchromatic - 1	High spatial resolution	Decommissioned, limited spectral resolution, expensive	Mitri and Gitas (2013), Mitri and Gitas (2008), Stow et al. (2007),
AVIRIS	Imagery	4 - 20m	430 channels ranging from 0.36 – 2.5µm	High spatial resolution, hyperspectral sensor	High cost, complicated data processing	Van Wagtendonk, Root and Key (2004), Jia et al. (2006), Riaño et al. (2002)
GOES	Imagery	1 - 4km	Visible – 1 SWIR – 1 Water vapor – 1 Surface/cloud temperature – 1 CO ₂ - 1	High temporal resolution, large area analysis	Lack of canopy penetration, coarse spatial resolution limits analysis of smaller areas	Zhang and Kondragunta (2008), Weaver et al. (2004), Yang et al. (2011)
Lidar	NIR Pulse Returns	Varys, typically 1.1 pts/m	Can be NIR or blue/green pulses	Canopy penetration, vegetation height measurements	High cost, restrictive data collections, complicated data processing,	Morsdorf et al. (2004), Mutlu et al. (2008), Koetz et al. (2008), Kane et al. (2014)
ERS-1, JERS-1, RADARSAT	Radar	3 – 100m	Varies by sensor	Large area analysis, canopy height estimates, can complement imagery data	High uncertainty in estimations, low sensitivity to high biomass levels	Bourgeau-Chavez et al. (2002), Hoffmann, Siegert and Hinrichs (1999), Liew et al. (1999)

Common techniques used for mapping fire risk potential involve the use of remotely sensed data to quantify and characterize land cover, vegetation conditions, surface conditions/characteristics, and, when fire risk is considered, human infrastructure. Land cover can be derived from remote sensing data due to differences in spectral responses among surface features (Anderson, 1976). These differences allow for implementation of a classification scheme which will find pixels with similar spectral properties and group them into thematic classes. This can be done through supervised or unsupervised classification. Data products which have already identified land cover types through these methods, such as the National Land Cover Database and MODIS land cover data are publicly available.

2.2 Remote Sensing and GIS applied to Fire Hazard Maps

Vegetation conditions are commonly obtained through the use of VIs. VIs use mathematical formulas to transform the raw or radiometrically corrected spectral data obtained from sensors into indices that provide information on the conditions of vegetation. The Normalized Differenced Vegetation Index (NDVI) uses the reflection of red and near-infrared (NIR) to examine the health of vegetation. The NDVI has been used for fire risk mapping due to its capability to identify areas of high vegetation abundance based off the red edge characteristics most vegetation exhibit (Yu et al., 2017). NDVI is derived through the following equation:

$$NDVI = \frac{NIR - Red}{NIR + Red} \quad (1)$$

Another VI used for identifying fire risk potential is the Normalized Difference Water Index (NDWI). The NDWI is used to estimate the water content of vegetation in a given area by using NIR and the shortest available short wave infrared (SWIR) reflection

(Gao, 1996). NDWI provides information on the wetness of the potential fuel for a wildfire and, along with other moisture indices, has been strongly correlated with fire (Yu et al., 2017). It is derived through the following equation:

$$NDWI = \frac{NIR - SWIR}{NIR + SWIR} \quad (2)$$

Surface conditions/characteristics that are important for fire risk mapping include land surface temperature (LST), elevation, slope, and aspect. LST data products are available from sensors that possess thermal infrared bands. LST is measured using the thermal infrared (TIR) section of the electromagnetic spectrum. This enables continuous temperature data to be used to generate fire risk maps.

Elevation, slope, and aspect are derived from digital elevation models (DEMs). DEMs can be obtained from sensors such as ASTER and STRM. Lidar can provide higher quality DEMs, although it is costlier than publicly available passive sensor data. Elevation is a factor in determining the probability of an ignition event occurring, with lower elevations generally being warmer, containing more oxygen, and being more densely vegetated than higher elevations, which leads to a higher fire risk (Schoennagel et al., 2004). Slope can influence the propagation of a wildfire as fires generally spread faster when traveling upslope (Weise and Biging, 1997;). Aspect is useful for determining if existing vegetation is on a surface facing the prevailing wind direction, and influences vegetation density, type, and moisture regimes.

Human infrastructure can be identified within an image and either classified as developed during supervised/unsupervised classification or simply digitized. Human infrastructure location is important as many wildfires are started by human activity. Due to this, many fire hazard mapping studies include proximity to features such as roads or

towns among their variables (Chuvieco and Congalton, 1989; Sowmya and Somashekar, 2010).

These data allow for continuous mapping of fire hazard potentials in an area, as opposed to fire danger ratings derived from interpolation of meteorological station data. Many studies have effectively demonstrated that remote sensing methods for fire risk mapping provide accurate estimations of fire risk potential (Jaiswal et al., 2002; Chuvieco et al., 2010; Yu et al., 2017). Fire risk is mapped similarly to fire hazard but also includes a vulnerability component based on values and expected losses (Hardy, 2005).

2.3 Remote Sensing of Burn Severity

Mapping burn severity estimates is achieved using NIR and SWIR data, with the SWIR wavelength generally being located in the longer end of the spectrum (2.08–2.35 μm range) (Miller and Thode, 2007). NIR (and delta NIR) were first used to identify burned and unburned areas (Garcia and Caselles, 1991). The ability of this index to determine varying degrees of burn severity within a burned area was explored in future research (Murphy, Reynolds and Koltun, 2008). Vegetation affected by a fire show drops in NIR reflectance and increases in SWIR reflectance (Veraverbeke et al., 2010). These wavelengths are used to derive NBR:

$$NBR = \frac{NIR - SWIR}{NIR + SWIR} \quad (3)$$

The NBR is calculated for an image before and after a fire event. The resulting NBRs are subtracted to calculate delta NBR (dNBR):

$$dNBR = NBR_{prefire} - NBR_{postfire} \quad (4)$$

While dNBR has become commonly used for burn severity estimates (Epting, Verbyla and Sorbel 2005), limitations to the technique have been widely documented

(Roy, Boschetti and Trigg, 2006; Epting, Verbyla and Sorbel, 2005; Murphy, Reynolds and Koltun, 2008). These limitations occurred when dNBR burn severity estimates were compared to those derived from CBI and found to have weak correlations in certain environments such as savannahs in South Africa (Roy, Keane and Trigg, 2006), temperate mountains of the Sierra Nevada Range of California (Miller and Thode, 2007), and boreal forests in Alaska (Murphy, Reynolds and Koltun, 2008).

As a result of these limitations, alternatives to dNBR are a current focus of research (Miller and Thode, 2007; Miller et al., 2009; Morgan et al., 2014; Parks, Dillon and Miller, 2014). Alternative methods for estimating burn severity include relative dNBR (RdNBR), revitalized burn ratio (RBR), and delta NDVI (dNDVI). dNDVI is not superior to dNBR, but it can be useful in circumstances where pre-burn biomass is lowly or highly variable, and in some areas dNBR only performs slightly better than dNDVI (Morgan et al., 2014).

RdNBR seeks to make NBR burn severity estimates relative to pre-fire vegetation cover, allowing for areas which experience high severity burns but possess less initial vegetation to be classified as a high burn severity by the index. NBR is calculated in a way where more densely vegetated stands that experience moderate burns will possess NBR values higher than less densely vegetated stands that experience severe burns (Miller and Thode, 2007). If NBR becomes relative, then stands experiencing a stand-replacing fire will fall into the high severity burn range despite pre-fire vegetation density. To accomplish this RdNBR is calculated:

$$RdNBR = \frac{dNBR}{\sqrt{|NBR_{prefire}|}} \quad (5)$$

RBR is a more recent burn severity index developed by Parks, Dillon and Miller

(2014) to mitigate difficulties associated with the denominator of the RdNBR equation. Parks, Dillon and Miller (2014) proposed this equation because it addresses the following issues: (1) The square root was removed because it resulted in extremely high or low values of RdNBR which were difficult to interpret. (2) The absolute value was removed due to the altering of negative pre-fire NBR values which alters the true variation in pre-fire NBR. While the concerns stated by Miller and Thode (2007) of altering the resulting index's sign due to a negative value in the denominator are legitimate, negative pre-fire NBR values compromise <1% of most fires. (3) In RdNBR, when pre-fire NBR equal zero the equation reaches infinity. The aim of RBR is to accurately estimate burn severity in areas of low vegetation density without the difficulties associated RdNBR. To accomplish this RBR is calculated:

$$RBR = \frac{dNBR}{NBR_{pre\ fire} + 1.001} \quad (6)$$

Remote sensing of burn severity is an evolving research effort that requires further exploration to find an ideal detection method. NBR is commonly used by land managers, but its limitations suggest the need for development of a more reliable index (Roy, Boschetti and Trigg, 2006; Epting, Verbyla and Sorbel, 2005; Murphy, Reynolds and Koltun, 2008). RBR has the potential to fulfill this need but as a relatively new burn severity index, further testing is required (Parks, Dillon and Miller, 2014).

1.2.4 Remote Sensing of Vegetation Recovery

Remote sensing of vegetation recovery is typically accomplished through one of three techniques: Image classification, VIs, and SMA. Additionally, recent research into vegetation recovery through the use of lidar technologies has been conducted (Bolton, Coops and Wulder, 2015; Gordon Price and Tasker, 2017). Image classification uses

supervised or unsupervised classification to identify areas of varying recovery. This method can categorize levels of recovery (Mitri and Gitas, 2010) or can be used for a binary, recovered/non-recovered classification (Stueve et al., 2009). A limitation of this approach is spatial resolution. Most available sensors spatial resolution is too coarse to pick up on individual plant regeneration, leading to mixed pixels (Gitas et al., 2012).

VIs are one of the most popular remote sensing techniques for monitoring vegetation recovery. NDVI has been strongly correlated to field estimates of post-fire vegetation cover (Vila and Barbosa, 2010; Van Leeuwen et al., 2010; Veraverbeke et al., 2012a). Studies have also used NDVI to estimate other post-fire environmental parameters including fractional vegetation cover (Pereira, 1999; Vila and Barbosa 2010), net primary production (NPP) (Amiro, Chen and Liu, 2000; Hicke et al., 2003) and leaf area index (LAI) (Boer et al., 2008). Other research has focused on making reliable recovery rate estimates, finding that modeling variations in NDVI achieves reliable estimates for plant recovery rates (Diaz-Delgado and Pons, 2001), however NDVI has proven less successful in coniferous environments where lower R^2 s are derived (Meng et al., 2015). Further research is needed to determine if the use of VIs based on SWIR can perform as well as NDVI when assessing vegetation recovery (Gitas et al., 2012).

Because of pixel size exceeding the size of individual plants, techniques such as SMA, which addresses the mixed pixel issue, are also used in vegetation recovery monitoring (Vila and Barbosa, 2010; Veraverbeke et al., 2012b). SMA determines the fraction of a pixel which belongs to a particular endmember. These endmembers are assumed to be representative of the cover types identified in the image (Gitas et al., 2012). Studies have documented consistent results using linear SMA models which

allowed for only one spectrum per endmember (Röder et al., 2008; Caetano et al., 1996; Vila and Barbosa, 2010). Endmember design presents a limitation to this approach as an endmember may not fully account for the natural variability in a given scene (Röder et al., 2008; Gitas et al., 2012). To address this issue, multiple endmember SMA (MESMA) has been used to allow for multiple endmembers for each cover type, and has shown high potential (Lippitt et al., 2018). Despite the previously mentioned limitation SMA still represents a practical means to monitor vegetation recovery at a sub-pixel level.

III. Need for Research

Fire risk mapping has become increasingly important with an increase of severe fire seasons (Keane et al., 2010). Fire risk mapping is an area of interest for land managers as it allows for identification of areas of fuel accumulation as well as providing an assessment of which areas are at the greatest risk of ignition events and fire propagation. The identification of at-risk areas enables land managers to better plan prescribed burns and mechanical thinning. These measures ultimately help protect large forest ecosystems, property that would be affected by a resulting wildfire, and human lives (Keane et al., 2010; Morgan et al., 2014). As a result, research in this area has received support from agencies and organizations in the U.S. such as the Joint Fire Sciences Program and the US Forest Service.

Burn severity is important to land managers as well as climate scientists. For land managers, knowledge of the severity of burns facilitates the assessment of a fire's impact on the landscape (Van Wagtendonk, Root and Key, 2004). For climate scientists, burn severity can be used in the calculation of carbon emissions resulting from a fire event (Epting, Verbyla and Sorbel, 2005) and organizations such as the National Science

Foundation (NSF), National Aeronautics and Space Administration (NASA), United States Forest Service (USFS), Bureau of Land Management (BLM), National Park Service (NPS), and others have supported research in this area.

Vegetation recovery monitoring is important to land managers because of the affects fire has on biological productivity and composition in an ecosystem. Additionally, these monitoring efforts facilitate estimates for long-term recovery (Gitas et al., 2012). These recovery time estimates allow for planning of long-term forestry activities and for predictions on when enough fuel will be built up for the area to be at risk of a new ignition event. Due to the importance of vegetation recovery monitoring, support for research in this area has been provided by the National Science Foundation and the National Geographic Society.

As previously mentioned, the relationship between fire risk, burn severity and vegetation recovery is an important area of research. The relationship between fire risk potential and burn severity allows for land managers to attempt to preemptively reduce the severity of future fire events by reducing the fire risk potential. The relationship between burn severity and vegetation recovery facilitates a better understanding of the impacts a fire will have on the composition of ecosystems. Finally, a relationship between fire risk potential and vegetation recovery can help land managers better prepare for eventual fire events as well as aid climate change scientist better project the effects of future fire regimes on ecosystem richness and endangerment of plant species.

IV. Study Area

Grand Teton National Park is located in western Wyoming; south of Yellowstone National Park (43.7904° N, 110.6818° W). The park encompasses approximately 130,000

ha of land that includes forests, mountains, and glacial lakes. When the surrounding area used in this study is included, the total area is approximately 222,620 ha (Figure 1). According to the National Park Service (NPS), this area has a semi-arid mountain climate with an average high of 25°C in the summer and an average low of -2 °C in the winter (NPS, 2016). On average, the area receives 440 cm of snowfall and has an average rainfall of 55 cm. The elevation ranges from approximately 1,900 m above sea level to 4,200 m. The sub-alpine forests are dominated by coniferous trees including *Pinus albicaulis* (whitebark pine), *Pinus flexilis* (limber pine), *Abies lasiocarpa* (subalpine fir), and *Picea engelmannii* (Engelmann spruce). Above the tree line in the alpine zone, tundra conditions prevail. Treeless regions are composed of grasses, wildflowers, mosses, and lichens. The northern section of the park experienced a wildfire event in the late summer of 2016.

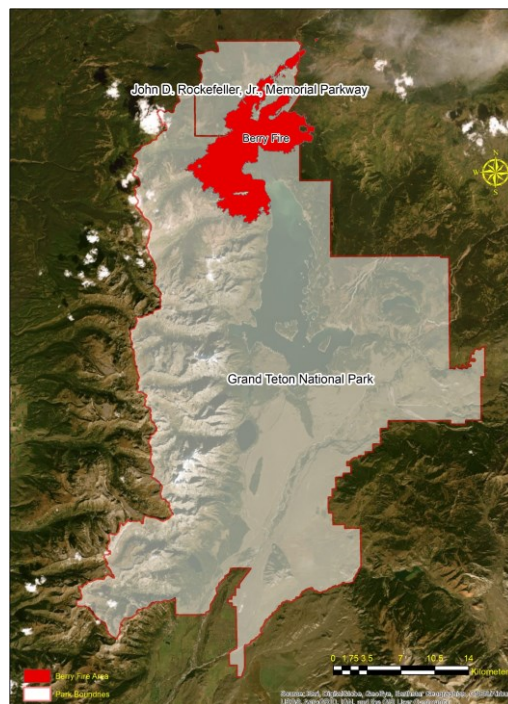


Figure 1. The study area for Grand Teton National Park and J.D. Rockefeller Parkway. The area affected by the Berry Fire is shown in red.

V. Research Questions

1. Are fire risk and burn severity related and if so how strong is this relationship?
2. Can traditional and red-edge based spectral indices be used to estimate quantitative assessments of burn severity?
3. Do “traditional”, red-edge, or MESMA products provide accurate estimations of fractional vegetation cover three-years postfire?

II. GRAND TETON FIRE HAZARD AND BURN SEVERITY

ABSTRACT: Fire risk maps are a useful tool which help land managers with wildfire mitigation planning. These maps are used for predicting the likelihood of fire ignition, the fire behavior, and the effects of a fire and can be generated using different techniques. However, the relationship between fire risk and the resulting burn severity has not been fully explored. This paper presents a new method for assessing fire risk and examines the relationship between fire risk and burn severity. The 2016 Berry Fire in Grand Teton National Park is used as a case study for this examination. Fire risk was calculated using a multicriteria evaluation based on fuel type, canopy cover, moisture conditions, topography, and infrastructure. Additionally, several previously proposed fire risk indices were generated for comparison. All fire risk indices were then compared to the burn severities for the Berry Fire to determine if a relationship exists between fire risk and burn severity. The proposed model exhibited a moderate relationship with two of the tested burn severity categories (unburned and moderate to high) and a weak relationship with the other categories (low, moderate, high). The other fire risk indices exhibited very weak relationships with burn severity and in some instances the relationship was the inverse of what was expected.

I. Introduction

Wildfires are a phenomenon that can alter ecosystems (Ahlgren and Ahlgren, 1960; Bond and Keeley, 2005), damage property and infrastructure (Stetler, Venn and Calkin, 2010), and harm the wellbeing of at-risk populations (Congressional Research Service, 2019). In recent years, wildfires have had dramatic effects on various parts of the United States, with 2015 being the worst wildfire year on record in terms of area

burned (CRS, 2019). With changing climate, the trend towards larger, more severe wildfires is expected to increase (Westerling and Bryant, 2008; de Groot, Flannigan and Cantin, 2013; Flannigan et al., 2013).

This trend in larger, more severe wildfires escalates the need for improved wildfire prevention planning by land managers. Improved planning requires fire risk mapping to identify the most at-risk areas. Fire risk mapping has been an ongoing area of research for decades but no agreed upon method has yet been developed (Chuvieco and Congalton, 1989; Chuvieco and Salas, 1996; Jaiswal et al., 2002; Adab, Kanniah and Solaimani, 2013). Typically, fire risk mapping applies remote sensing and existing geographic data to acquire variables entered into a spatially explicit model to determine the hazard for specific areas and then evaluate the risk on the consequences of these hazards. This enables the land managers to address areas of high fire risk and reduce the current risk to better prepare for future fire events.

It is important to differentiate between fire hazard, risk and danger as these terms have different meanings. Fire hazard is a rating of the chance of an ignition event and propagation potentials based off conditions in the landscape (Chuvieco and Congalton, 1989). Fire risk builds upon fire hazard by adding vulnerability into the assessment which is based on value and loss estimates for the landscape (Chuvieco et al., 2010). Fire danger maps fire potential based on meteorological conditions for an area (Burgan et al., 1997).

Characterizations of fire hazard, risks and danger have been accomplished through climatic interpolation (Burgan et al., 1997), hybrid models (Beverly, Herd and Conner, 2009; Keane et al., 2010), and remote sensing/GIS (Watts, 1997; Hernandez-Leal, Arbelo and Gonzalez-Calvo, 2006; Adab, Kanniah and Solaimani, 2013; Yu et al.,

2017). Each of these methods possesses advantages and limitations. Climatic interpolation is used in the U.S. by the Wildland Fire Assessment System (WFAS) which was founded in 1994 by the Northern Forest Fire Laboratory (now the Missoula Fire Sciences Laboratory). This fire danger assessment system is used by private, local, state, and federal agencies and is updated on a daily basis. Its primary limitation is the use of interpolation to calculate fire risk potentials (Yu et al., 2017).

Hybrid models use a combination of spatially explicit daily climate data and continuous data from pre-existing databases and/or remote sensing systems to assess fire risk. An example of a hybrid model is FIREHARM. Keane et al. (2010) introduced FIREHARM, a method for mapping fire risk and potential risk. FIREHARM is a C++ program which uses spatially explicit daily climate data with weather models to simulate fuel moisture for the calculation of fire behavior, danger, and effects across multiple spatial scales. These outputs are calculated using LANDFIRE vegetation data, topography data from the USGS National Elevation Dataset, LAI data generated from MODIS, and soil inputs summarized from the STATSGO database. Researchers found FIREHARM to be advantageous in the creation of risk maps at fine spatial resolution, but its limitations include stringent data requirements and lengthy processing time. Due to these limitations, FIREHARM is seen as an effective method for mapping potential fire risk at fine scale but it does not replace other fire risk mapping techniques.

Studies that use remote sensing and GIS for fire risk mapping span across decades and use similar variables, but they implement these variables in diverse ways and in different environments. Before fire risk mapping, the focus of research was on fire hazard mapping which maps the likelihood of ignition and propagation events. This was

accomplished through the use of cartographic modeling with weights assigned by on how much the input variable influences fire ignition and spread. Chuvieco and Congalton (1989) used remote sensing and GIS to assess fire hazard for an area on the southeastern coast of Spain. They used land cover, elevation, distance from trail, and road locations to assess the risk of a fire event. They found these variables adequately identified areas of a higher fire hazard. Fire hazard methods have since been developed to include the economic perspective of potential damages (i.e., fire risk).

Recently, Adab, Kanniah and Solaimani (2013) composite fire risk indices of Structural Fire Index (SFI) and Fire Risk Index (FRI) into Hybrid Fire Index (HFI). The variables used in their HFI study included vegetation moisture, elevation, slope, aspect, distance from roads, and proximity to settlement. While SFI does not use proximity to settlement and FRI does not use elevation, both indices also use different weight assignments. The HFI includes both elevation and proximity to settlement and a novel weight assignment. By comparing the indices and verifying against MODIS active fire data products, Adab, Kanniah and Solaimani (2013) found that HFI outperformed the other two indices.

An alternative approach to mapping fire risk potentials is to model the distribution of fuel, referred to as the fuel loading, for a given area and to use these fuel loading models to assist in the simulation of fire spread. Simulations of fire spread use data on weather conditions, wind, topography, and fuel characteristics as inputs into fire behavior models (Finney, 1995; Finney and Ryan, 1995; Finney, 2006). This allows for a series of simulations of fire spread based on various ignition points that are used to assess fire risk. An example of a simulation model used to assess fire risk is FlamMap, a commonly used model for risk assessments (Finney, 2006).

Studies which attempt to simulate fire spread provide a means of assessing where potential fires have the greatest chance of negatively affecting lives and property. However, this approach is limited due to the need for accurate and up-to-date meteorological conditions for the area being assessed, accurate data on fuel conditions, and the need for constant updates in changing environmental and atmospheric conditions. Because of this, risk assessments based on less dynamic data can still be useful for assessing short- and long-term fire risk.

Currently, the relationship between fire hazard and burn severity has not been adequately explored. Several fire risk studies briefly mention burn severity but do not attempt to compare post-fire burn severity to the generated fire hazards (Chuvieco and Congalton, 1989; Pradhan, Dini Hairi Bin Suliman and Arshad Bin Awang, 2007; Adab, Kanniah and Solaimani, 2013). While these models are primarily designed to estimate the hazard of an ignition event, the variables used to generate these models have been shown to be related to burn severity and therefore the resulting fire hazards should have a relationship with post-fire burn severity (Lentile, Smith and Shepperd, 2006; Prichard and Kennedy, 2014).

With the launch of the Sentinel-2 platforms, research into the capability of the sensors for fire hazard mapping is warranted. The Sentinel satellite constellation possesses a temporal resolution of 5 to 7 days, which allows for regular updates to fire risk assessments on a weekly basis. Additionally, the Sentinel-2 satellites have both high spatial and spectral resolutions compared to other moderate resolution satellites (e.g., Landsat 8 OLI/TRIS). This makes these sensors ideal for rapid and regular fire risk assessment for moderate to large areas. Currently the only research related to wildfire

using Sentinel-2 is a study which attempted to determine the sensor's ability to detect burn severity using red-edge wavelengths (Fernández-Manso, Fernández-Manso and Quintano, 2016).

The objective of this research is to integrate a LANDFIRE fuel model and canopy cover data into a modification of the hybrid fire risk index (HFI) created by Adab, Kanniah and Solaimani (2013). This approach builds upon past research to enhance the modeling of fire hazard by providing accurate estimates based on fuel type, canopy cover, relative moisture conditions, topography, and distance from human infrastructure. This index is applied to an area of recent wildfire activity in Grand Teton National Park in Wyoming, USA using Sentinel-2 imagery acquired prior to the fire for estimating moisture conditions. The resulting fire hazard maps are compared to the burn severities identified by the Monitoring Trends in Burn Severity (MTBS) project to determine if a relationship exists between fire hazard and burn severity. Additionally, three other common fire hazard models are generated and the relationship between these models' fire hazards and burn severity is tested and compared to the results for the proposed model.

II. Methods

2.1 Study Area

Grand Teton National Park is located in western Wyoming; south of Yellowstone National Park (43.7904° N, 110.6818° W). The park encompasses approximately 130,000 ha of land that includes forests, mountains, and glacial lakes. This study includes the surrounding area that totals up to approximately 222,620 ha. The elevation ranges from approximately 1,900 m above sea level to 4,200 m. The sub-alpine forests are dominated by coniferous trees including *Pinus albicaulis* (whitebark pine), *Pinus flexilis* (limber

pine), *Abies lasiocarpa* (subalpine fir), and *Picea engelmannii* (Engelmann spruce).

Above the tree line in the alpine zone, tundra condition prevails. Treeless regions are composed of grasses, wildflowers, mosses, and lichens.

The northern section of the national park experienced a wildfire event in the late summer of 2016. The wildfire, named the Berry Fire, was discovered on July 25, 2016 and burned until early September 2016 (Figure). The fire affected approximately 8,750 ha of land in and around the national park, causing the closure of Highway 89/191/287. After discovery, the fire was managed by park authorities for ecological benefits. The Berry Fire is the largest recorded fire in Grand Teton National Park's history.

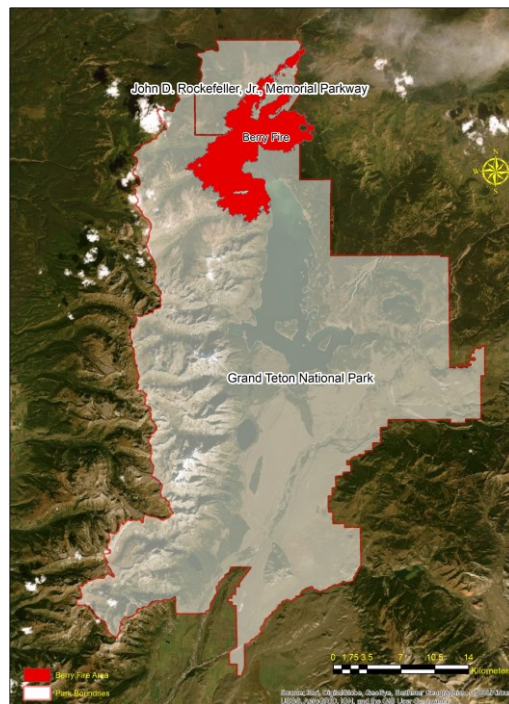


Figure 2. Grand Teton National Park and John D. Rockefeller Parkway. The area affected by the 2016 Berry Fire is represented by the red polygon in the northern section of the study area.

2.2 Data Collection and Preprocessing

Sentinel-2 is a moderate-resolution multispectral scanner with 13 spectral bands (Table 4). Sentinel-2 imagery is acquired by two sensors on the same orbit about 180° apart from each other. This allows for a temporal resolution of five days at the equator. Sentinel-2A was launched by the European Space Agency (ESA) on June 23, 2015 and Sentinel-2B was launched on March 7, 2017.

Table 4. Sentinel-2A spectral and spatial resolutions.

Band Number	Spectral Resolution Central Wavelength (μm)	Spatial Resolution (m)
1	0.4304 - 0.4574	60
2	0.4476 - 0.5456	10
3	0.5375 - 0.5825	10
4	0.6455 - 0.6835	10
5	0.6955 - 0.7134	20
6	0.7312 - 0.7492	20
7	0.7685 - 0.7965	20
8	0.7626 - 0.9076	10
8a	0.8483 - 0.8813	20
9	0.941 - 0.967	60
10	1.336 - 1.411	60
11	1.5422 - 1.6852	20
12	2.0814 - 2.3234	20

Sentinel-2A imagery were acquired prior to the Berry Fire (image acquisition July 15th) and was downloaded from the ESA's Copernicus database. The data were processed to apply atmospheric corrections and converted to surface reflectance using the Sen2Cor application. The visible-NIR bands were resampled to a 30m spatial resolution to match the other inputs of the fire hazard model. From the imagery, the normalized difference moisture index (NDMI) was calculated using bands 8a and 11 in the ERDAS IMAGINE

image processing system.

A DEM was downloaded from the USGS Elevation Derivatives for National Applications (EDNA) dataset. This DEM provides 30m spatial resolution elevation data for the contiguous USA. The DEM was clipped to the study area and used to calculate aspect and slope values for the study area. The database was completed from 2000-2003 and was designed to be vertically consistent. It is possible that some minor changes to elevation values for parts of the DEM (due to flooding, debris flows, etc.) have occurred since its generation, however these changes are not expected to have changed the elevation values significantly enough to make the DEM obsolete.

Road, trail and structure data were obtained via the National Park Service datastore. The structures shapefile was last updated in 2015 and the roads and trails were updated in 2016. For the purpose of this research, settlements were identified as lodges, docks, and other structures/compounds located within the park, as these are the areas where repair/rebuilding costs, and potentially the loss of human lives, would be highest in the event of a fire.

The LANDFIRE 40 Scott and Burgan Fire Behavior Fuel Models (40FBFM) for 2014 was acquired from the LANDFIRE database for the study area. This model groups various vegetation covers into fuel types which exhibit similar fire behavior when burned. Existing canopy cover data were also downloaded from LANDFIRE.

Burn severity data were acquired from the MTBS project conducted by the U.S. Geological Survey Center for Earth Resources Observation and Science (EROS) and the USDA Forest Service Geospatial Technology and Applications Center (GTAC). These data were generated using the delta Normalized Burn Ratio (dNBR) applied to pre- and

post-fire Landsat 8 imagery. These data are useful for determining the relationship between fire hazard and burn severity.

2.3 Analysis

2.3.1 Risk rankings

The fire hazard model was derived using a multicriteria evaluation (MCE), where the inputs were assigned rankings based on their contribution to potential ignition/propagation of fire and the vulnerability they represent. The greater the hazard represented by the input, the larger the assigned ranking. Determination of rankings assigned to variables was achieved via literature on how these inputs influence fire hazard.

Vegetation conditions and fuel arrangement have a large influence on fire hazard and fire behaviors (He et al., 2004; Krasnow, Schoennagel and Veblen, 2009). Fuel categories are determined by the type of vegetation present, the danger of an ignition event for this vegetation, and how the vegetation will influence the fire characteristics. This study uses the 40FBFM method of categorizing fuels and has ranked the hazard presented by each fuel based on the descriptions from Scott and Burgan, 2005 (Table 5). However, fuel categories alone are not enough of an indication of the hazard presented by the vegetation of an area. In combination with fuel type, canopy cover was also used for the hazard assessment. The hazard rankings for canopy cover are based on the ranking system used by the FlamMap fire behavior simulator (Table 6).

Table 5. Hazard rankings for 40FBFM fuel categories.

Hazard Ranking	40FBFM
1	GR1, GR2, GS1, SH1, SH2
2	GR4, GS2, TU1, TL1
3	TU2, TL2, TL3, TL4, TL7
4	TU5, TL5, TL8
5	TL6

Table 6. Hazard rankings for canopy cover.

Canopy Cover	Hazard Ranking
0%	0
1-20%	1
21-50%	2
51-80%	3
81-100%	4

Moisture content is an important factor when determining the ease with which a fire can ignite and spread (Chuvieco and Congalton, 1989; Adab, Kanniah and Solaimani, 2013). Drier conditions allow for ignition events to occur more easily, whereas wet conditions can be less vulnerable to an ignition event. As a result, low moisture values are associated with higher fire hazard and high moisture values are associated with low fire hazard. NDMI was used as a proxy for moisture content and was broken into five classes based on natural breaks which were then reclassified into hazard rankings (Table 7).

Table 7. Hazard rankings for NDMI.

NDMI range	Hazard Ranking
-0.993443 - -0.082426	5
-0.082426 - 0.075685	4
0.075685 - 0.226266	3
0.226266 - 0.504842	2
0.504842 - 0.933998	1

Topographic variables are also important for determining fire hazard as they can influence fire occurrence and have a large effect on fire propagation. In environments where large variations in elevation occur it can be useful as an indicator of hazard due to elevations influence on precipitation occurrence and temperature (Pradhan, Dini Hairi Bin Suliman and Arshad Bin Awang, 2007; Adab, Kanniah and Solaimani, 2013). This makes lower elevations more vulnerable to fire occurrences. Slope does not influence fire occurrence but does influence the rate at which fire will spread, with steeper slopes causing a more rapid fire propagation (Viegas, 2004). Elevation was broken into four classes based on natural breaks which were then reclassified into hazard rankings (Table 8).

Table 8. Hazard rankings for elevation

Elevation(m)	Hazard Ranking
1926 - 2260.1561	4
2260.1561 - 2620.6929	3
2620.6929 - 2981.2297	2
2981.2297 - 4177.1567	1

Aspect influences the amount of solar illumination received by an area on the Earth's surface. At 43.47° N, south facing slopes receive the greatest amount of sunlight,

followed by western facing slopes. As solar illumination can increase temperatures and reduce moisture content, south facing slopes receive the highest hazard ranking, western slopes received the second highest ranking, eastern slopes receiving the second lowest, and northern slopes receiving the lowest ranking. Slope was broken into four classes based on natural breaks which were then reclassified into hazard rankings and aspect was assigned higher hazard rankings for southern and western slopes (Tables 9 and 10).

Table 9. Hazard rankings for slope.

Slope(degrees)	Hazard Ranking
0 - 8.5809	1
8.5809 - 21.3043	2
21.3043 - 36.6908	3
36.6908 - 75.7488	4

Table 10. Hazard rankings for aspect.

Aspect	Hazard Ranking
-1 - 0	1
0 - 45	1
45 - 135	2
135 - 225	4
225 - 315	3
315 - 360	1

Areas of higher rates of anthropologic activities can increase fire hazard. Most fires ignitions in the United States are caused by human activity (CRS, 2019), which means any fire hazard model must incorporate the distance from areas of human activity. Additionally, the potential loss of lives and the economic cost of infrastructure destroyed by a fire play a key role in assessing vulnerability, which is necessary for a hazard

assessment. In the model presented in this study, distances from road, trail, and park structure were used as indicators of fire hazard associated with anthropogenic activity. The greater the distance the lower the hazard, with distance determined by the path distance over the DEM from each of the aforementioned layers. A raster layer for proximity to roads, trails and structures was generated using path distance with the DEM as the surface. This raster was the classified using natural breaks to categorize the data into nine classes and then was reclassified into four fire hazard rankings for roads and trails and five for structures (Table 11).

Table 11. Hazard rankings for roads, trails, and structures.

Hazard Ranking	Path distance from roads	Path distance from trails	Path distance from structures
1	8609.4 - 19371.2	6169.9 - 11105.9	10002.2 - 21161.6
2	4304.7 - 8609.4	3701.9 - 6169.9	5455.7 - 10002.2
3	2152.3 - 4304.7	1233.9 - 3701.9	3471.8 - 5455.7
4	0 - 2152.3	0 - 1233.9	1735.9 - 3471.8
5	N/A	N/A	0 - 1735.9

2.3.2 Weight Assignment

The variables for fire hazard modeling do not have equal importance when it comes to influencing the hazard of wildfire. Because of this, weights must be assigned to more accurately represent the influence variables have on fire hazard. Determining these weights can be difficult, as the most important variables can change from one environment to the next, and there is disagreement in the literature and among experts about what the appropriate weights are. However, there are certain trends in the assignment of weights for fire hazard assessments when the variables are viewed in more general categories. Generally, moisture content receives the highest weighting (Chuvieco

and Congalton, 1989; Jaiswal et al., 2002; Adab, Kanniah and Solaimani, 2013). This is because moisture content controls the ignition and fire spread potential for fuel and so its relative level plays a critical role in assessing fire hazard (Yebra, Chuvieco and Riaño, 2008). For this reason, the moisture variable was assigned the highest weight.

In previous research, fuel type and canopy cover are often not included in MCE fire hazard assessments due to lack of available data (Chuvieco and Congalton 1989; Jaiswal et al., 2002; Erten, Kurgun and Musaoglu, 2004; Adab, Kanniah and Solaimani, 2013). However, when available, these data can provide valuable information for the assessment of fire hazard. As fuel conditions have been shown to have a large influence on the chance of an ignition event, fire spread, and fire behavior (Rollins, 2009; Prichard and Kennedy, 2014), the summation of the fuel and canopy cover hazard rankings was assigned the second highest weight.

Generally, the slope of an area receives the second highest weighting across various environments in other fire hazard assessments (Adab, Kanniah and Solaimani, 2013). This is because of the importance of slope in fire propagation. For this specific study area slopes are of great importance, as there are large variations which can drastically affect wildfire behavior. However, the proposed model includes fuel variables which are not typically found in other fire hazard assessments. Because of this, slope was assigned the third highest weight. Aspect is important due to its influence on solar illumination, which in turn affects moisture content of an area and vegetation abundance (Prasad, Badarinath and Eaturu, 2008). Typically, aspect is assigned a weight slightly lower than slope (Adab, Kanniah and Solaimani, 2013). For the proposed model aspect was assigned the fourth highest weight.

The literature consistently assigns proximity to human activity a low weight (Chuvieco and Congalton, 1989; Adab, Kanniah and Solaimani, 2013). This is due to the rapid diminishing of human influence on fire occurrence and vulnerability as the distance from human activity increases. Additionally, the resources needed to fight fires are most easily transported to areas via this infrastructure. In the context of this study area, human activity is largely limited to trails, roads, and structures which are strictly enforced by rangers in the National Park Service. For these reasons, variables associated with human activity were assigned the second lowest weight.

Finally, elevation can influence fire occurrence as lower elevations in mountainous regions tend to have less frequent precipitation and are warmer. However, elevation is typically seen as the least important variable and is frequently assigned the lowest weight (Chuvieco and Congalton, 1989; Adab, Kanniah and Solaimani, 2013). Because of this, elevation was assigned the lowest weight in this research. The final weights were assigned in a based on the weight assignments in Adab, Kanniah and Solaimani (2013) with the addition of a weight of 75 for the sum of fuel type and canopy cover.

2.3.3 Analysis

All layers were entered into a MCE using cartographic modeling and map algebra. Weights were assigned based on a modification to the weight assignment used for the hybrid fire index (HFI) (Adab, Kanniah and Solaimani, 2013). Moisture content received the highest weight, fuel and canopy cover receiving the second highest weight, and the other variables receiving lower weights. Finally, the output was normalized based on the maximum possible value which could be obtained (Equation 1).

$$\frac{100m + 75(f + cc) + 50s + 25a + 10(r + t + b) + 5e}{max} \quad (1)$$

Where m represents moisture content, f represents fuel type, cc represents canopy cover, s represents slope, a represents aspect, r represents distance from roads, t distance from trails, b represent proximity to buildings/structures, and e represents elevation. The weights assignment for all variables are based on the HFI except for the weight assigned to the summation of fuel type and canopy cover. Seventy-five is selected as the weight for these variables because the presence and amount of fuel is more important than any factor other than the moisture content.

Additionally, the standard fire index (SFI), fire hazard index (FRI) and HFI were generated using their corresponding input variables. To make these indices more comparable to the proposed model, structures were substituted for settlements and trail data were included with roads in their generation. The fire hazard model was categorized into four fire hazard classes (low, moderate, high, extreme) by analyzing the distribution of hazard rankings and applying a Jenks natural breaks classification scheme to the data.

2.3.4 Comparison to Burn Severity

After the fire hazard map was generated, it was compared to the burn severity of the Berry Fire using logistic regression and the dNBR for the 2016 Berry Fire. One-thousand five-hundred points were generated in a stratified random sample proportional to the areas belonging to each burn severity category. While other studies have relied on historical spatial data for fire locations to determine if fires in a region were located in higher hazard pixels, this study instead examines a single fire to explore the relationship between hazard and burn severity. The number of points used in this study exceeds the

required points for a 95% confidence multinomial distribution. The values from the fire hazard model and the dNBR datasets were extracted to these points and their relationship was examined using logistic regression. Additionally, fire hazard values for the three other indices were also extracted to these points and examined.

Logistic regression is used for assessing the ability of a variable to predict the passing (1) or failing (0) of an event. In the context of this research the event which is being passed or failed is the burn severity category. Four separate pass/fail scenarios were created, one for each primary burn severity category (unburned, low, moderate, and high) as well as a fifth, broader, category which combined moderate and high, dubbed 'moderate to high'. For each category, points with a burn severity belonging to this category were coded as 1 and all other points were coded 0. These tables were combined, and logistic regression was performed within JMP with the binary success serving as the y variable and hazard ranking as the x variable.

Finally, the receiver operating characteristic (ROC) method was used to quantitatively determine the effectiveness of the proposed model for predicting different levels of burn severity. The ROC technique involves plotting the true-positive rate against the false-positive rate. The area under the curve (AUC) was used to determine how well the model performed. The AUC describes how adequately a model predicts the occurrence or nonoccurrence of 'events' (Yesilnacar and Topal, 2005; Adab, Kanniah and Solaimani, 2013). The closer the AUC is to one, the better the model, with one representing 100% accuracy.

III. Results

3.1 Sensitivity analysis of inputs

To determine the sensitivity of the output fire hazard to each input, variable importance was assessed in JMP. JMP allows for the assessment of model factors independent from the model. Indices are calculated based on the range of variability in each variable. If variations in a variable result in a larger variation for the model output, then the model is sensitive to this variable. This sensitivity is measured using:

$$\text{Var}(E(y | x_j)) / \text{Var}(y) \quad (2)$$

Where $\text{Var}(E(y | x_j))$ measures the variation in the expected output value ($E(y)$) over the distribution of the input (x_j ; when the input is fixed), and $\text{Var}(y)$ is the variance of the output. JMP reports an estimate of this as the main effect, with higher values indicating a variable which the output is more sensitive to. The total effect is impact on variance of x_j for all terms that contain x_j . This provides an additional measurement for the sensitivity of the output values to variations in the input variables, with higher total effect values indicating greater sensitivity.

When assessing the importance of variables, multicollinearity is an important consideration. Table 12 contains the measured correlation between the input variables. The only strong positive correlations were Buildings/Roads (0.85) and Canopy Cover/40FBFM (0.59) with the remaining variables only weakly correlated at best. Because of this weak correlation between the input variables, the sensitivity analysis was run with the assumption of independence in the inputs.

Table 12. Correlation matrix for model input variables.

Variable	Canopy Cover	40FBFM	DEM	Slope	Aspect	NDMI	Roads	Buildings	Trails
Canopy Cover	1.00	0.59	0.08	-0.04	-0.15	-0.21	-0.04	0.00	-0.07
40FBFM		1.00	0.11	0.03	-0.15	-0.02	-0.05	-0.01	-0.08
DEM			1.00	-0.32	0.05	-0.07	0.43	0.39	0.11
Slope				1.00	-0.03	0.16	-0.36	-0.44	0.15
Aspect					1.00	0.05	0.17	0.14	-0.03
NDMI						1.00	-0.13	-0.09	0.00
Roads							1.00	0.85	-0.37
Buildings								1.00	-0.32
Trails									1.00

The result of the sensitivity analysis for the proposed fire hazard model is provided in Table 13. Interestingly, the Fuel Model (40FBFM) was identified as possessing the strongest effect on model outputs despite being weighted lower than NDMI. The fuel model was identified as the most important variable, with NDMI and Canopy Cover also having a large impact on the variation in the output. Roads, Trails, Buildings and DEM all had little effect on the model output, which is likely related to the lower weights assigned to these variables.

Table 13. First sensitivity analysis for proposed model input variables based on the assumption of variable independence. This report was generated using the proposed models weighting scheme.

	Main Effect	Total Effect
40FBFM	0.33	0.342
NDMI	0.301	0.313
Canopy Cover	0.194	0.206
Slope	0.058	0.07
Aspect	0.03	0.039
Buildings	0.004	0.007
Roads	0.004	0.006
Trails	0.001	0.003
Elevation	0.001	0.001

To determine the importance of variables without the model weights, a separate sensitivity analysis was conducted where the inputs were not weighted and were instead simply summed and normalized (Table 14). In this basic summation model, the variable Roads was identified as the variable of greatest importance, with 40FBFM, Buildings and Aspect also possessing relatively large main and total effect values. This highlights the importance of using weights to ensure that variables which have been consistently identified in the literature as possessing the most importance for fire hazard assessment possess the strongest effect on the model.

Table 14. Second sensitivity analysis for model inputs based on the assumption of variable independence. This report was generated using a simple summation of variables.

	Main Effect	Total Effect
Roads	0.172	0.188
40FBFM	0.152	0.168
Buildings	0.139	0.155
Aspect	0.138	0.154
Canopy Cover	0.073	0.09
Slope	0.069	0.086
NDMI	0.063	0.079
Trails	0.033	0.047
Elevation	0.025	0.038

Evaluation of model performance

3.2 Fire hazard model output

Fire hazard for Grand Teton National Park was estimated using a MCE with the reclassified variables as inputs (Figure 3). The hazard values ranged from 0.127 to 0.848, with a mean of 0.503 (Table 12). Jenk’s natural breaks were used to organize these values into categories corresponding to estimated hazard. The northern section of the park possessed the most extreme hazard, with the southern and eastern section of the park possessing extreme hazard in dry, forested areas.

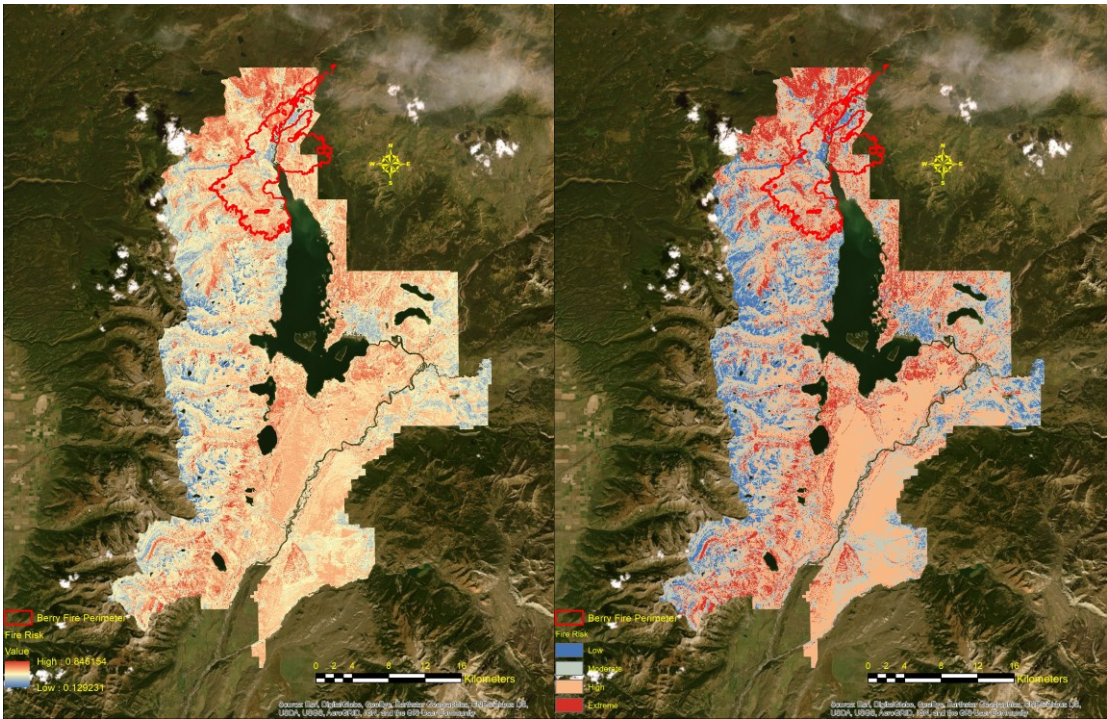


Figure 3. Fire hazard output. (A) The image on the left shows the raw, normalized output for the fire hazard model. Lower hazards are in blue and higher hazards are in red. (B) the image on the right shows the hazard broken into four broad categories: low, moderate, high, and extreme. Low hazards are shown in dark blue and extreme hazards are displayed as dark red.

Table 15. Descriptive statistics for the fire hazard model output.

Descriptive Statistic	Fire Hazard Output
Min	0.129
Max	0.846
Mean	0.494
Standard Deviation	0.091
Mode	0.523
Median	0.501
Low Fire Hazard	11.15% of area
Moderate Fire Hazard	29.58% of area
High Fire Hazard	43.15% of area
Extreme Fire Hazard	16.11% of area

Low fire hazard was the smallest category in the output, comprising 11.15% of the area. Low hazard was most frequently found in the mountains in the western section of the park and in areas with low hazard fuel/little canopy cover. Moderate hazard was the second largest hazard category, making up 29.58% of the study area. High hazard comprises 43.15% of the park, with a large area of high hazard being located in the dry southern section of the study area. Areas of extreme fire hazard comprise 16.11% of the park, being primarily located in the northern sections of the park.

The first recorded Berry Fire perimeter (July 27, 2016) was located in an area of primarily moderate hazard pixels, with parts of four high hazard pixels and an extreme hazard pixel located within the perimeter. The area in which the Berry Fire was first located had an average fire hazard of 0.465, with a max of 0.590 and a min of 0.421.

3.3 Comparison to burn severity

To compare fire hazard to burn severity, a dNBR product generated by the MTBS project was used for estimates of burn severity. This product is generated at a 30m spatial resolution using Landsat data and breaks the burn severity into four categories: unburned,

low, moderate and high. Using these data, the proportion of each burn severity category were calculated and 1,500 random points were generated based on the proportional composition of each burn severity category. The raw hazard values and the burn severity category were extracted for each point and were used to perform several logistic regressions where:

- Unburned was coded as 1 and all other severities coded as 0
- Low burn severity was coded as 1 with all other severities coded as 0
- Moderate burn severity was coded as 1 with all other severities coded as 0
- High burn severity was coded as 1 with all other severities coded as 0
- Moderate to high burn severity were coded as 1 and all other burn severities were coded as 0

The normalized fire hazard values were used as the independent variable and the coded burn severity values as the dependent variable to perform nominal logistic regression. The results of the logistic regression indicate that the modeled fire hazards had a significant relationship with all burn severity categories except the low burn severity category (Table 16).

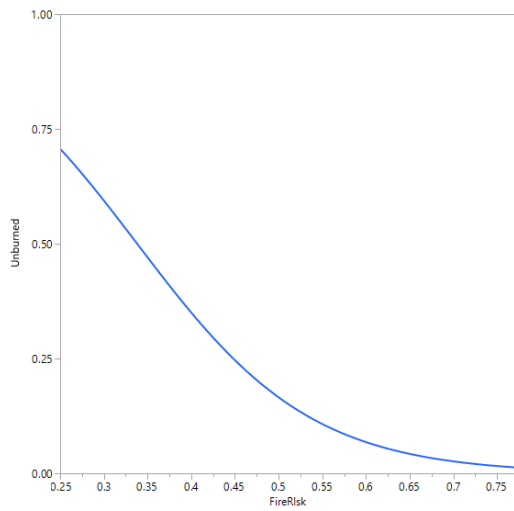
Table 16. Summary of logistic regression results for each run.

Logistic Test	Odds Ratio	Standard Error	Chi Square	<i>p</i>
Unburned and Fire Hazard	0.0073	0.8555	155.4910	<0.0001
Low Burn Severity and Fire Hazard	1.2497	0.6765	0.4489	0.5028
Moderate Burn Severity and Fire Hazard	3.7494	0.7246	14.0909	0.0002
High Burn Severity and Fire Hazard	8.2174	0.6859	41.1249	<0.0001
Moderate to High Burn Severity and Fire Hazard	16.8322	0.6504	84.3702	<0.0001

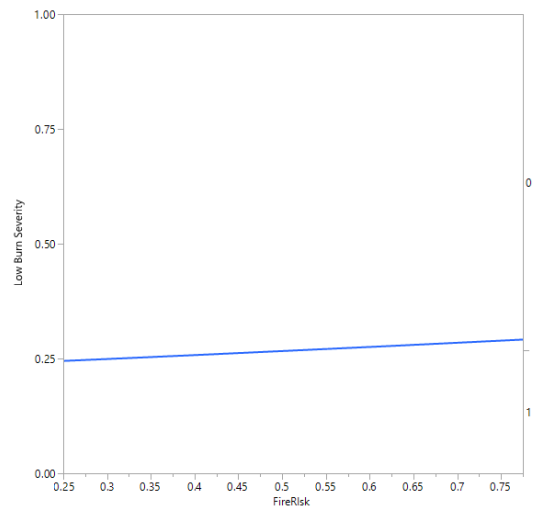
The logistic regression models exhibit a moderate relationship for fire hazard and

moderate to high burn severity and unburned (Figure 4). On their own, high burn severity and moderate burn severity possess a weak relationship with fire hazard. Low burn severity does not possess a statistically significant relationship with burn severity.

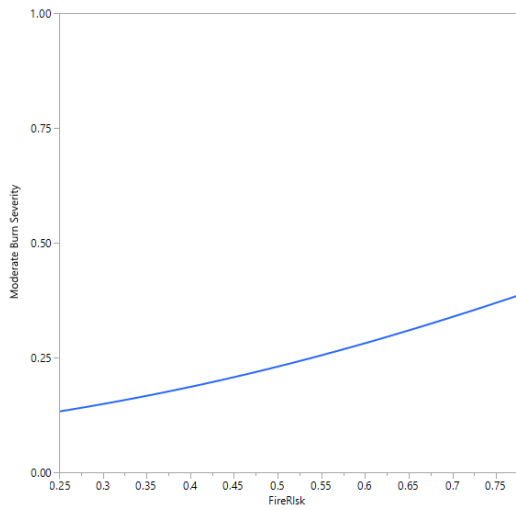
(a)



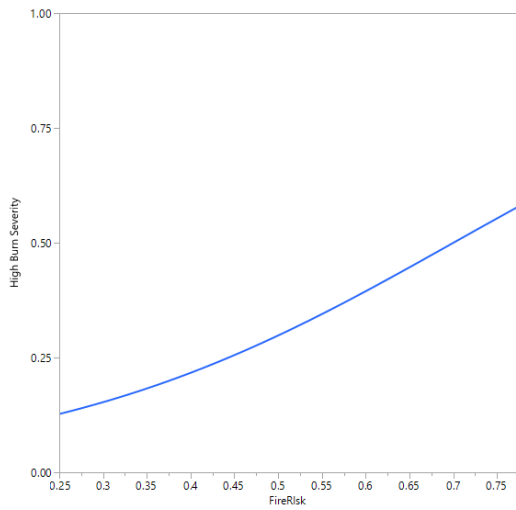
(b)



(c)



(d)



(e)

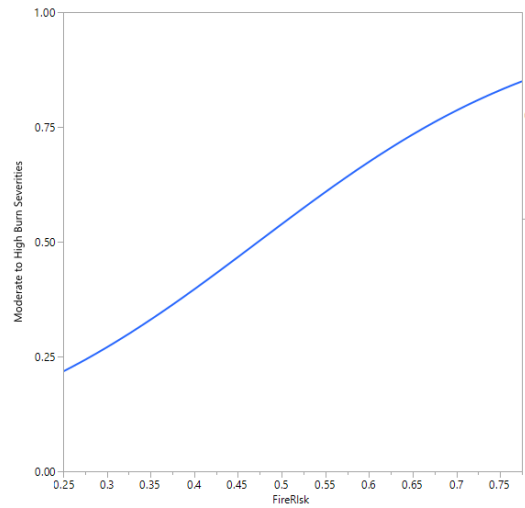
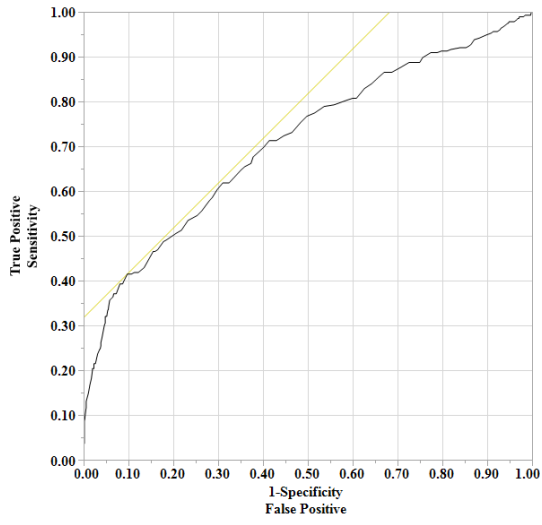


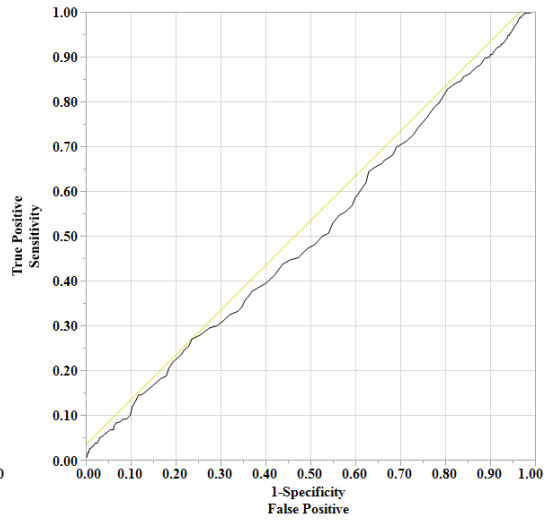
Figure 4. Logistic regression plots of fire hazard and burn severity: for unburned (a), low burn severity (b), moderate burn severity (c), high burn severity (d), and moderate to high burn severity (e).

The ROCs for the burn severity categories were generated inside of JMP (Figure 5). The unburned category possessed the best AUC value (0.709), followed by the moderate to high burn severity category (0.623). These values suggest a model which is better than fair (0.5). High, moderate and low burn severities had AUCs of 0.595, 0.555 and 0.504 respectively.

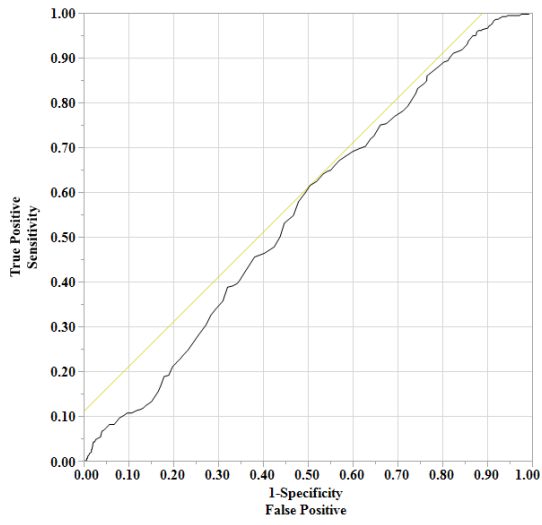
(a)



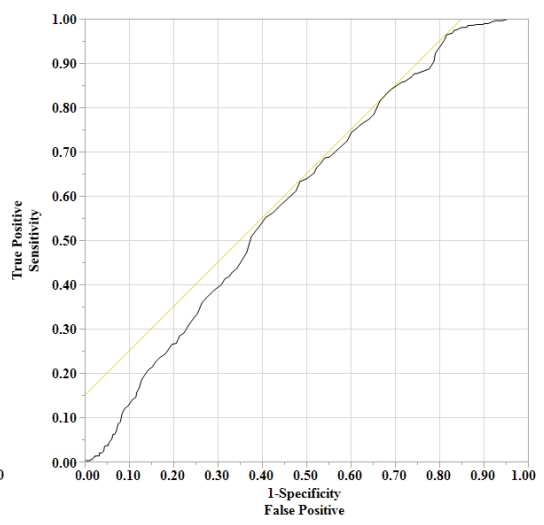
(b)



(c)



(d)



(e)

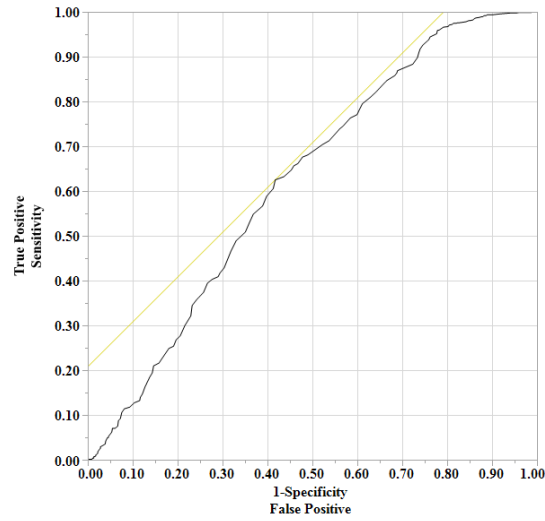


Figure 5. ROC curves of fire hazard and burn severity: for unburned (a), low burn severity (b), moderate burn severity (c), high burn severity (d), and moderate to high burn severity (e).

Multinomial logistic regression was used to further evaluate the ability for fire hazard to predict burn severity levels. Multinomial logistic regression estimates $k-1$ models, where k in this instance is the level of burn severity. In Table 17 unburned is treated as the referent group which low, moderate and high are estimated relative to. The positive odds ratios and estimates for fire hazard indicate that as fire hazard increases the odds of predicting high, moderate or low burn severity instead of unburned increase.

Table 17. Multinomial logistic regression with unburned as reference group.

Burn Severity	Term	Estimate	Std Error	Chi Square	<i>p</i>	Odds Ratio
High	Intercept					
	t	-5.027	0.490	105.450	<.0001	2.020
Moderate	Fire Hazard	11.301	0.993	129.420	<.0001	
	Intercept					
Low	t	-4.794	0.508	88.890	<.0001	1.386
	Fire Hazard	10.339	1.029	100.890	<.0001	
	Intercept					
	t	-3.684	0.473	60.680	<.0001	1.625
	Fire Hazard	8.426	0.973	74.930	<.0001	

3.4 Comparison of proposed model to other models in the literature

In addition to customized model, three other fire hazard models were generated. The HFI, FRI, SFI are models which have been used to successfully estimate fire hazard in previous studies (Chuvieco and Congalton, 1989; Erten, Kurgun and Musaoglu, 2004; Siachalou et al. 2009; Adab, Kanniah and Solaimani, 2013). The relationship of these models and burn severity has not fully been explored. To compare these models to the model presented in this paper, logistic regression was used to determine if the fire hazards estimated by the HFI, FRI and SFI performed better than the proposed fire hazard model. Each index was individually compared to the five burn severity categories previously outlined. (Figures 6 and 7).

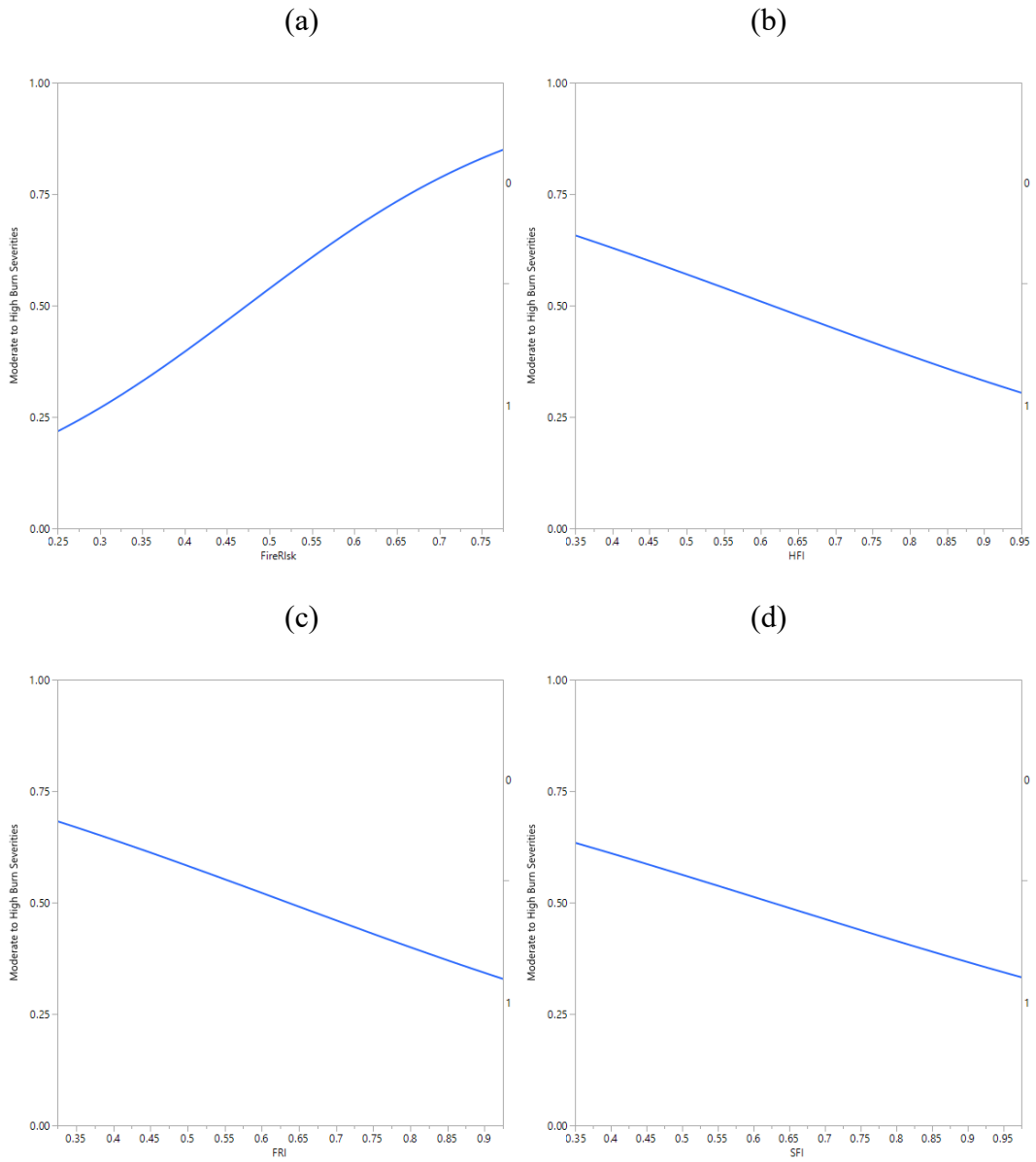


Figure 6. Moderate to high burn severity logistic regression results: for the proposed model (a), the HFI (b), the FRI (c), and the SFI (d).

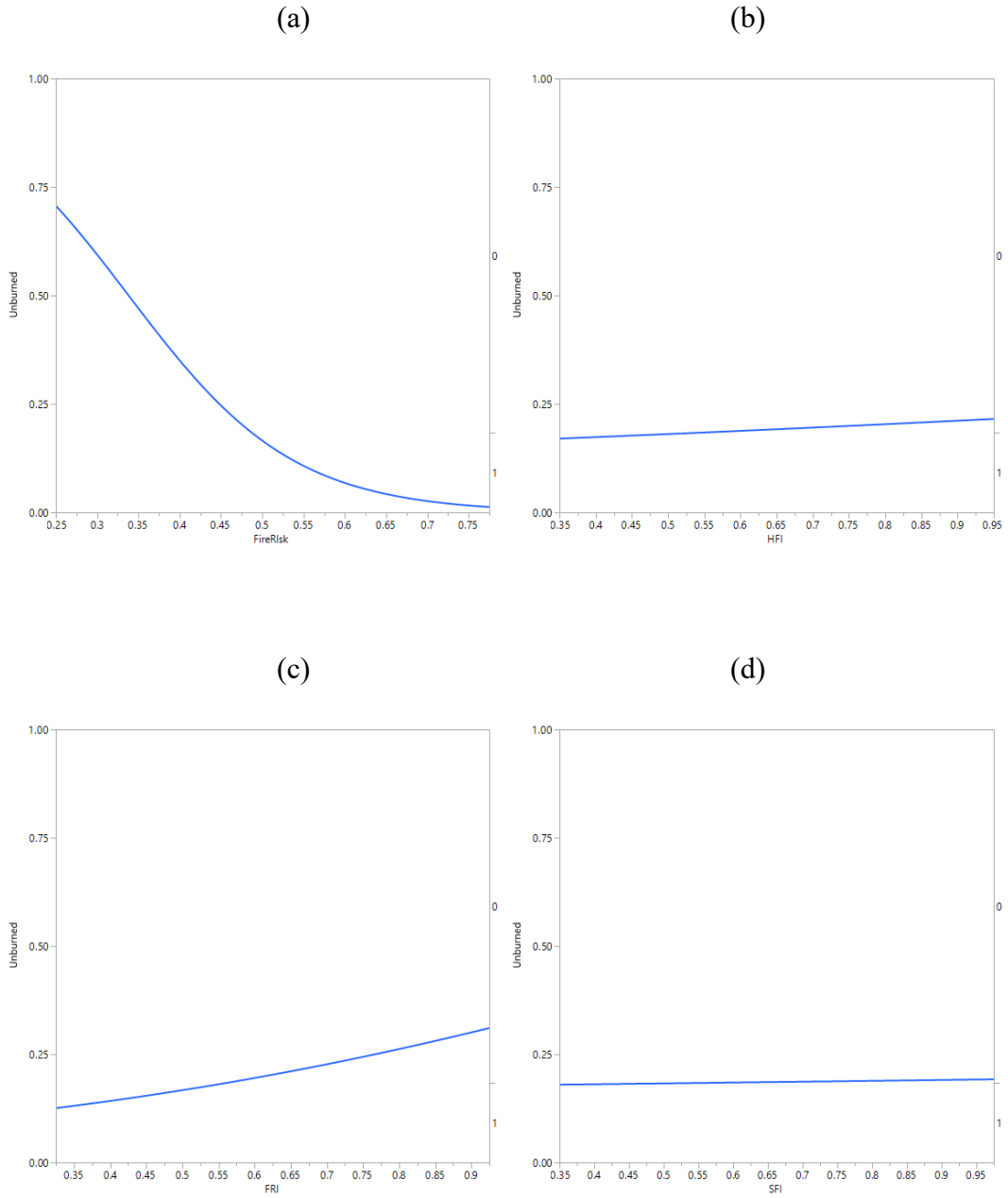


Figure 7. Unburned logistic regression results: for the proposed model (a), the HFI (b), the FRI (c), and the SFI (d).

Logistic regression results indicate that a predictive relationship between burn severity and fire hazard does not exist for any of the other fire hazard models. While

other models do possess significant p -values for some burn severity categories, the relationship is weak, and in the case of moderate to high burn severities the relationship is the inverse of what would be expected (i.e. higher hazards are less likely to predict moderate to high severity burns). This suggests that the proposed model is the best suited model for determining the hazard of moderate to high severity burns in the event of a wildfire, and for predicting burn severity in general.

Fire hazard indices are generally used to identify areas where an ignition event is most likely to occur. Because of this, the proposed model's hazards for the first identified fire perimeter for the Berry Fire were compared to the hazards for the other three indices. The categorical fire hazards for the proposed model, SFI, FRI, and HFI pixels located in the initial Berry Fire perimeter (July 27th) can be seen in Figure 8. The proposed model was the only model which had high and extreme pixels located within the initial fire perimeter. For the Berry Fire as a whole, the proposed model possessed a greater number of pixels identified as being at high or extreme hazard than the other fire indices (Figure 9).

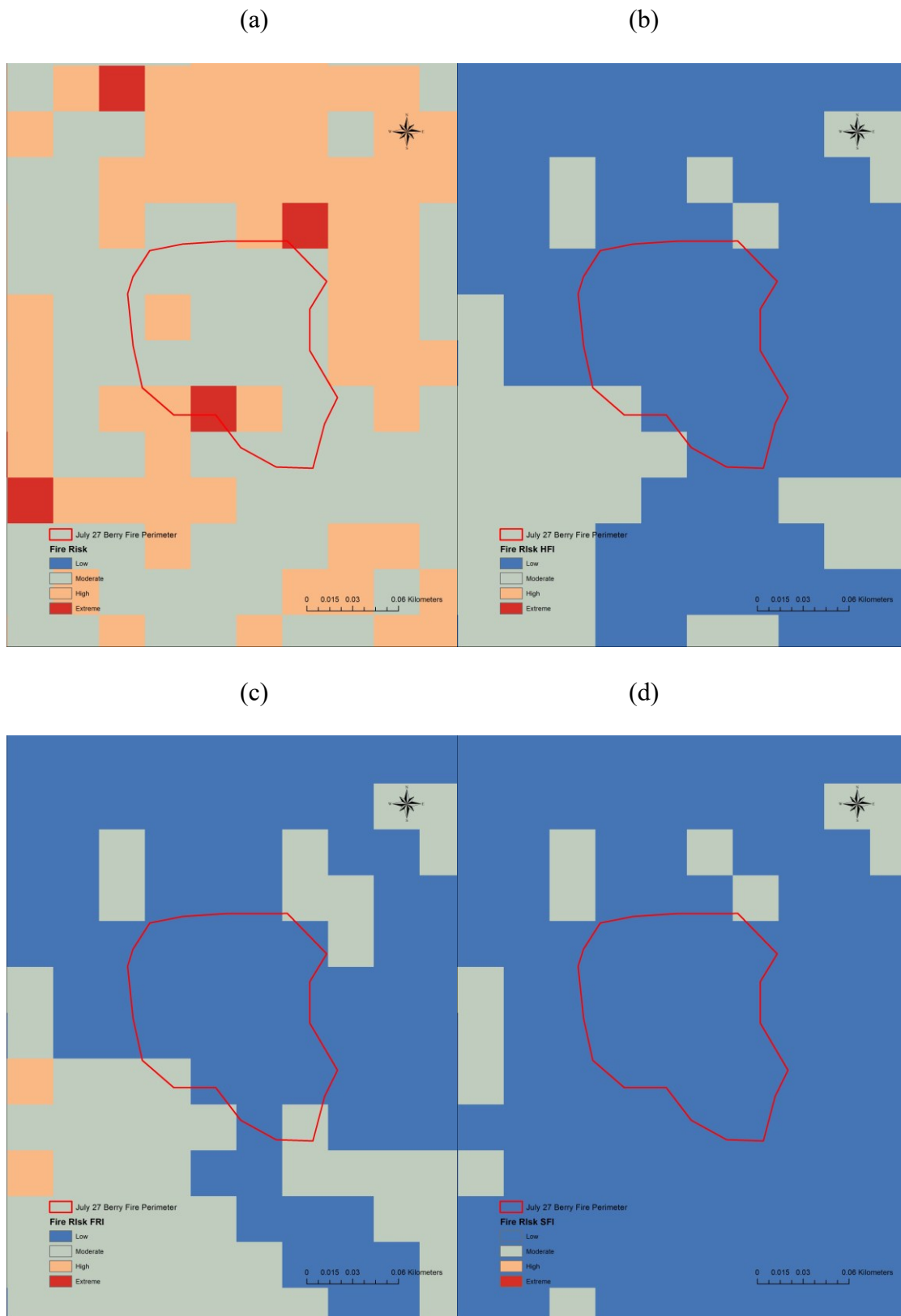


Figure 8. Fire hazards for initial Berry Fire perimeter (July 27th, 2016). The top left

figure is the proposed model (a), (b) is the HFI, (c) is the FRI, and (d) is the SFI.

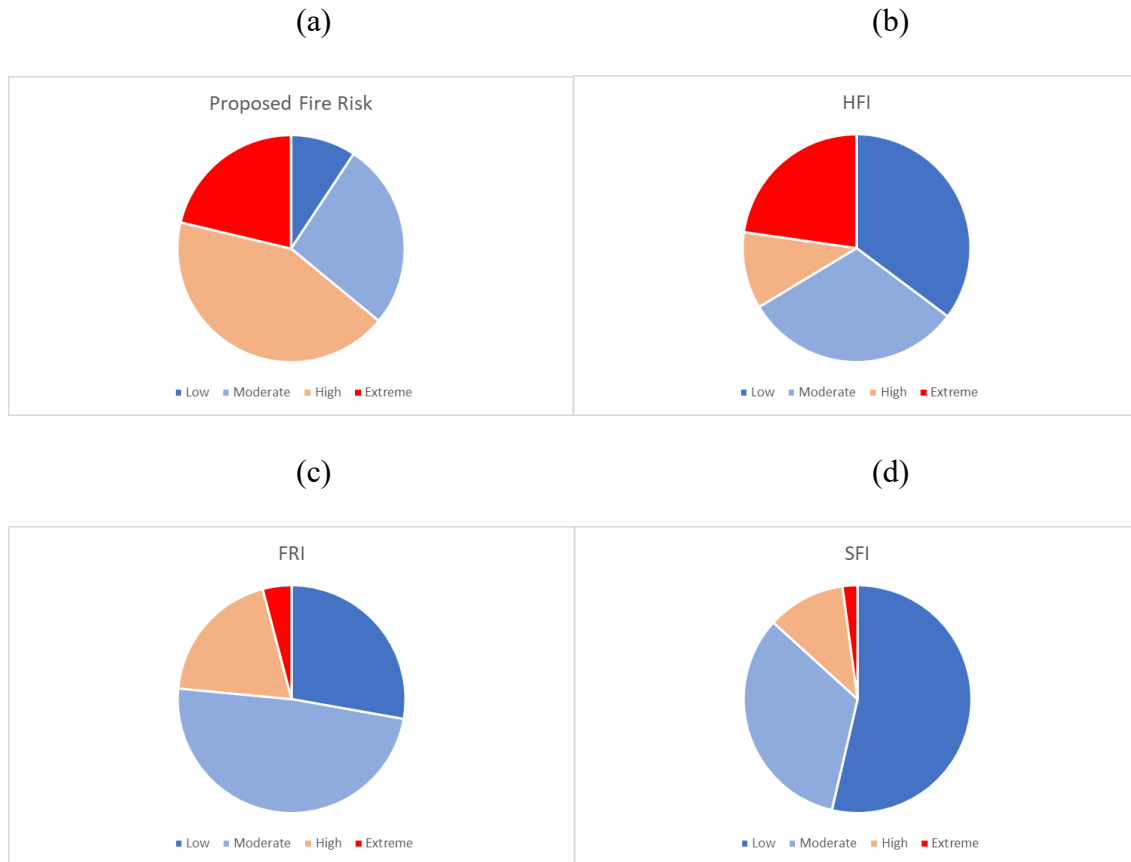


Figure 9. Proportion of pixels belonging to each fire hazard category: for the proposed model (a), HFI (b), FRI (c), and SFI (d).

I. Discussion

The proposed model identified areas of extreme fire hazard throughout Grand Teton National Park using a MCE based on fuel type, canopy cover, moisture conditions, topography, and infrastructure. Most MCE based fire hazard indices use similar variables, but do not include fuel type/canopy cover in their assessment of hazard (Chuvieco and Congalton, 1989; Jaiswal et al., 2002; Adab, Kanniah and Solaimani, 2013). The

inclusion of fuel data was expected to increase the accuracy of fire hazard estimates, creating a more robust model. The results indicate that the addition of fuel created a fire hazard model which more accurately estimates hazard of an ignition event, the measure generally used to assess the performance of fire hazard models (Adab, Kanniah and Solaimani, 2013). Additionally, the proposed model exhibits a stronger relationship with the resulting burn severity than the other fire hazard models tested in this paper, however, this relationship is rather weak. This is due to the other fire hazard models not being designed for predicting burn severity but instead for determining hazard of ignition (Chuvieco and Congalton, 1989; Adab, Kanniah and Solaimani, 2013).

Concentrations of high fire hazard estimates were most prominent in the northern and northwestern sections of the park but were also found on the eastern side of Jackson Lake in the southwestern mountain valleys. The primary fuel type for the high hazard areas in the northern and northwestern section of the park is Timber Understory 5 which according to Scott and Burgan (2005) consists of “very high load, dry climate timber-shrub”. Additionally, this area has many sections of moderate to steep slopes, which can increase the hazard of fire spread (Viegas, 2004; Butler, Anderson and Catchpole, 2007). The relative moisture content, estimated using NDMI, was moderate to very low for much of the area made up by the TU5 fuel category, which increased the fire hazard values. Proximity to roads and building increased fire hazard for the northern section of the park, whereas proximity to trails increased fire hazard for the northwestern section. Elevation increased fire hazard in the northern section but Aspect only minimally affected the fire hazard of this area.

The high fire hazard concentration to the east of Jackson Lake can be attributed to

the fuel composition and high canopy cover of this area. The Timber Understory 5, Timber Litter 3 and Timber Litter 4 fuel types are mixed throughout the areas of high fire hazard in this eastern area. The Timber Litter 3 and 4 fuel types consist of “moderate load conifer litter” and “small downed logs” respectively (Scott and Burgan 2005). The slopes of this area minimally influenced the resulting fire hazard due to the area being relatively flat. The NDMI for the TU5, TL3 and TL4 in this area were mostly moderate with some low moisture content pixels, generally increasing the fire hazard. The proximity to roads, trails and buildings all increased the fire hazard for this area. Elevation increased fire hazard in this area, whereas aspect minimally affected resulting fire hazard.

The southwestern concentration of high fire hazard results from a combination of canopy cover, TU5 fuel and moisture conditions. This area possesses higher hazard moisture conditions which increase the hazard of fire ignition and spread. Steep slopes and close proximity to trails also contribute to the higher fire hazard, whereas elevation, proximity to roads and proximity to buildings only minimally affected the fire hazard.

The major objective of this paper was to examine the relationship between fire hazard and burn severity. Based on the logistic regression results, the model’s fire hazard values possessed a moderate relationship with unburned and the broad burn severity category (i.e. moderate to high grouped together) but possessed a weak relationship with individual burn severity categories. This suggest that the proposed model can provide an indication of which areas are likely to experience moderate to severe burn severities but cannot predict the precise burn severity category for an area.

When compared to the HFI, SFI and FRI, the proposed model’s fire hazard values possess a stronger probability of estimating burn severity. Generally, these three fire

hazard models' values exhibited the opposite of the expected relationship to burn severity (i.e., lower hazard values having a higher probability for higher severity burns). Several factors can account for this including differences in data types (no fuel variable), and differences in weighting schemes. The relationship between fire hazard and burn severity was not explored in the papers that these fire hazard indices were proposed in as these models were designed for predicting ignition and spread (Chuvieco and Congalton, 1989; Erten, Kurgun and Musaoglu, 2004; Adab, Kanniah and Solaimani, 2013). However, the likelihood of ignition events is based upon variables which have been shown to influence burn severity (Butler, Anderson and Catchpole, 2007; Rollins, 2009; Prichard and Kennedy, 2014). Because of this, a stronger relationship with burn severity was expected.

Of the input variables, canopy cover and the fuel type possessed the strongest correlation with burn severity. This is consistent with studies which have found a significant but weak relationship between fuel/landscape structure and burn severity (Lee et al., 2009; Davies et al., 2015). This correlation between burn severity and fuel/canopy cover explains the stronger relationship between the proposed model's hazard values and resulting burn severity. The impact of including fuel characteristics into fire hazard assessments suggest that when fuel/vegetation data are available it is beneficial for these data to be included in fire hazard assessments. However, fuel data are limited for most of the world. Future research should examine if the inclusion of less robust, but easily generated fuel datasets improve fire hazard assessments to a similar degree as the LANDFFIRE fuel dataset has been shown to do. This would be beneficial for increasing the accuracy of fire hazard assessments in areas which do not already have available fuel data.

V. Conclusion

An approach for assessing fire hazard which integrates fuel type and canopy cover into a modification of the HFI outperformed other methods for assessing fire hazard. The proposed model better predicted the ignition of the 2016 Berry Fire and possessed a stronger relationship with burn severities. However, the relationship between fire hazard values and burn severity was only moderately strong for broad burn severity categories, and weak for individual burn severity categories. Additionally, as this research only examined a single wildfire event, further research examining more fires in the Greater Yellowstone Ecosystem as well as fires in other ecosystems need to be examined to better determine the relationship between fire hazard and burn severity. Future research should focus on the creation of models which better predict likelihood of ignition events and resulting burn severity. Additionally, future research should explore the ability of fuel datasets, generated for parts of the world which do not already have available fuel data, to increase the accuracy of fire hazard assessments.

III. Assessing Fire Effects in the Greater Yellowstone Ecosystem Using Burn

Ratios and Red-edge Spectral Indices

ABSTRACT: Burn severity is commonly assessed using Burn Ratios and field measurements to provide land managers with estimates on the degree of burning in an area. However, less commonly studied is the ability of spectral indices and Burn Ratios to estimate field measured fire effects. Past research has shown low correlations between fire effects and Landsat derived Burn Ratios, but with the launch of the Sentinel-2 constellation more spectral bands with finer spatial resolutions have become available. This paper explores the use of several red-edge based indices and Burn Ratios along side more ‘traditional’ spectral indices for predicting fire effects measured from the Maple and Berry fires in Wyoming, USA. The fire effects include ash depth, char depth, postfire dead lodgepole pine (*Pinus contorta*; PICO) density/stumps, mean basal diameter, cone density on dead postfire trees, coarse wood percent cover/volume/mass, percent cover ghost logs, and initial regeneration postfire PICO/aspen density. All-possible-models regression was used to determine the best models for estimating each fire effect. Models with satisfactory R^2 values were constructed for postfire dead PICO stumps (0.663), coarse wood percent cover (0.691), coarse wood volume (0.833), coarse wood mass (0.838), ash depth (0.636) and percent cover ghost logs (0.717). Red-edge based indices were included in all of the satisfactory models, which shows that the red-edge bands may be useful for measuring fire effects.

I. Introduction

Burn severity is an important measurement of the effect that a wildfire had upon a

landscape. Burn severity impacts vegetation mortality, soil nutrient composition, and causes increased runoff due to decreased infiltration resulting from soil hydrophobicity. The degree of burn severity can influence how long it takes for an ecosystem to recover and can change the composition of flora within an ecosystem. Because of these impacts, it is important for land managers to be able to assess the varying degrees of burn severity that result from fire events.

Burn severity can be measured differently depending on the interpretation of what it represents. Some studies have interpreted burn severity as a measurement of fire severity metrics and ecosystem responses (Keeley, 2009). Other researchers interpret burn severity solely as the loss of organic matter in or on the soil surface. The latter approach is used for Burned Area Emergency Response (BAER) assessments, which commonly use delta Normalized Burn Ratio (dNBR) to derive a burn severity map designated as the Burned Area Reflectance Classification (BARC). BARC maps generally provide adequate assessments of post-fire vegetation conditions and allow for rapid assessment of the immediate impacts of a fire event (Robichaud et al., 2007). BAER assessments commonly use the Composite Burn Index (CBI) for validation as it is heavily weighted towards the effects a fire has had on vegetation (Morgan et al., 2014).

Although commonly used, the CBI possesses a major limitation because it is based on ocular measurements as opposed to more quantitative field methods (Key and Benson, 2006). This is because of how difficult it can be to take a significant number of accurate quantitative field measurements for each wildfire to calibrate spectral indices. However, this can lead to different assessments of CBI depending on the individual performing the assessment. Other measurements of burn severity provide a quantitative assessment of the

level of burn severity, such as the amount of downed coarse wood, number of live trees per unit area, and ash depth.

The robustness of the dNBR index has come into question, with several studies suggesting that the index does not always provide accurate estimates and needs improvement (Epting, Verbyla and Sorbel, 2005; Roy, Keane and Trigg, 2006; Miller and Thode, 2007). Miller and Thode (2007) found that dNBR performs poorly for pixels containing sparse vegetation because of dNBR detecting absolute change. dNBR detects change through the use of the whole image and so a large change relative to the land cover within a given pixel may not be considered a large change in the context of the image as a whole. Different vegetation compositions affected by the same fire and possessing the same degree of burning can be assigned dissimilar dNBR values. To address this issue, RdNBR was proposed.

RdNBR is designed to assess the relative change instead of absolute change. This is accomplished with an additional step to the dNBR procedure in which the square root of the absolute value of the pre-fire NBR is used to calculate the quotient of dNBR. Miller and Thode (2007) found that RdNBR more accurately identified high severity burns in areas of heterogenous vegetation compositions. However, the proposed equation possessed its own issues, namely that the square root used to calculate RdNBR produces large, difficult to interpret numbers.

An alternative burn severity index was proposed by Parks, Dillon and Miller (2014) and named the revitalized burn ratio (RBR). This index replaces the square root and absolute functions with the addition of 1.001 to ensure all NBR values are greater than zero and altered in a way that preserves the level of NBR assigned to pixels. The RBR

provides an index that estimates relative change without altering the output to the degree that the square-root in RdNBR does.

Although most studies using remote sensing data for assessing burn severity use Burn Ratios based on NIR and shortwave infrared (SWIR) (Chuvieco, 2009), a proposed alternative to the Burn Ratios is to include land surface emissivity (LSE). The inclusion of LSE adds a surface characteristic separate from incoming solar radiation for the assessment of burn severity (Harris, Veraverbeke, Hook, 2007). Quintano et al. (2015) found that LSE-enhanced vegetation indices resulted in better burn severity estimates when compared to standard spectral indices, with an increase of about 16% when used to map burn severity in Sierra del Teleno, Spain. However, LSE-enhanced vegetation indices can be difficult to generate as they require the LSE and temperature to be differentiated from surface radiance and atmospheric conditions.

Spectral mixture analysis (SMA) has also been proposed as an alternative to the Burn Ratios. SMA is a technique which uses the spectral reflectance of the 'pure' spectral response of a land cover, referred to as endmembers, to determine the proportion of a mixed pixel belonging to different cover types. This is accomplished by using the endmembers to analyze a pixel and determine the degree to which the radiance from a mixed pixel agrees with each endmember (Gitas et al. 2012). Currently, SMA is not commonly used as a burn severity estimation technique. Studies that have compared spectral indices and SMA for estimating burn severity have shown the two approaches to be analogous (Robichaud et al., 2007; Veraverbeke and Hook, 2013). However, SMA has not been shown to consistently outperform dNBR, as seen in Veraverbeke and Hook (2013) which compared SMA to several spectral indices (NBR, dNBR, RdNBR) for burn

severity estimates. They found that dNBR outperformed SMA but also noted that both approaches performed adequately and that SMA has the benefit of providing transferable quantitative data which does not need field data for calibration.

Recently, the Sentinel-2 sensor system was launched by the European Space Agency (ESA). The system contains additional red-edge bands that facilitate the calculation of more indices which may be useful for burn severity estimates. Fernández-Manso et al. (2016) used Sentinel-2 imagery to calculate several red-edge indices, as well as several more 'traditional' spectral indices, for estimating burn severity. They found that two of the red-edge indices outperformed the other indices which were tested, showing the potential for red-edge indices to aid in the assessment of burn severity. However, the capabilities of the red-edge bands for assessing burn severity have not been fully explored and further research is needed.

Although most burn severity studies that use remote sensing to assess severity rely on field measured CBI (Epting, Verbyla and Sorbel, 2005; Roy, Boschetti and Trigg, 2006; Miller and Thode, 2007), few attempts have been published to determine which indices can be used for assessing more quantitative measurements of fire effects such as tree mortality by basal area and number of trees, char height and surface char. The CBI is useful for rapid ocular assessment of burn severity but is limited and may vary depending on the subjective judgement of the individual assessor in the field. Saberi and Harvey (forthcoming) found CBI estimates to correspond best to field measurements of tree canopy attributes but did not correspond as well to other field measurements like the deep char index. The authors suggest that spectral indices can be used to map CBI which in turn can be used to map various fire effects (particularly those related to tree canopy

attributes) using regression analysis. Hudak et al. (2007) attempted to relate several Landsat 5 TM derived burn indices to fire effects, finding that none of the indices were highly correlated with the fire effects.

The objective of this study is to test the ability of several indices for estimating field measured fire effects using Sentinel-2 imagery. Commonly used burn indices such as dNBR, RdNBR and RBR are calculated and compared to several red-edge indices to determine which index best estimates several measures of burn severity. In Fernández-Manso et al. (2016) only post fire indices were calculated, so this research aimed to determine the effectiveness of using the delta index from pre- and post-fire imagery as well as the post-fire indices. Additionally, alterations to the commonly used burn indices were made in which the narrow NIR band is replaced with a red-edge band to generate the indices and assess whether this substitution results in a more robust index. By testing a broad range of indices this paper seeks to determine the appropriate indices for estimating field measured fire effects for two fires in the Greater Yellowstone Ecosystem.

II. Methods

2.1 Study Area

The Greater Yellowstone Ecosystem is located in northwestern Wyoming and includes Yellowstone National Park, Grand Teton National Park, and their surrounding area (Figure 10). This study uses data collected from fires within Yellowstone National Park and Grand Teton National Park. Yellowstone National Park encompasses approximately 898,985ha of land including forests, mountains, and glacial lakes. The northwestern portion of the park experienced the Maple Fire in the summer of 2016. The Maple Fire was started on August 8th 2016 and burned until late October. The fire

affected approximately 18,383 ha of land (NPS, 2017).

Grand Teton National Park encompasses approximately 130,000 ha of land that includes forests, mountains, and glacial lakes. The northern section of Grand Teton National Park experienced a wildfire event in the late summer of 2016. The Berry Fire was discovered on July 25th 2016 and burned until early September of 2016. This fire affected approximately 8,750 ha of land in and around the national park, causing the closure of Highway 89/191/287.

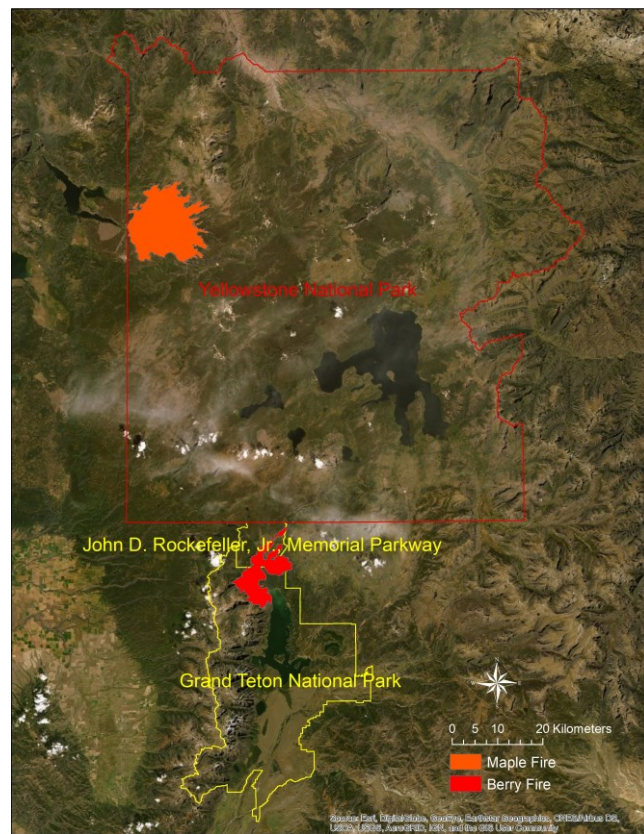


Figure 10. Study area within Greater Yellowstone Ecosystem including Yellowstone National Park and Grand Teton National Park.

2.2 Field Data

The field data used in this research was collected by Turner et al. (2019) in the summer of 2017. Turner et al. (2019) collected several quantitative measurements for the Berry and Maple fires in the Greater Yellowstone Ecosystem to examine the effects of reburns on lodgepole pine (*Pinus contorta*; PICO) forests (Figure 11). Burn severity measurements for twenty-seven field plots were quantified using circular subplots 30 m in diameter. The measurements collected within these plots included ash depth, char depth, postfire dead PICO density/stumps, mean basal diameter, cone density on dead postfire trees, coarse wood percent cover/volume/mass, percent cover ghost logs, and initial regeneration postfire PICO/aspen density (Table 18).

Table 18. Field measurement definitions and units of measurement.

Field Measurement	Definition	Unit of Measurement
Postfire Dead PICO Density	For plots that reburned, the density of fire-killed lodgepole pine trees	Number per hectare
Postfire Dead PICO Stumps	For plots that reburned, the density of stumps remaining for which the prefire lodgepole pine tree was completely combusted	Number per hectare
Mean Basal Diameter	The mean value from 25 measure live trees (in plots that did not reburn) or fire-killed trees or stumps (in reburned plots)	centimeters
Cone Density on Dead Postfire Trees	In plots that reburned, remaining identifiable cones on fire-killed lodgepole pine trees	Number per hectare
Coarse Wood Percent Cover	Percent of surface covered by downed coarse wood, estimated from line intercept	Cubic meters per hectare
Coarse Wood Volume	Volume of coarse wood estimated from Brown's planar intercept transects; in reburned plots, this is volume of wood remaining after the short-interval fire	Megagrams per hectare
Coarse Wood Mass	Mass of coarse wood estimated from Brown's planar intercept transects; in reburned plots, this is volume of wood remaining after the short-interval fire	Millimeters
Ash Depth	Where recent ash was visible, depth on soil surface	
Char Depth	If soil showed evidence of charring, depth from surface to which soil charring was evident	Millimeters
Percent Cover Ghost Logs	In reburned plots, areas of soil surface covered by log shadows where downed coarse wood had been combusted completely	Dimensionless
Initial Regeneration Postfire PICO Density	Density of first year seedlings of lodgepole pine	Number per hectare
Initial Regeneration Postfire Aspen Density	Density of aspen stumps that resprouted from surviving roots; if multiple leaders came from the same stump, it was scored as one.	Number per hectare

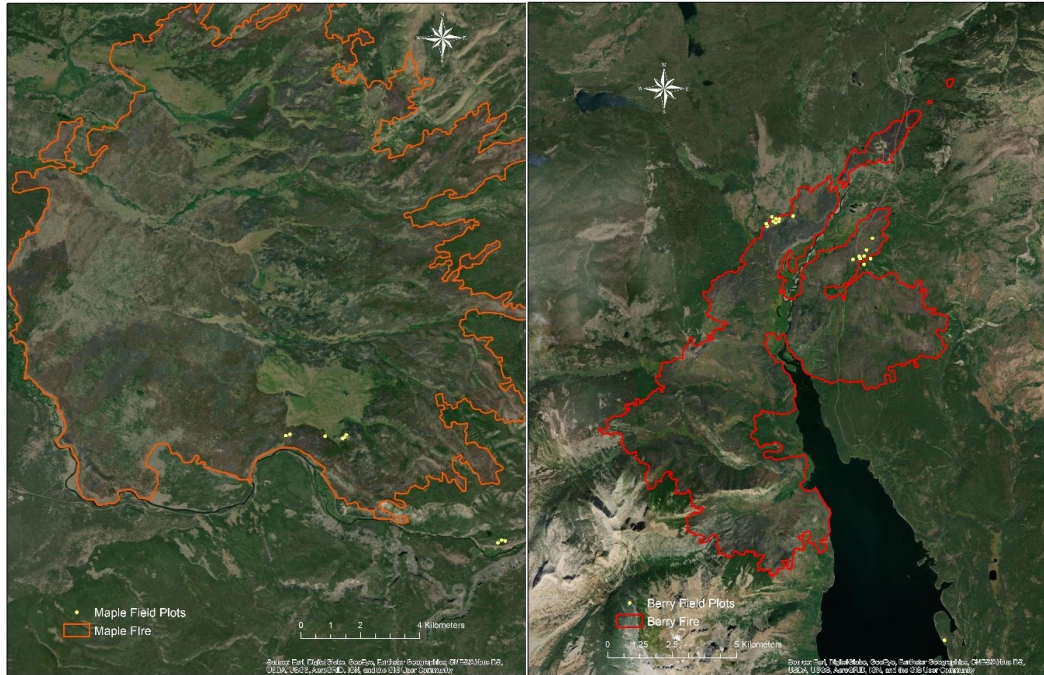


Figure 11. Locations of the twenty-seven field plots collected by Turner et al. (2019).

Plots are shown as yellow points for the Maple (left) and Berry (right) fires.

2.3 Image Preprocessing and Index Generation

Sentinel-2a data acquired on July 15th 2016 (pre-fire, Berry), November 22nd 2016 (post-fire, Berry), August 4th 2016 (pre-fire, Maple) and June 7th 2017 (post-fire, Maple) were downloaded from the ESA open access data hub (<https://scihub.copernicus.eu/dhus/#/home>) and from the USGS's EarthExplorer (<https://earthexplorer.usgs.gov/>). To ensure image pixel values were comparable, atmospheric corrections were performed using the Sen2Cor to convert the data to surface reflectance. Two images were needed to capture the extent of the Maple fire for August 4th and June 7th which were mosaiced together using nearest neighbor and most nadir seamline. For the Berry fire, the Monitoring Trends in Burn Severity's (MTBS) burned area shapefile was buffered by 6.5 km for use in this analysis, and for the Maple Fire a 2

km buffer was applied to the MTBS burned area shapefile for analysis. These buffers were used to ensure that the collected control plots fell within the image data for analysis. The reason for the variation in buffer size is the control plots for the Maple Fire were located within 2 km of the fire perimeter and the control plots for the Berry Fire were located within 6.5 km of the fire perimeter. The Berry and Maple fire images were then used to calculate several spectral indices (Table 19). Each of these indices were calculated for both the pre- and post-fire imagery and then the delta for each index was calculated by subtracting the post-fire image from the pre-fire image.

Table 19. List of indices generated for estimating burn severity.

Spectral Indices		Equation
NBR	Normalized Burn Ratio	$\frac{B8a - B12}{B8a + B12}$
NDVI	Normalized Difference Vegetation Index	$\frac{B8a - B4}{B8a + B4}$
GNDVI	Green Normalized Difference Vegetation Index	$\frac{B8a - B3}{B8a + B3}$
NDVIre1n	Normalized Difference Vegetation Index red-edge 1 narrow	$\frac{B8a - B5}{B8a + B5}$
NDVIre2n	Normalized Difference Vegetation Index red-edge 2 narrow	$\frac{B8a - B6}{B8a + B6}$
NDVIre3n	Normalized Difference Vegetation Index red-edge 3 narrow	$\frac{B8a - B7}{B8a + B7}$
PSRI	Plant Senescence Reflectance Index	$\frac{B4 - B3}{B6}$
Clre	Chlorophyll Index re-edge	$\frac{B7}{B1} - 1$
NDre1	Normalized Difference re-edge 1	$\frac{B6 - B5}{B6 + B5}$
NDre2	Normalized Difference red-edge 2	$\frac{B7 - B5}{B7 + B5}$
MSRren	Modified Simple Ratio red-edge narrow	$\frac{\left(\frac{B8a}{B5}\right) - 1}{\sqrt{(B8a/B5) + 1}}$

Additionally, RdNBR and RBR were calculated using the dNBR and $NBR_{prefire}$ (Equations 1 and 2). These indices were calculated using the narrow NIR band (8a) to calculate dNBR, as shown in table 19.

$$RdNBR = \frac{dNBR}{\sqrt{|NBR_{prefire}|}} \quad (1)$$

where dNBR was calculated using the difference between pre- and post-fire NBR.

$$RBR = \frac{dNBR}{NBR_{prefire} + 1.001} \quad (2)$$

Further, alternative red-edge based dNBRs, RdNBRs and RBRs were generated (three each) by replacing the narrow NIR band (0.8483 - 0.8813 μm) with Sentinel-2 bands five (0.6955 - 0.7134 μm), six (0.7312 - 0.7492 μm) and seven (0.7685 - 0.7965 μm). This was done to determine how accurately red-edge versions of dNBR, RdNBR and RBR estimated the various burn severity metrics. The red-edge is a region within the electromagnetic spectrum from 0.680 to 0.750 μm . The spectral response curve for healthy vegetation with high chlorophyll content will display a sharp increase in spectral reflectance in this region (Gitelson and Merzlyak, 1994). In the past, the lack of freely-available red-edge remote sensing data made it difficult to explore the potential for these wavelengths to enhance burn severity assessment. The resulting dNBR indices for Beery Fire study area can be seen in Figure 12.

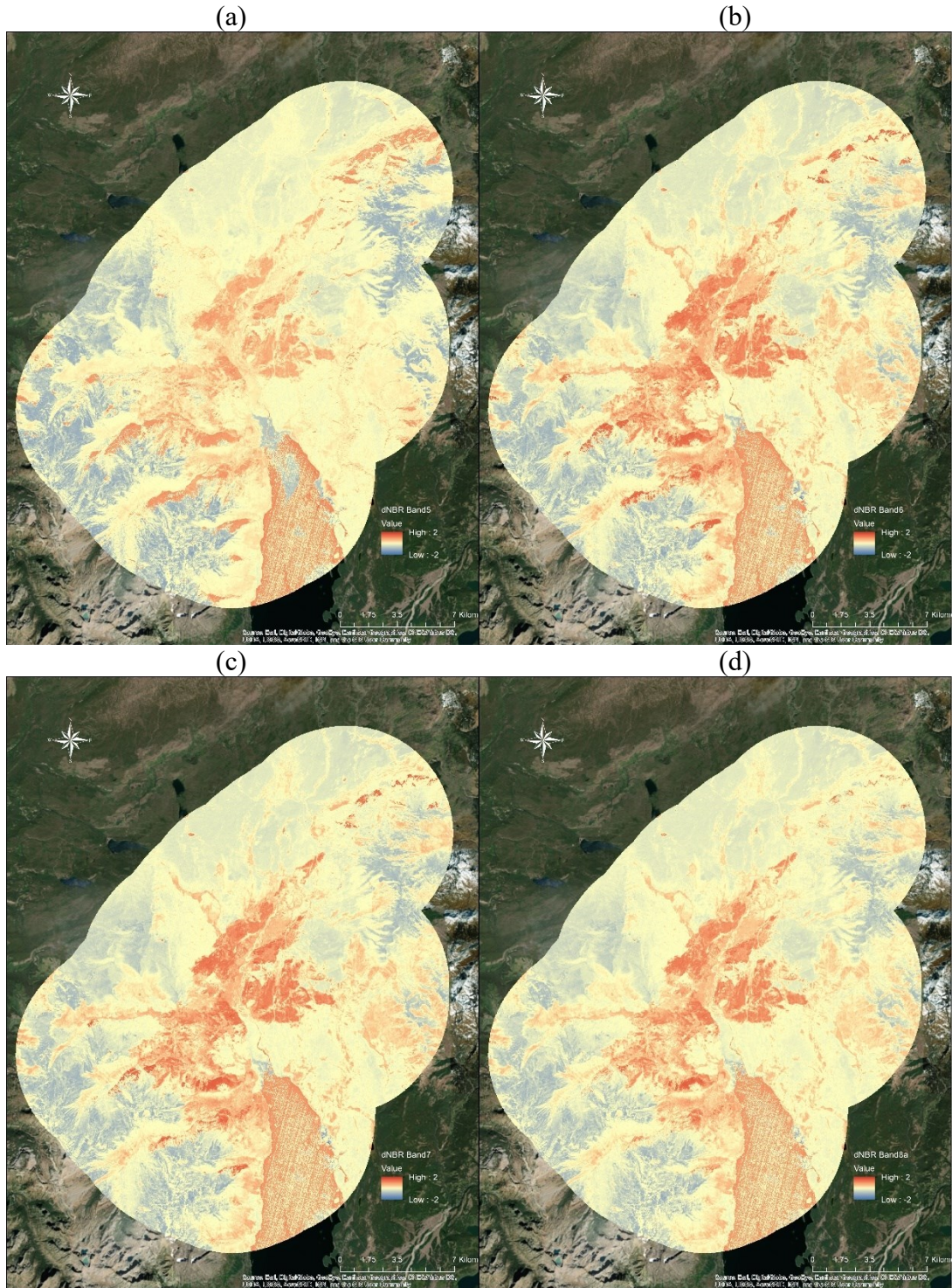


Figure 12. The dNBR index. Calculated using bands five (0.6955 - 0.7134 μm ; a), six (0.7312 - 0.7492 μm ; b), seven (0.7685 - 0.7965 μm ; c) and eight-a (0.8483 - 0.8813 μm ;

d). The symbology is stretched to a range of -2 to 2 so the indices can be more easily compared.

2.3 Analysis

The x, y locations for each field data point were entered into a GIS environment with the recorded field measurements as attributes. Next, a 30m buffer was applied to each plot point and zonal statistics were calculated to determine the mean value of pixels which fell within buffer. This was done because the field plots collected by Turner et al. (2019) were collected in 30 m circular plots, and so will encompass multiple 20 m Sentinel-2 pixels. By buffering and using zonal statistics the mean of these pixels can be extracted and this value will better correspond to the field measurements than using just the value of the pixel that plot centers fell into. Finally, the mean values for each index were extracted to these points. A correlation matrix was generated to determine if a relationship between the field measurements and the spectral indices exists. Finally, using all-possible-models regression, models for predicting the field measured burn severity metrics using the spectral indices were constructed. These models were validated using the prediction error sum of squares (PRESS) statistic, a form of leave-one-out cross-validation.

III. Results

3.1 Descriptive statistics for spectral indices

The spectral indices were generated for a 6.5 km buffered area around the Berry Fire and for the 2 km buffered area of the Maple Fire. Table 3 shows the descriptive statistics for each spectral index calculated for the Berry Fire grouped into five categories: postfire

normalized red-edge indices, difference normalized red-edge indices, difference normalized burn ratios, other burn ratios and other indices (n = 1,478,229 pixels). The non-burn ratio indices are defined in table 19. In table 20 the PF following the index acronym signifies post fire while the d before the index acronym signifies the result of the delta between pre- and post-fire imagery. For the burn ratios, the B# following the index signifies which red-edge band was used for NIR in the NBR equation. Table 4 shows the same breakdown of indices for the Maple Fire (n = 970,055 pixels). Note that the CLre, MSRren and PSRI indices are also red-edge indices which are not normalized and so are grouped under other indices, whereas the GNDVI indices are normalized but are not red-edge indices and so are also under other indices.

Table 20. Descriptive statistics for Berry Fire indices.

Index	Min	Max	Mean	Standard Deviation
<i>Postfire Normalized Red-edge Indices</i>				
NDre1_PF	-0.994	0.997	0.130	0.222
NDre2_PF	-0.994	0.998	0.154	0.244
NDVIre1n_PF	-0.996	0.998	0.178	0.264
NDVIre2n_PF	-0.986	0.993	0.060	0.109
NDVIre3n_PF	-0.987	0.992	0.031	0.078
<i>Difference Normalized Red-edge Indices</i>				
dNDre1	-1.202	1.805	0.025	0.152
dNDre2	-1.719	1.946	0.026	0.151
dNDVIre1n	-1.857	1.892	0.017	0.145
dNDVIre2n	-1.747	1.787	-0.011	0.094
dNDVIre3n	-1.886	1.798	-0.013	0.078
<i>Difference Normalized Burn Ratios</i>				
dNBR_B8a	-1.749	1.637	0.010	0.423
dNBR_B5	-1.798	1.666	-0.036	0.436

Table 20. Continued

dNBR_B6	-1.769	1.627	0.026	0.479
dNBR_B7	-1.736	1.693	0.030	0.460
<i>Other Burn Ratios</i>				
RdNBR_B8a	-73.309	32.330	-0.133	1.612
RdNBR_B5	-84.548	42.966	-0.318	2.002
RdNBR_B6	-68.660	48.944	-0.214	1.937
RdNBR_B7	-75.090	28.094	-0.148	1.765
RBR_B8a	-70.076	0.994	-0.014	0.442
RBR_B5	-198.320	0.996	-0.073	0.609
RBR_B6	-161.290	0.997	-0.021	0.657
RBR_B7	-159.930	0.997	-0.007	0.534
<i>Other Indices</i>				
GNDVI_PF	-0.997	0.999	0.270	0.436
PSRI_PF	-280.000	80.000	-2.107	17.112
MSRren_PF	-0.997	28.284	0.466	1.194
CLre_PF	-3836.000	3662.000	217.252	365.007
dGNDVI	-1.627	1.624	0.012	0.205
dPSRI	-295.300	279.860	1.944	17.172
dMSRren	-27.486	15.185	-0.081	1.048
dCLre	-2740.000	4979.000	297.265	523.168

Table 21. Descriptive statistics for Maple Fire indices.

Index	Min	Max	Mean	Standard Deviation
<i>Postfire Normalized Red-edge Indices</i>				
NDre1_PF	-0.829	0.947	0.168	0.138
NDre2_PF	-0.991	0.967	0.204	0.155
NDVIre1n_PF	-0.990	0.941	0.238	0.165
NDVIre2n_PF	-0.981	0.882	0.077	0.047
NDVIre3n_PF	-0.974	0.994	0.037	0.027
<i>Difference Normalized Red-edge Indices</i>				

Table 21. Continued

dNDre1	-0.912	0.708	0.049	0.123
dNDre2	-0.867	0.735	0.057	0.128
dNDVIre1n	-0.828	0.893	0.059	0.117
dNDVIre2n	-1.172	0.997	0.015	0.022
dNDVIre3n	-1.022	0.762	0.005	0.020
<i>Difference Normalized Burn Ratios</i>				
dNBR_B8a	-0.888	1.229	0.159	0.294
dNBR_B5	-1.207	0.938	0.072	0.181
dNBR_B6	-1.028	1.260	0.140	0.301
dNBR_B7	-0.969	1.268	0.154	0.306
<i>Other Burn Ratios</i>				
RdNBR_B8a	-59.367	18.309	0.248	0.652
RdNBR_B5	-15.804	23.850	0.352	1.120
RdNBR_B6	-45.937	26.669	0.275	0.994
RdNBR_B7	-56.675	23.814	0.257	0.827
RBR_B8a	-7.268	0.985	0.114	0.214
RBR_B5	-1.747	0.983	0.076	0.196
RBR_B6	-69.379	0.852	0.106	0.259
RBR_B7	-53.673	0.989	0.112	0.243
<i>Other Indices</i>				
GNDVI_PF	-0.985	0.995	0.409	0.250
PSRI_PF	-9.818	1.238	0.053	0.087
MSRren_PF	-0.993	5.488	0.423	0.319
CLre_PF	-1447.000	4516.000	556.645	540.477
dGNDVI	-0.717	1.349	0.058	0.113
dPSRI	-1.211	13.981	-0.014	0.097
dMSRren	-5.318	1.423	0.130	0.262
dCLre	-1447.000	13.981	-0.014	0.097

3.2 Correlation Results

To determine whether the indices and field measurements were related, Pearson correlations between the field measurement and spectral indices were assessed (Table 22; $n = 27$). Coarse wood percent cover and coarse wood mass were correlated with the most indices, with each field measurement possessing strong correlations with twenty-two spectral indices. Other field measurements which possessed strong correlations with spectral indices were postfire dead PICO stumps, ash depth, coarse wood volume and percent cover ghost logs.

Coarse wood mass possessed the strongest positive relationship with a spectral index, with NDre2_PF having a correlation of 0.886. The NDre2_PF index also possessed a strong positive correlation with coarse wood percent cover and coarse wood volume. Coarse wood mass also possessed the strongest negative correlation, possessing a correlation of -0.811 with both dNDre2 and GNDVI_PF.

The dNDre2_PF was significantly related to the most field measurements, with six field measured fire effects being strongly correlated with this index. The RdNBR_B8a index was significantly related to only one field measurements, coarse wood percent cover. Several indices were found not to possess strong correlations with any field measurements, including dPSRI, dNDVIre2n, dNDVIre3n, NDVIre2n_PF, NDVIre3n_PF and RdNBR_B5.

Table 22. Correlations between field measurements and spectral indices. Strong positive ($r \geq 0.60$) correlations are highlighted in green and strong negative correlations ($r \leq -0.60$) are highlighted in red.

Index	Postfire dead PICO Density	Postfire dead PICO Stumps	Mean Basal Diameter	Postfire Cone Density	Coarse Wood Percent	Coarse Wood Volume	Coarse Wood Mass	Ash Depth	Char Depth	Percent cover Ghost Logs	Initial Regen PICO	Initial Regen Aspen
dClre_Avg	0.294	0.358	-0.167	0.443	-0.669	-0.551	-0.617	0.674	0.227	0.518	0.274	0.346
dPSRI_Avg	-0.170	-0.078	0.001	-0.295	0.529	0.367	0.438	-0.515	-0.440	-0.387	-0.038	-0.328
MSRren_AVG	0.283	0.636	-0.417	0.345	-0.636	-0.754	-0.742	0.572	-0.195	0.491	0.484	0.094
NDre1_Avg	0.352	0.565	-0.354	0.462	-0.756	-0.765	-0.798	0.696	0.088	0.581	0.414	0.190
NDre2_AVG	0.346	0.658	-0.428	0.418	-0.752	-0.793	-0.811	0.697	-0.021	0.580	0.450	0.139
NDVlr1n_A	0.291	0.726	-0.481	0.291	-0.657	-0.777	-0.763	0.626	-0.160	0.552	0.460	0.065
NDVlr2n_A	-0.139	0.228	-0.183	-0.326	0.243	0.037	0.126	-0.194	-0.477	-0.111	0.070	-0.240
NDVlr3n_A	-0.040	0.344	-0.537	-0.172	-0.057	-0.430	-0.354	0.107	-0.315	0.201	0.131	-0.005
CLre_PF_Avg	-0.316	-0.347	0.204	-0.379	0.671	0.587	0.658	-0.673	-0.281	-0.587	-0.260	-0.286
PSRI_PF_AVG	0.142	0.018	0.034	0.263	-0.499	-0.337	-0.413	0.469	0.472	0.371	0.001	0.318
MSR_PF_AVG	-0.145	-0.623	0.524	-0.026	0.650	0.808	0.776	-0.485	0.185	-0.580	-0.331	-0.120
NDre1_PF_AVG	-0.258	-0.557	0.431	-0.257	0.821	0.855	0.883	-0.668	-0.139	-0.688	-0.312	-0.212
NDre2_PF_AVG	-0.235	-0.658	0.522	-0.174	0.805	0.879	0.886	-0.649	0.001	-0.686	-0.337	-0.162
NDVlr1_PF_A	-0.167	-0.707	0.570	-0.022	0.671	0.826	0.798	-0.548	0.153	-0.630	-0.330	-0.085
NDVlr2_PF_A	0.133	-0.280	0.259	0.367	-0.172	0.035	-0.059	0.153	0.485	0.038	-0.062	0.181
NDVlr3_PF_AVG	0.168	-0.162	0.147	0.375	-0.260	-0.042	-0.137	0.230	0.431	0.089	-0.020	0.161
dNBR_B5_AVG	0.415	0.326	-0.277	0.551	-0.612	-0.569	-0.641	0.667	0.290	0.443	0.372	0.195
dNBR_B6_AVG	0.418	0.358	-0.299	0.539	-0.626	-0.589	-0.656	0.683	0.238	0.477	0.359	0.230
dNBR_B7_AVG	0.412	0.385	-0.293	0.549	-0.641	-0.600	-0.667	0.687	0.266	0.484	0.380	0.197
dNBR_8a_AVG	0.417	0.414	-0.319	0.547	-0.644	-0.619	-0.682	0.703	0.257	0.499	0.397	0.190
RBR_B5_AVG	0.388	0.272	-0.249	0.519	-0.610	-0.552	-0.626	0.650	0.333	0.463	0.325	0.346
RBR_B6_AVG	0.382	0.334	-0.278	0.501	-0.658	-0.603	-0.671	0.678	0.314	0.520	0.274	-0.328
RBR_B7_AVG	0.387	0.356	-0.294	0.501	-0.660	-0.608	-0.675	0.688	0.306	0.518	-0.038	0.094
RBR_8a_AVG	0.396	0.390	-0.322	0.503	-0.663	-0.630	-0.693	0.706	0.293	-0.387	0.484	0.190
RdNBR_B5_AVG	0.383	0.326	-0.180	0.520	-0.425	-0.414	-0.479	0.468	0.227	0.491	0.414	0.139
RdNBR_B6_AVG	0.208	0.172	-0.253	0.273	-0.615	-0.554	-0.614	0.674	-0.440	0.581	0.450	0.065

Table 22. Continued

RdNBR_B7_AVG	0.228	0.205	-0.250	0.296	-0.673	-0.584	-0.617	-0.515	-0.195	0.580	0.460	-0.240
RdNBR_8a_AVG	0.353	0.349	-0.325	0.441	-0.687	-0.551	0.438	0.572	0.088	0.552	0.070	-0.005
GNDVI_AVG	0.237	0.709	-0.541	0.124	-0.669	0.367	-0.742	0.696	-0.021	-0.111	0.131	-0.286
NDVI_AVG	0.357	0.705	-0.479	0.443	0.529	-0.754	-0.798	0.697	-0.160	0.201	-0.260	0.318
GNDVI_PF_AVG	-0.131	-0.673	-0.167	-0.295	-0.636	-0.765	-0.811	0.626	-0.477	-0.587	0.001	-0.120

3.3 Regression Results

Within the statistical analysis software JMP, all-possible-models was used to construct models for predicting field measurements using the spectral indices. With a sample size of twenty-seven field plots a maximum of three dependent variables were allowed for model construction. Each model was assessed based on the significance of its independent variables and on the variable multicollinearity. The p-value of each model covariate had to be less than 0.05 for the model to be accepted. Multicollinearity was assessed using the Variance Inflation Factor (VIF), where all input variables had to possess VIF values of < 10 . The models for one, two, and three input variables which met these criteria and possessed the highest R^2 for a given field measurement are reported in Table 23.

Of the field measurements, coarse postfire dead PICO stumps, coarse wood percent cover, coarse wood volume, coarse wood mass, ash depth and percent cover ghost logs possessed models with R^2 s above 0.6. Of these coarse wood mass achieved the highest R^2 (0.847) followed by Coarse wood volume ($R^2 = 0.833$). Ash depth possessed the lowest R^2 (0.636) with postfire dead PICO stumps possessing the second lowest ($R^2 = 0.663$) of the variables with R^2 s greater than 0.6.

Of the single variable models, Coarse wood volume possessed the highest R^2 (0.784) with NDre2_PF as the input variable. The single variable model for postfire dead PICO density performed the worst with an R^2 of 0.174 when dNBR_B6 is used as the input variable. For two variable models coarse wood mass performed the best with an R^2 of 0.847 and initial regeneration postfire aspen density performed the worst with an R^2 of 0.249. Of the three variable models, coarse wood mass possessed the highest R^2 (0.847)

whereas initial regeneration postfire aspen density had the lowest R^2 (0.448). Several field measurements did not have any models which met the p-value and/or VIF criteria and so the variables are reported as none and the statistics as N/A.

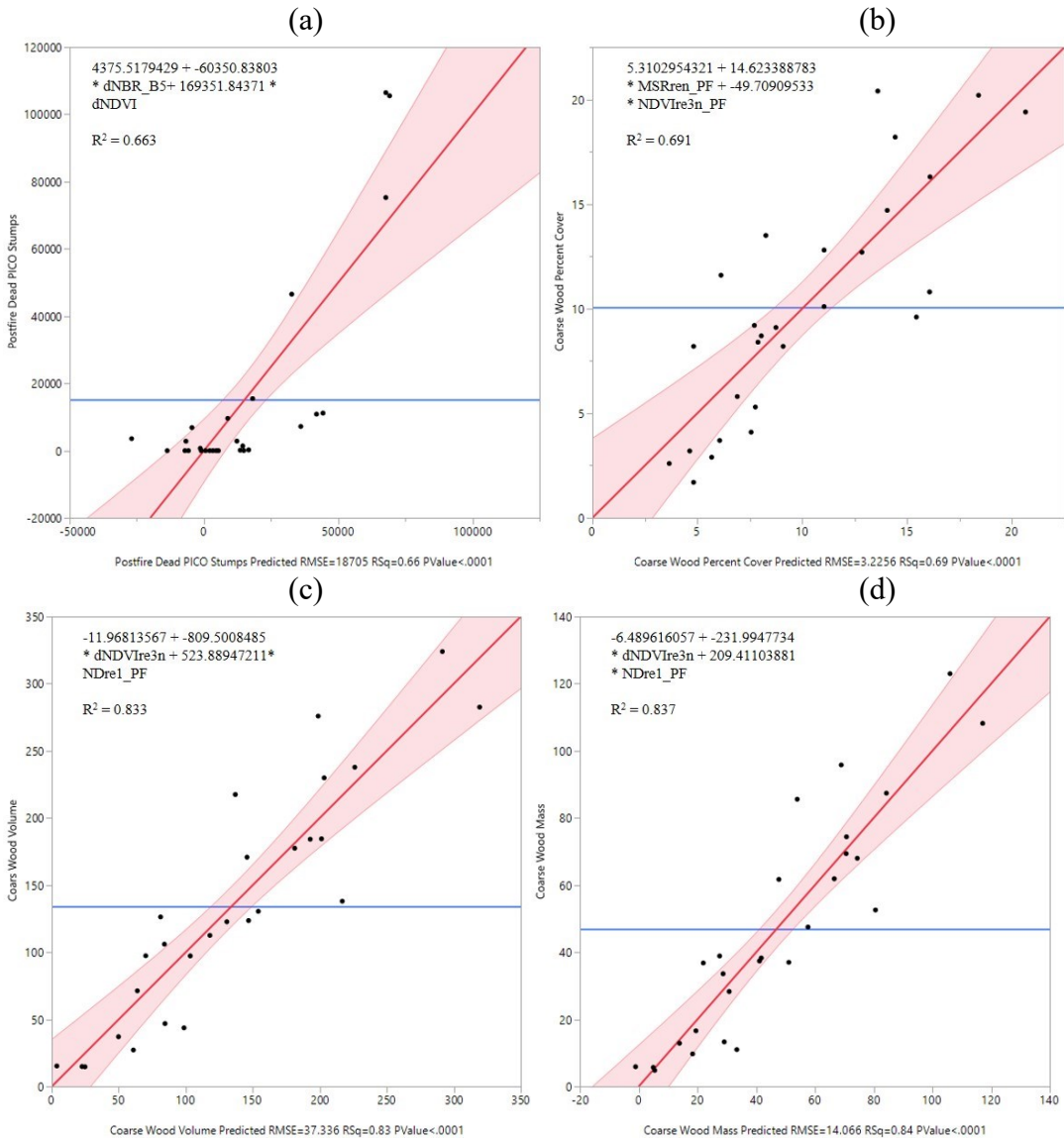
Table 23. Results from all-possible-models regression. Models with moderately strong models ($0.6 < R^2s < 0.7$) are highlighted in yellow while models ($0.70 < R^2$) are highlighted in green.

Field Measurement	Model Variables	R^2	RMSE	PRESS R^2	PRESS RMSE
Postfire Dead PICO Density	dNBR_B6	0.174	16859.88	0.066	17255.543
Postfire Dead PICO Density	None	N/A	N/A	N/A	N/A
Postfire Dead PICO Density	None	N/A	N/A	N/A	N/A
Postfire Dead PICO Stumps	dNDVIre1n	0.527	21687.91	0.383	23854.682
Postfire Dead PICO Stumps	dNBR_B5, dNDVI	0.663	18705.19	0.502	21414.479
Postfire Dead PICO Stumps	None	N/A	N/A	N/A	N/A
Mean Basal Diameter	GNDVI_PF	0.349	2.542	0.248	2.629
Mean Basal Diameter	dNDVIre3n, NDre2_PF	0.440	2.406	0.2853	2.562
Mean Basal Diameter	None	N/A	N/A	N/A	N/A
Cone Density on Dead Postfire Trees	dNBR_B5	.304	75553.4	0.184	78703.305
Cone Density on Dead Postfire Trees	dNDre2, NDVIre1n_PF	0.419	70417.16	0.2411	75900.966
Cone Density on Dead Postfire Trees	dPSRI, dMSRren, NDVIre2n_PF	0.571	61865.44	0.333	71184.947
Coarse Wood Percent Cover	NDre1_PF	0.674	3.244	0.620	3.370
Coarse Wood Percent Cover	MSRren_PF, dNDVIre3n	0.691	3.226	.627	3.341
Coarse Wood Percent Cover	None	N/A	N/A	N/A	N/A

Table 23. Continued

Coarse Wood Volume	NDre2_PF	0.773	42.735	0.7403	43.944
Coarse Wood Volume	dNDVIre3n, NDre1_PF	0.833	37.336	0.782	40.229
Coarse Wood Volume	None	N/A	N/A	N/A	N/A
Coarse Wood Mass	NDre2_PF	0.784	15.878	0.753	16.367
Coarse Wood Mass	dNDVIre3n, NDre1_PF	0.838	14.066	0.787	15.175
Coarse Wood Mass	dNDVIre3n, NDre2_PF, NDVIre2n_PF	0.842	14.157	.770	15.776
Ash Depth	dNDVI	0.548	3.455	0.493	3.520
Ash Depth	dCLre, dNDVIre3n	0.581	3.396	0.486	3.543
Ash Depth	dPSRI, dNDVIre2n, dNBR_B5	0.636	3.233	.392	3.853
Char Depth	NDVIre2n_PF	0.235	0.177	-0.008	0.195
Char Depth	dNDre2, RBR_B8a	0.328	0.169	0.148	0.179
Char Depth	None	N/A	N/A	N/A	N/A
Percent Cover Ghost Logs	NDre1_PF	0.473	2.430	0.361	2.574
Percent Cover Ghost Logs	NDVIre1n_PF, RdNBR_B5	0.587	2.194	.421	2.450
Percent Cover Ghost Logs	dNDre2, NDVIre1n_PF, RdNBR_B5	0.717	1.855	0.574	2.100
Initial Regeneration Postfire PICO Density	dMSRren	0.234	8440.969	0.030	9140.458
Initial Regeneration Postfire PICO Density	RBR_B6, PSRI_PF	0.328	8071.69	0.078	8915.812
Initial Regeneration Postfire PICO Density	None	N/A	N/A	N/A	N/A
Initial Regeneration Postfire Aspen Density	None	N/A	N/A	N/A	N/A
Initial Regeneration Postfire Aspen Density	MSRren_PF, GNDVI_PF	0.249	81.299	0.037	86.791
Initial Regeneration Postfire Aspen Density	dCLre, dNDVIer3n, dNDVI	0.448	71.177	0.224	77.933

The PRESS statistic was used to determine which of the models generated for each field measurement possessed the best predictive power. This statistic determines model performance by leaving one sample out at a time to determine how well the data predicts the left-out sample (Haaland and Thomas, 1988). The model with an $R^2 > 0.60$ which yielded the highest PRESS R^2 for each field measurement was determined to be the best model for predicting the field measured fire effect. Standard least squares was then used to plot these models and determine their corresponding prediction equation (Figure 4).



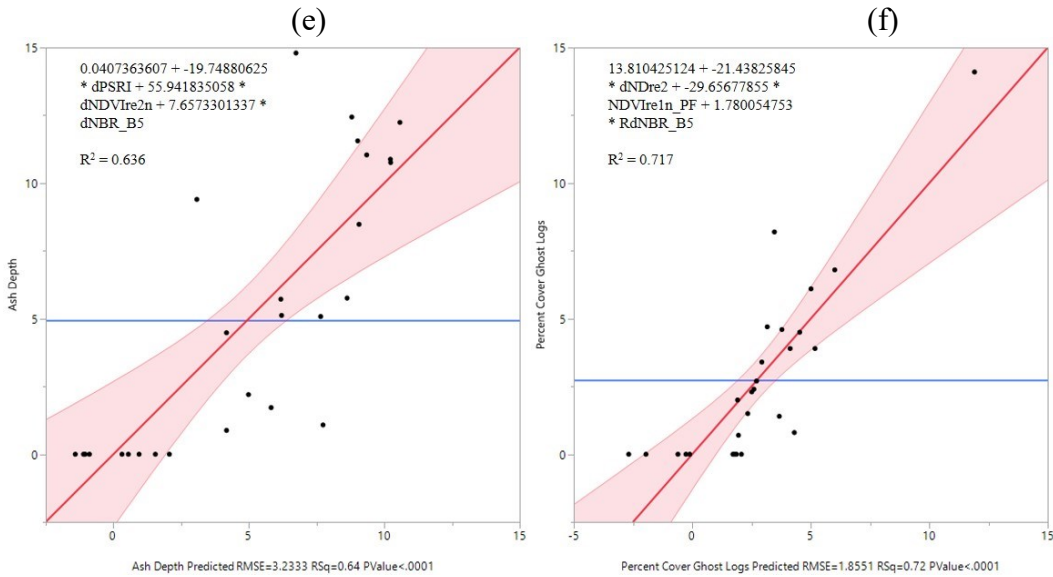


Figure 13. Standard least squares for models with best predictive capabilities. Models for postfire dead PICO stumps (a), coarse wood percent cover (b), coarse wood volume (c), coarse wood mass (d), ash depth (e) and percent cover ghost logs (f). The red line is the line of fit, the blue line is the mean line and the red buffer zone is the confidence interval.

Of the variables used to construct these models dNDVire3n, NDre1_PF and dNBR_B5 were the only indices used in more than one model. A total of three Burn Ratio indices were used across all the models whereas ten red-edge indices were used. Of the Burn Ratio indices, all the selected input variables for the models used red-edge bands in place of narrow NIR.

IV. Discussion

4.1 Correlations Between Spectral Indices and Field Measurements

When examining the correlation between the various spectral indices and the fire effects measurements, the strongest correlations were found to involve indices generated using band 5 for all field measurements. Of the red-edge indices, the only indices to possess strong correlations with field measurements not generated using band 5 were the CLre_PF and dCLre. Of the red-edge NDVI indices, both postfire and difference NDVIre1n outperformed their NDVIre2n and NDVIre3n counterparts. Previous research has reported similar findings, with red-edge indices generated closer using the band closest to red, band 5, outperforming the other red-edge indices as well as more traditional spectral indices for burn severity detection (Fernández-Manso, Fernández-Manso and Quintano 2016; Navarro et al. 2017).

4.2 Spectral Indices Ability to Estimate Field Measurements

Although many studies have estimated burn severity using spectral indices (Epting, Verbyla and Sorbel, 2005; Roy, Boschetti and Trigg, 2006; Miller and Thode, 2007), only a few have attempted to estimate field measured fire effects using these indices (Hudak et al., 2007; Verbyla and Lord, 2007; Lentile et al., 2009). Although field measured fire effects are not as commonly assessed because of the time intensive nature of these measurements, they provide valuable ecological information which can be used in fire recovery efforts. However, previous research has shown little relationship between Landsat derived burn indices and field measured fire effects (Hudak et al., 2007; Verbyla and Lord, 2007; Lentile et al., 2009). This can be attributed to a number of variables including the spatial resolution of Landsat images, the radiometric resolution of the sensors used during the time of these studies being inadequate to capture the slight

variations in radiance, and the lack of spectral bands in the red-edge region. Previous research has shown slight improvement in the performance of Sentinel-2 NBR-based indices when compared to Landsat 8 NBR-based indices (García-Llamas et al., 2019). However, this research was limited to indices which could be calculated by both sensor systems, which eliminates the use of red-edge indices. The results of this research suggest that several field measured fire effects can be estimated using the Sentinel-2 sensor constellation and the use of red-edge indices improved the Sentinel-2's performance of this task.

Of the fire effects estimated by the spectral indices, those related to tree canopy characteristics resulted in the best estimates. This agrees with the findings of Saberi and Harvey (forthcoming) who found that CBI and the three primary burn severity indices (dNBR, RdNBR, RBR) were more highly correlated with tree canopy fire effects than they were with other effects. Additionally, we found that the red-edge spectral indices explained approximately 64% of field-measured variation in ash depth and 72% of the variation in percent cover ghost logs.

Of the best performing models, coarse wood mass and coarse wood volume possessed the highest R^2 values, at 0.837 and 0.833 respectively. Both models were generated using the same red-edge indices, with neither of the models requiring a Burn Ratio index. These high accuracies combined with the use of solely red-edge indices suggest that further research into the utility of using red-edge indices for estimating and mapping various fire effects should be explored.

4.3 Performance of Red-edge Bands and Indices

With the launch of the Sentinel-2 sensor constellation, red-edge bands for index

generation have become freely available. Fernández-Manso, Fernández-Manso and Quintano (2016) show that red-edge indices can accurately discriminate between levels of burn severity and found that indices generated using Sentinel-2 band five were most suited for this task. Our results show that indices which were generated using band five were included in all six of the best performing models, suggesting agreement with other research (Chuvieco et al. 2006; Fernández-Manso, Fernández-Manso and Quintano 2016; Navarro et al. 2017).

Interestingly, of the best performing models only one contained a non-red edge index (percent dead PICO stumps). The two best performing models (coarse wood volume and mass) both only used red-edge indices, and both achieved $R^2 > 0.8$. The indices used in these models relied on bands 5, 7 and 8a. This suggests that red-edge indices, which have been shown promising results in estimating burn severity (Korets et al., 2010; Fernández-Manso, Fernández-Manso and Quintano 2016; Navarro et al. 2017), may also be useful for estimating fire effects.

4.4 Sources of Uncertainty

Although these results are promising, there are a few sources of uncertainty. The field measurements were collected for circular subplots 30m in diameter, but the spatial resolution of the Sentinel-2 data is 20m. We used the average of the pixels which fell in a 30m buffer to address this issue, but some of these pixels lay partially outside the buffer and other pixels were excluded because too small a proportion of these pixels fell within the buffer. This may lead to the spectral reflectance of the pixels corresponding to these measurements only partially representing the measured conditions and/or including reflectance from outside the buffer in the average.

Additionally, geolocation error between images can create uncertainty in index calculation and value to points extraction. For Sentinel-2 this error is less than 1 pixel in most cases, with errors exceeding this threshold primarily because of coarse corrections. No coarse corrections are documented for any of the images used in this analysis, however a single pixel error could potentially impact the results.

The use of samples from two separate fires is also a source of uncertainty. These fires started and ended around the same time (summer 2016 to fall 2016) and were both located in the Greater Yellowstone Ecosystem possessing similar vegetation and landcovers. However, different image acquisition dates and a more limited number of samples for the Maple Fire could create uncertainty in the results. However, because of the lack of snow cover in the November imagery and the evergreen forests which make up the majority of the in-scene vegetation for both fires we do not expect the difference in acquisition dates to considerably influence our results. After examining the residuals for the primary regression models it was noted that overall the two fires residuals were similarly distributed, except in the case of postfire dead PICO stumps where the upper end of the predicted values for the Maple Fire possessed larger negative and positive residuals than any residual for the Berry Fire. This can be explained by the limited sampling for both fires, which ideally would have at least thirty sample plots per fire. Because of this limited sample size, these results should be considered preliminary and further research should be conducted to determine their validity.

V. Conclusion

This study assessed the ability of spectral indices, both traditional and red-edge based, to estimate various field measured fire effects. Several fire effects were able to be

accurately estimated using a combination of red-edge and Burn Ratio indices and multivariate regression. These fire effects include postfire dead PICO stumps, coarse wood percent cover, coarse wood volume, coarse wood mass, ash depth and percent cover ghost logs. Of the indices generated the most useful for estimating these fire effects were red-edge indices especially those generated using Sentinel-2 band five.

This research shows that red-edge indices have potential for mapping various fire effects when used in combination. However, the field data used for this study has a limited sample size from a single ecosystem. Because of this, these results should be considered preliminary and require further research with more field data from other ecosystems to verify.

IV. BERRY FIRE VEGETATION RECOVERY

ABSTRACT: The monitoring of post-fire vegetation recovery provides important information which land managers can use to formulate recovery efforts for an ecosystem. This research attempts to assess vegetation recovery using fractional vegetation cover (FVC) derived from a combination of field plots, regression fitted spectral indices and multiple endmember spectral mixture analysis (MESMA). A total of sixty field plots were collected in the summer of 2019 in each of which eight downward and eight upward hemispherical photographs were taken. The FVC was then calculated for each photograph belonging to a plot within CAN-EYE from which the average FVC was calculated. Thirty-one of these plots were then used to derive the regression fits for the spectral indices, which were implemented using raster algebra. The resulting regression fit values were then compared to the remaining plots via linear regression to determine how accurately FVC was mapped. The MESMA, derived using three forest and three herbaceous endmembers, was compared to all sixty plots using linear regression. We found that of the spectral indices, an altered form of NDVI which uses Sentinel-2 band five performed the best, achieving an $R^2 = 0.69$. The MESMA results failed to achieve significance. Our findings are in line with similar fire-related research which compared indices generated using Sentinel-2 red-edge bands with more “traditional” indices and found that red-edge indices based on band five outperformed the other spectral indices. Future research should test if these red-edge indices increase the accuracy of recovery trajectories as well as if they outperform more “traditional” indices in other environments.

I. Introduction

Post-fire vegetation recovery monitoring provides important information to land managers on which areas are in need of intervention for recovering vegetation, which areas should be barred from access, and how much time is expected to elapse before an ecosystem has recovered. Vegetation monitoring also assists ecological and biological research in understanding and identifying patterns of recovery and what factors affect this process. This facilitates a greater understanding of the effects that vegetation types, geographic attributes, and land management practices have on post-fire vegetation recovery.

Post-fire vegetation recovery monitoring can be conducted either *in situ* with field measurements or via remote sensing. Field measurements usually involve some combination of optical estimates, photography, and the use of plots or transects to measure various vegetation attributes in an area (Gitas et al., 2012). As the area affected by a wildfire increases in size, performing these tasks becomes more burdensome. This makes remote sensing an attractive alternative since large areas can be monitored with greater efficiency. Remote sensing techniques for estimating vegetation recovery are grouped into three categories: (1) Image classification; (2) Vegetation indices (VIs); and (3) Spectral mixture analysis (SMA) (Gitas et al., 2012).

Image classification attempts to use spectral responses to determine the presence of healthy vegetation in individual pixels. Stueve et al. (2009) used supervised classification to identify patterns of alpine tree recovery in Mount Rainer National Park. This was accomplished using KH-4B imagery from the CORONA mission, a digital orthophoto quarter quadrangle (DOQQ) image, and a lidar derived DEM. The supervised classification method proved successful, which can be attributed to the very high spatial

resolution of the data used in this study. Results of other studies which use image classification to determine vegetation recovery have indicated that larger pixel sizes can lead to “salt and pepper” effects, which is seen as the primary limitation to this technique (Gitas et al., 2012). Recently, object-based image analysis (OBIA) has been introduced as an alternative to pixel-based classifications (supervised and unsupervised classification). Currently this approach is not widely used for vegetation recovery monitoring, however there are a few studies which have attempted to use it for this purpose (Mitri and Fiorucci, 2012; Mitri and Gitas, 2013; Polychronaki, Gitas and Minchella, 2014). Polychronaki, Gitas and Minchella (2014) used OBIA to map major land cover types for two fires on the Mediterranean island of Thasos. They were able to accurately map post-fire land cover types, achieving a Kappa coefficient of 0.84 and an overall accuracy of 90.5%.

VIs are the most commonly used vegetation recovery monitoring method (Gitas et al., 2012). To determine the most appropriate red-near infrared (NIR) VI for accurately assessing vegetation recovery, Veraverbeke et al. (2012a) evaluated thirteen indices. Their study found that soil-adjusted vegetation index (SAVI) outperformed the normalized difference vegetation index (NDVI) in areas with a single type of vegetation; NDVI outperformed SAVI in areas with heterogeneous vegetation cover and a single soil type, and overall NDVI was the most robust VI for assessing vegetation recovery.

Bisson et al. (2008) used a novel VI which included vegetation type, soil type, geology, and topography to determine the natural capability of vegetation to recover post-fire. The Vegetation Resilience After Fire (VRAF) index is calculated:

$$VRAF = PsS + PvV + PslSL + PaA + PgG \quad (11)$$

Where S , V , SL , A , and G are the parameters and P_x are the weights assigned to the parameters. S is soil stability, V is capability of vegetation to regenerate, SL is slope, A is aspect, and G is the geological parameter related to the alterability of bedrock. The results were evaluated against field and remote sensing data. Validation remote sensing data was processed via a multi-temporal dataset of the temporal-spectral profile, the feature space, and NDVI. Results indicate that the VRAF index is appropriate for constructing recovery trajectories in Northern Mediterranean environments. Gitas et al. (2012) notes that an area that is currently insufficiently studied is the use of indices that include SWIR.

SMA is considered a robust technique that aims to resolve the concern associated with objects that are smaller than the pixel size of an image. SMA uses the spectral reflectance of 'pure' pixel spectral response (endmembers) to determine what fraction of a mixed pixel is comprised of individual cover types (Figure 14). This is accomplished by analyzing the degree to which the radiance from a mixed pixel corresponds with the endmembers. The product allows for the detection of low cover fractions and results in quantitative abundance maps (Gitas et al., 2012).

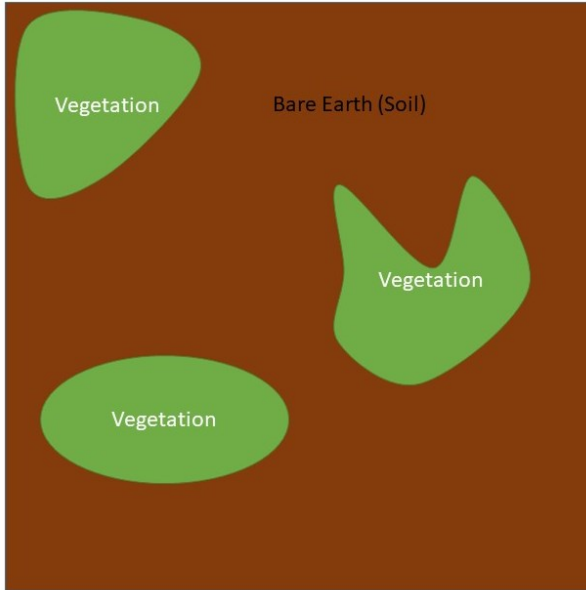


Figure 14. Example of a mixed pixel consisting of vegetation and bare earth.

Sankey, Moffet and Weber (2008) used a matched filtering SMA technique on a SPOT-5 image acquired after a fire in eastern Idaho and developed a spectral unmixing model to estimate percent shrub canopy cover within each pixel. Linear regression was used to test the accuracy of the SMA unmixing results compared to field measurements. The SMA model performed well, with an adjusted $R^2 = 0.82$ ($p < 0.0001$).

Veraverbeke et al. (2012b) published a study using a simple SMA, a multiple endmember SMA (MESMA), and a segmented SMA (a SMA that includes ancillary data) to estimate vegetation regrowth while accounting for variations in soil brightness due to the presence of two different lithological units. The simple SMA resulted in reasonable regression fits ($R^2 = 0.67$ and 0.72) for the two lithological subsets when evaluated separately, but indicated poor performance with the pooled dataset owing to the inability to separate the lithological subsets ($R^2 = 0.65$). Overall, the segmented SMA provided the most robust results, outperforming both the simple SMA and the MESMA.

The European Space Agency (ESA) launched the Sentinel-2A and B sensors on dates. This high-resolution multispectral sensor system provides a relatively high temporal resolution when compared to similar sensor systems such as Landsat 8 Optical Land Imager. The system has moderately high spatial and spectral resolutions. Currently, the Sentinel-2 system's red-edge bands have shown promise for detecting differing degrees of burn severity (Fernández-Manso, Fernández-Manso and Quintano 2016; Navarro et al. 2017), land use/land cover change (Forkuor et al., 2018), vegetation mapping (Bayle et al., 2019) and improved quantification of vegetation biophysical characteristics (Korhonen et al., 2017). Evangelides and Nobajas (2020) used an alteration to NDVI based on the Sentinel-2 red-edge band centered at $.705\mu\text{m}$ (band 5) to examine postfire vegetation recovery and reported their modified NDVI provided a rapid and efficient means for monitoring postfire vegetation recovery. However, research into the use of Sentinel-2 red-edge spectral indices for post-fire vegetation recovery monitoring is still limited. Additionally, the impact of the addition of red-edge bands have on SMA has not been explored.

The objective of this research was to conduct a comparison of several VIs and MESMA to estimate vegetation recovery after the 2016 Berry Fire in Grand Teton National Park and to evaluate the utility of the Sentinel 2 red-edge bands to improve estimates of post-fire vegetation recovery by quantifying the fractional vegetation cover observed for within the study area.

II. Methods

2.1 Study Area

Grand Teton National Park is located in Wyoming, USA, south of Yellowstone

National Park (43.7904° N, 110.6818° W). The park is situated in a semi-arid climate and covers approximately 130,000 ha of land comprised of forests, mountains, and glacial lakes. Including the surrounding area analyzed in this study, the total study area extent is approximately 222,620 ha. This area receives, on average, 440 cm of snowfall and 55 cm of precipitation. The elevation ranges from approximately 1,900 m to 4,200 m above sea level. The sub-alpine forest is dominated by coniferous trees including *Pinus albicaulis* (whitebark pine), *Pinus flexilis* (limber pine), *Abies lasiocarpa* (subalpine fir), and *Picea engelmannii* (Engelmann spruce). Treeless regions are composed of grasses, wildflowers, mosses, and lichens.

The northern section of the national park was impacted by the Berry Wildfire starting in July of 2016 and ending in September 2016. The fire burned approximately 8,750 ha of land in and around the national park. The Berry Fire is the largest recorded fire in Grand Teton National Park's history. Since this event, vegetation has been regenerating in the afflicted areas at varying rates.

2.2 Field Data

In situ measurements of vegetation recovery were conducted from July 2nd to July 19th, 2019 and involved establishing sixty 20x20m field plots. For each plot, hemispherical photos were collected. GPS positions of each plot center were acquired, none of which exceeded a horizontal error of 1.5m (Figure 15).

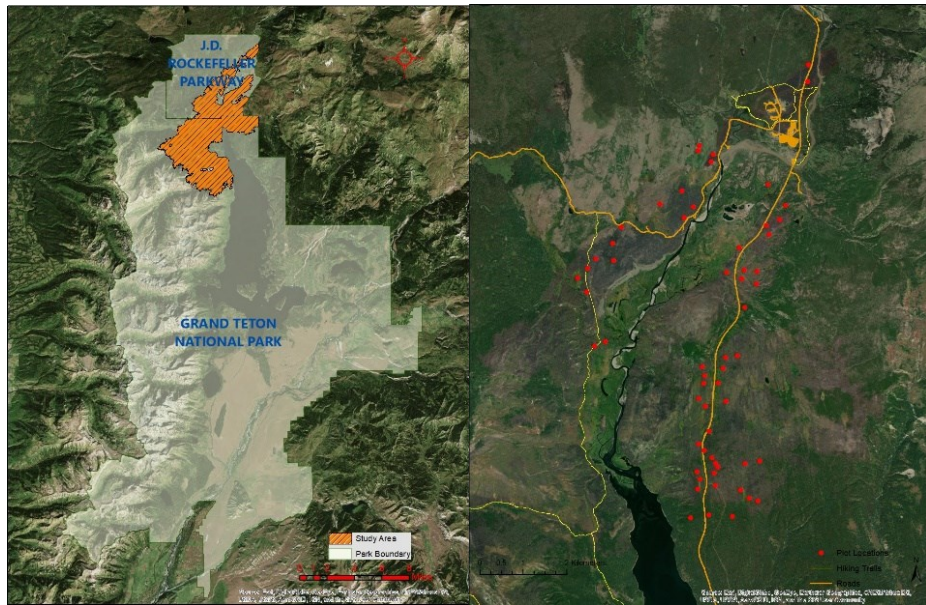


Figure 15. Study area and plot locations. (a) Map of study area as it relates to Grand Teton National Park and J.D. Rockefeller Parkway and (b) Plot locations within the study area.

2.2.1 Sample Plot Generation

Plot locations were generated by a stratifying criterion including burn severity, cover type, and topography. Burn severity was based on dNBR generated from Sentinel-2 imagery for the Berry Wildfire. Three burn severity categories were used: low, moderate, high. Two different cover types were identified as being important to sample from for this study area: herbaceous and evergreen forest. Slope was grouped into three categories using natural breaks, two of which were used for sampling: low ($\text{slope} \leq 7.76^\circ$) and moderate ($7.76^\circ \geq \text{slope} \leq 15.76^\circ$). The proportion of the study area which belonged to each of these groupings was used to determine how many plots would be allocated for that grouping. Additionally, eight plots were collected in areas not affected by the Berry Fire to serve as controls. Sample plot distributions are provided in Table 24; most plots were in evergreen forest with moderate to high burn severities (Table 24).

Table 24. Plots broken down by category.

Cover Type	Slope	Burn Category	Number of Plots
Evergreen Forest	Low	Low	3
Evergreen Forest	Moderate	Low	4
Evergreen Forest	Low	Medium	5
Evergreen Forest	Moderate	Medium	8
Evergreen Forest	Low	High	12
Evergreen Forest	Moderate	High	13
Herbaceous	Low	Medium	2
Herbaceous	Moderate	Medium	3
Herbaceous	Moderate	High	2
Evergreen Forest	Low	Control	2
Evergreen Forest	Moderate	Control	2
Herbaceous	Low	Control	2
Herbaceous	Moderate	Control	2

2.2.2 Plot Collection Procedure

Downward and upward facing hemispherical photos were collected using a Canon EOS 4000D camera with an Altura 0.35x fisheye lens. For each plot, we first collected a GPS position for plot center using a Trimble GeoXH and Zephyr 2 antenna. Next, we acquired a photo from plot center, four photos 9m from center in each cardinal direction, and three photos using random bearings and directions generated prior to going into the field (Figure 16). Any random point that was within a meter and less than 30 degrees from a previously collected photo was skipped for the next random point to avoid overlap. The collection method involved the use of 1x1m plots created from PVC pipe placed over the point of interest. The camera was held 1.3m above each photo station using a monopod facing downward. The camera was then centered as best as possible,

focused and an upward-facing photo was taken. Next the monopod was placed in the center of the quadrant and pointed toward the sky with the lens 1.3m above the ground. Another photo was taken and then the team moved to the next point of interest. After each photo, notes were taken on the image number, direction, and distance from center and the general field conditions. In the event that debris or vegetation hindered photo acquisition, an offset was applied and documented in the field notes.

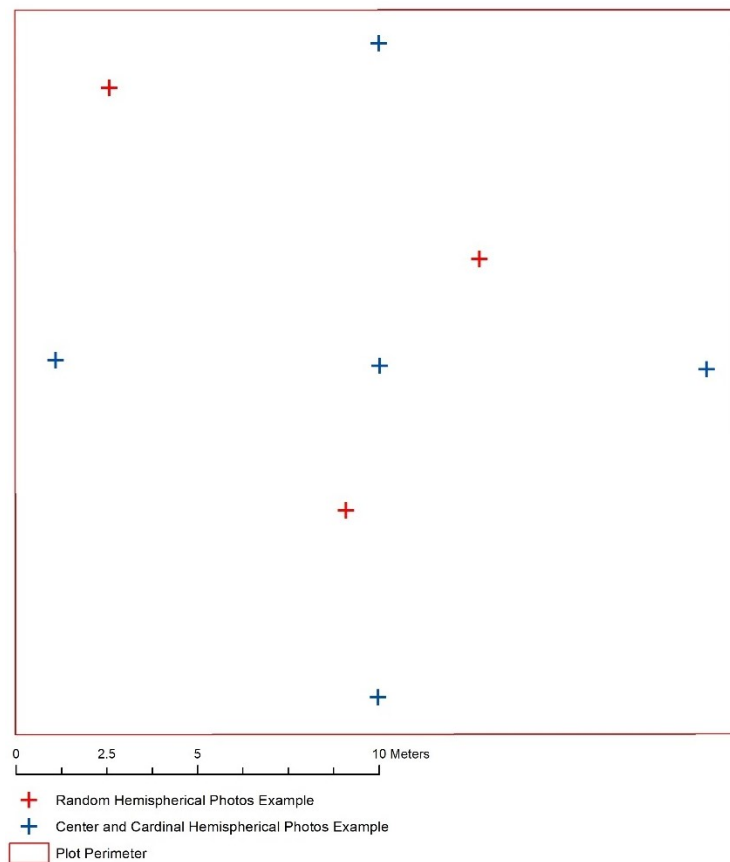


Figure 16. Example plot layout. Blue symbols represent the hemispherical photos taken at center and for the four-cardinal directions. Red symbols represent possible locations for the three random hemispherical photos.

2.2.3 Hemispherical Photograph Processing in CAN-EYE

The hemispherical photos were processed in CAN-EYE (Weiss and Baret, 2017) to derive fractional vegetation cover. CAN-EYE is an open source image processing software that can be used to extract various vegetation structure characteristics from images acquired with a fisheye lens. Each plot's images were stored in an upward and downward directory allowing CAN-EYE to process the images as an elementary sampling unit (ESU). The directories for all downward facing ESUs were loaded one at a time into CAN-EYE and each photo was masked to remove vegetation outside of the 1x1m sub-plot from the analysis. Then, fractional vegetation cover was estimated in CAN-EYE by classifying vegetation in the image based on image segmentation. After an initial segmentation, we identified vegetation pixels which were used to help the algorithm group all remaining pixels in the ESU.

For the upward facing ESUs, only units which possessed at least one image containing live vegetation within the plot were used. In total, twenty-five upward facing ESUs were processed. The procedure for processing these ESUs was similar to that of the downward facing units with the exception of masking vegetation outside the 1x1m plot. After all ESUs were processed, the average fractional vegetation cover for both surface and canopy vegetation were associated with their respective plot center points. The surface FVC and the Canopy FVC values were then summed and divided by 200 (the maximum possible vegetation cover) to calculate a total FVC.

2.3 Image preprocessing and index generation

Cloud free, atmospherically corrected Sentinel-2 data were downloaded from the ESAs open access data hub (<https://scihub.copernicus.eu/dhus/#/home>) for July 20, 2019. The area of the imagery corresponding to the final Monitoring Trends in Burn Severity

(MTBS) fire perimeter for the Berry Fire was buffered 6.5km and the image was clipped to this buffered perimeter. We calculated several indices to estimate post-fire fractional vegetation cover (Table 25). Band 8a was used as the standard NIR band because it has previously been used for calculating NDVI in other research (Mandanici and Bitelli, 2016; Zhang et al., 2018) and is collected at the same 20m spatial resolution as the red-edge bands.

Table 25. List of indices generated for estimating fractional vegetation cover.

Spectral Indices		Equation
NDVI	Normalized Difference Vegetation Index	$\frac{B8a - B4}{B8a + B4}$
GNDVI	Green Normalized Difference Vegetation Index	$\frac{B8a - B3}{B8a + B3}$
NDVIre1n	Normalized Difference Vegetation Index red-edge 1 narrow	$\frac{B8a - B5}{B8a + B5}$
NDVIre2n	Normalized Difference Vegetation Index red-edge 2 narrow	$\frac{B8a - B6}{B8a + B6}$
NDVIre3n	Normalized Difference Vegetation Index red-edge 3 narrow	$\frac{B8a - B7}{B8a + B7}$
PSRI	Plant Senescence Reflectance Index	$\frac{B4 - B3}{B6}$
Clre	Chlorophyll Index re-edge	$\frac{B7}{B1} - 1$
NDre1	Normalized Difference re-edge 1	$\frac{B6 - B5}{B6 + B5}$
NDre2	Normalized Difference red-edge 2	$\frac{B7 - B5}{B7 + B5}$
MSRren	Modified Simple Ratio red-edge narrow	$\frac{\left(\frac{B8a}{B5}\right) - 1}{\sqrt{\left(\frac{B8a}{B5}\right) + 1}}$

2.4 Multiple Endmember Spectral Mixture Analysis

The subpixel analysis tools in ERDAS Imagine 2018 (Hexagon Geospatial, 2018) were used to perform a MESMA analysis for forest and herbaceous covers within the study area. The MESMA process within Imagine involves: (1) preprocessing of the imagery, (2) environmental corrections for the imagery, (3) collection of ‘pure’ pixels for each land cover to use in endmember generation, (4) manual signature derivation from the collected pixels, (5) combining the signatures created in the previous step into a single signature file, (6) material of interest classification based on the combined signature file. Because of variations in vegetation type and lighting, three sets of pure pixels were required to classify the majority of in-scene forests and three sets of pure pixels were required to classify the majority of in-scene herbaceous land cover. These ‘pure’ pixels were collected using the scene as a whole (the un-clipped imagery) but were applied to the image subset. This was done because the subset image lacked enough good, contiguous ‘pure’ pixels to use as endmembers for endmember selection. To ensure that the pixels used for signature creation were ‘pure’, 3m spatial resolution imagery acquired by Planet’s PlanetScope satellites (provided by the Education and Research Program) were used to help determine Sentinel-2 pixel composition.

2.5 Analysis

Plot center points for each field measurement were buffered by 20m and the mean spectral index values as well total percent cover value from the MESMA were extracted for each plot. We used JMP statistical software package (SAS Institute) where a set of thirty-one plots were used to calibrate the spectral indices to obtain a regression fit for predicting fractional vegetation cover. These regression fits were then implemented using raster algebra inside of ArcMap and the resulting values for each spectral index were

extracted. The remaining twenty-nine points were compared to the values extracted from the regression fit models to determine which best estimated fractional vegetation cover. All sixty field plots were used in a regression with the MESMA values to determine how well these values estimated FVC.

III. Results

3.1 Field Data

A total of nine-hundred and sixty hemispherical photographs were collected across sixty field plots. The GPS position of each plot center was taken for a total of sixty GPS points with an average horizontal precision of 0.197m. Six-hundred and eighty of the photographs (480 downward, 200 upward) were processed using CAN-EYE to provide a measurement of FVC. The remaining 280 upward photographs were excluded because there was not a single photograph which possessed living vegetation in the plot these photos were associated with and so the living canopy cover was assumed to be zero. The result of the CAN-EYE analysis found an average total cover of 28.08% (Table 26). Interestingly, the herbaceous control plots possessed a lower total and surface cover than the burned herbaceous plots.

Table 26. Descriptive statistics of *in situ* FVC based on CAN-EYE processing.

Cover Type	FVC Type	Average	Median	Min	Max
Burned Evergreen Forest	Total Cover	26.42%	25.50%	4.00%	62.00%
Burned Evergreen Forest	Surface Cover	45.71%	45.00%	8.00%	87.00%
Burned Evergreen Forest	Canopy Cover	7.13%	0.00%	0.00%	44.00%
Control Evergreen Forest	Total Cover	52.00%	49.75%	43.50%	65.00%
Control Evergreen Forest	Surface Cover	47.00%	50.50%	25.00%	62.00%
Control Evergreen Forest	Canopy Cover	57.00%	59.50%	40.00%	69.00%
Burned Herbaceous	Total Cover	31.71%	31.50%	21.50%	40.00%
Burned Herbaceous	Surface Cover	61.43%	60.00%	39.00%	80.00%
Burned Herbaceous	Canopy Cover	2.00%	0.00%	0.00%	8.00%
Control Herbaceous	Total Cover	16.50%	13.50%	3.50%	35.50%
Control Herbaceous	Surface Cover	29.75%	23.50%	7.00%	65.00%
Control Herbaceous	Canopy Cover	3.40%	4.00%	0.00%	6.00%
All	Total Cover	28.08%	28.25%	3.50%	65.00%
All	Surface Cover	46.57%	47.50%	7.00%	87.00%
All	Canopy Cover	9.60%	0.00%	0.00%	69.00%

3.2 Spectral Index Regression Fits

The mean values of each spectral index were extracted for each plot and a training set of thirty-one calibration plots were used in a regression analysis with total vegetation cover as the dependent variable and the indices as independent variables. This was done to derive the regression fits for each index which achieved significant ($p < 0.05$) R^2 values greater than 0.7 (Table 27). Based on the training model R^2 s, NDVI performed the best with an R^2 of 0.805. Of the indices, CLre and NDVIre2n were not statistically significant ($p > 0.05$) and NDVIre3n only accounted for 13.5% of field-measured variation so these indices were excluded from further analysis.

Table 27. Significant models from subset regression analysis.

Model	R²	RMSE	PRESS R²	PRESS RMSE
NDVI	0.805	0.069	0.769	0.073
MSRren	0.789	0.072	0.760	0.074
NDVIre1n	0.788	0.072	0.758	0.075
GNDVI	0.786	0.073	0.748	0.076
NDre2	0.784	0.073	0.753	0.075
NDre1	0.778	0.074	0.745	0.077
PSRI	0.705	0.085	0.584	0.098

The regression equation derived for each of these variables was implemented in ArcMap using raster algebra (Figure 17). After using zonal statistics to find the mean value for each plot, the new values were extracted and used in a second regression to predict the values of the remaining 29 validation plots (Table 28). Interestingly, the model generated using NDVIre1n best explained the variation of postfire FVC, with an R² of 0.690 (Figure 18). NDVI was outperformed by NDVIre1n, GNDVI and MSRren when the regression fit models were used to predict the field plots' FVC.

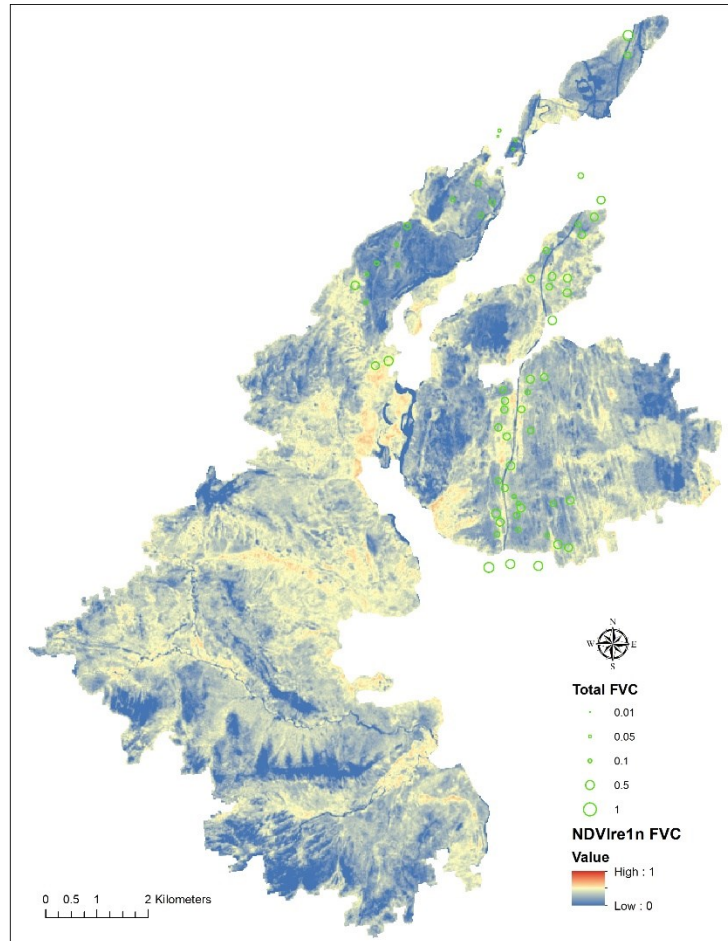


Figure 17. NDVIre1n derived fractional vegetation cover for the Berry Fire. Lighter yellow and orange pixels represent higher FVC while the darker blue pixels represent lower FVC. The field plots are displayed with green circles sized in proportion to the field measured total FVC. The plots outside of the Berry Fire perimeter (white background) are control plots.

Table 28. Validation plots regression results from calibration regression fit.

Model	R ²	RMSE	PRSS R ²	PRESS RMSE
NDVIre1n	0.690	0.080	0.642	0.083
GNDVI	0.687	0.080	0.634	0.084
MSRren	0.687	0.081	0.638	0.083
NDVI	0.683	0.081	0.636	0.084
NDre2	0.679	0.082	0.628	0.085
NDre1	0.668	0.083	0.617	0.086
PSRI	0.602	0.091	0.545	0.094

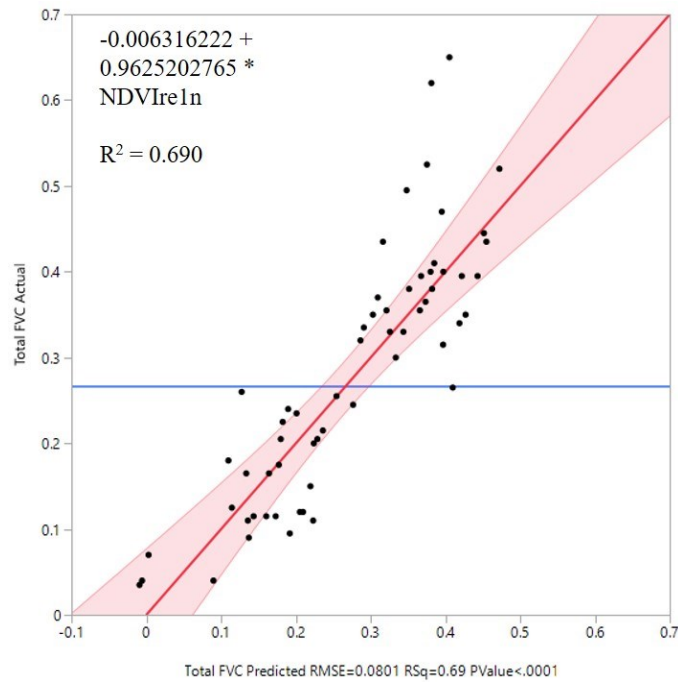


Figure 18. Standard least squares output for NDVIre1n FVC.

3.3 MESMA Regression Analysis

The output for the MESMA broke vegetation cover into eight broad categories starting at 0.2 FVC, with each category possessing a range of 1.0 (Figure 19). The averages of these values were extracted and regression analysis implemented to determine the robustness of these values (Figure 20). The MESMA possessed an

insignificant p-value (0.901) and low R^2 .

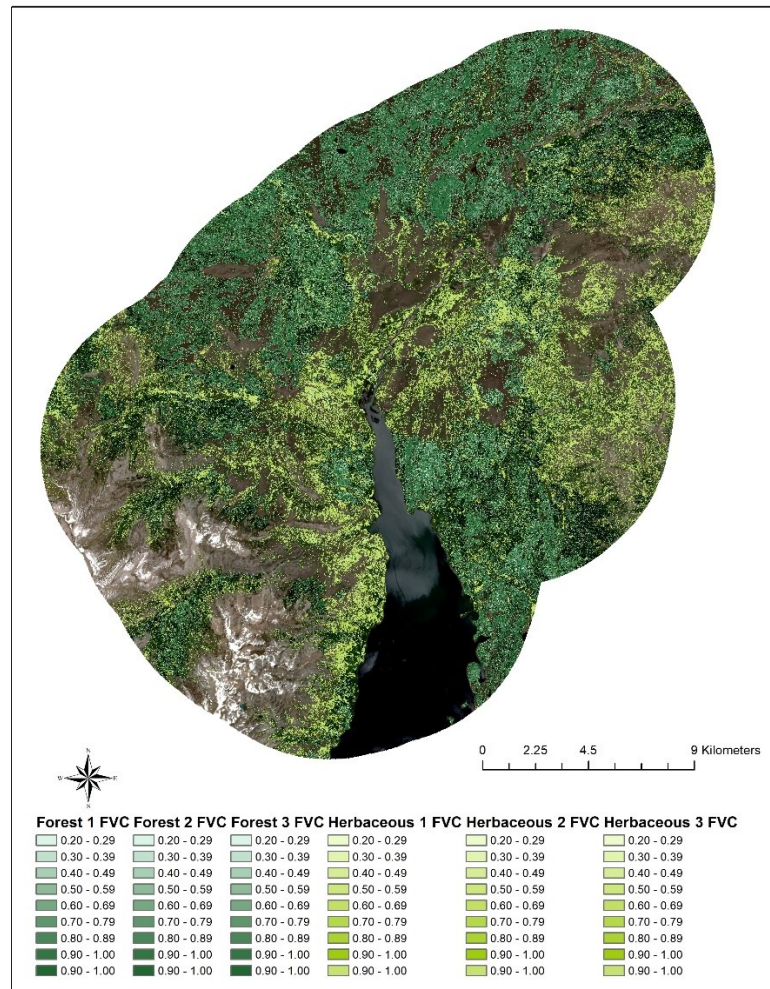


Figure 19. MESMA output. The three forest classifications are displayed in increasing intensities of dark green for increasing cover and the two herbaceous are displayed in increasing intensities of light green for increasing cover.

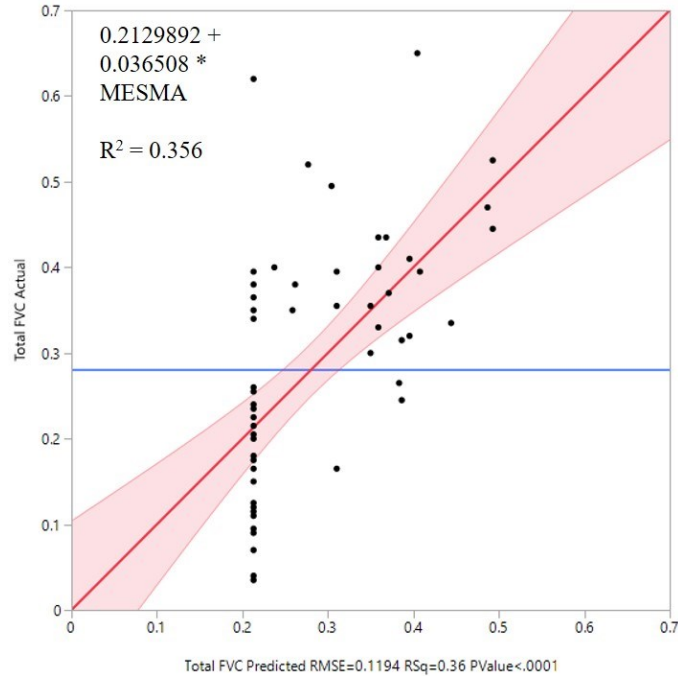


Figure 20. Standard least squares output for the MESMA FVC.

IV. Discussion

4.1 Field Data

Post-fire vegetation recovery was present in all sixty field plots, with the greatest FVCs found in plots with lower burn severities (Table 29). A moderately strong correlation between field measured FVC and a MTBS derived dNBR image was found (-0.604). This agrees with other studies which have found that burn severity measured via NBR and CBI are strongly correlated with post-fire measurements of vegetation recovery (Chen et al., 2011; Jin et al., 2012; Lee and Chow, 2015). However, Chen et al. (2011) notes that this strong correlation drops after two years postfire, which explains why the correlation between our FVCs and the MTBS dNBR image is only moderately strong. This diminishing of a relationship between burn severity and vegetation recovery can be seen in the average surface covers of the low and medium burn severities, which are only separated by 3.69%.

Table 29. Field measured FVC by burn severity category.

Burn Severity	Average Total Cover	Average Surface Cover	Average Canopy Cover
Low	40.86%	55.86%	25.86%
Medium	30.29%	52.17%	8.44%
High	21.46%	42.85%	7.41%

4.2 Ability of Spectral Indices to Assess FVC

Of the spectral indices used to assess FVC, the regression fit based on NDVI_{re1n} performed the best. This is interesting, as the initial regression analysis suggested that NDVI to be most optimal based on its R^2 . However, this is consistent with other studies which have found red-edge bands to be useful for vegetation and land cover monitoring (Forkuor et al., 2017; Korhonen et al., 2017; Bayle et al., 2019). Because of how sensitive the red-edge region is to vegetation with high chlorophyll content, this region may be better suited to respond strongly to spectral reflectance of vegetation (Horler, Dockray and Barber, 1983). However, while NDVI_{re1n} outperformed NDVI and the other models it only achieved an R^2 of 0.69, which resulted in a model unable to accurately map the highest and lowest field measured FVCs.

Even though the NDVI_{re1n} R^2 is only moderately strong, it slightly outperforms the best performing model in Veraverbeke et al. (2012a). Vereverbeke et al. (2012a) tested 12 “traditional” spectral indices using a similar methodology to that presented in this paper and found that the NDVI regression fit model outperformed the others, achieving an $R^2 = 0.68$. This study examined an area in southern Greece which had a vegetation composition dominated by shrublands and pine forests (*Pinus nigra*). The

NDVI regression fit model used in this paper achieved a similar R^2 (0.683). However, unlike the Vereverbeke study this study included red-edge based bands, two of which slightly outperformed standard NDVI.

The red-edge based models were both indices which included Sentinel-2's band 5, which has been noted in several other studies as providing a slight improvement over more standard NIR bandwidths for various vegetation, land cover change and fire-related analyses (Fernández-Manso, Fernández-Manso and Quintano 2016; Navarro et al. 2017; Korhonen et al., 2017; Forkuor et al., 2017; Evangelides and Nobajas, 2020). This builds upon the findings from our previous research on burn severity for which the best performing models all included at least one index which was generated using Sentinel-2 band 5. Although further research into the uses of this band is needed to better understand how it can be used to improve postfire vegetation monitoring and other remote sensing vegetation studies, early results are promising.

4.3 MESMA's Assessment of FVC

This study attempted to use MESMA, derived in ERDAS Imagine, to estimate FVC. Unfortunately, the effort proved unsuccessful with a low R^2 and insignificant p -value. One of the reasons for this can be attributed to the lack of low FVC classes in the output of the MESMA analysis. The MESMA output's lowest FVC class ranges from 20-29% cover, which is unable to capture the low vegetation covers found in many postfire pixels.

Additionally, Zhang et al. (2019) have found that unmixing error originates from the deviation signal, which increases as the spectral variability of an endmember increases. The vegetation found in this study area possesses considerable spectral

variation, which is enhanced by the topography of the area. To address this, we implemented MESMA as suggested by Zhang et al. however a different approach may be necessary to increase the accuracy of the output.

4.4 Sources of Uncertainty

Efforts were taken to reduce sources of uncertainty, although several still remain. For the collected field data, only eight 1x1m subplots were collected for each 20m plot. This means 392 square meters were unaccounted for in each plot. Our field methodology was based off of a review of the literature and time constraints. Although there is currently no standard to the number of photographs which should be collected per field plot, after a review of the literature we chose to capture eight downward and eight upward photographs in each plot (Martinez et al., 2004; Hopkinson and Chasmer, 2009; Ryan et al., 2014; Mu et al. 2014). However, it is possible that had more photographs been collected within each plot, our field measured FVC results may have changed. Additionally, the CAN-EYE processing does possess limitations when shadows are present (Weiss and Baret, 2017). Shadows and overexposure (due to sun glare in upward photographs) can cause some vegetation to be misclassified. As a result, our CAN-EYE derived FVC values were likely underestimated for several plots because of shadows.

The spectral indices were derived from Sentinel-2 imagery which is subject to geolocation error. However, this error does not usually exceed one pixel in Sentinel-2 imagery unless a course correction takes place during or shortly before acquisition. However, no course corrections are documented for the imagery used in this study.

V. Conclusion

This research attempted to determine whether one of several spectral indices or

MESMA best estimated FVC three years after the 2016 Berry Fire in Grand Teton National Park and John D. Rockefeller Parkway. To accomplish this task a field campaign was conducted from July 2nd to July 19th, 2019 in which 60 plots consisting of nine-hundred and sixty hemispherical photographs were collected. Sentinel-2 imagery acquired on July 20th, 2019 was downloaded for index generation and use in MESMA. Ten spectral vegetation indices, including eight red-edge based indices, were generated from the imagery. A MESMA was performed with three forest and three herbaceous endmembers. Our results indicated that of the tested approaches, the NDVIre1n regression fit model best estimated FVC.

Our findings agree with other research that the Sentinel-2 band 5 provides wavelengths which can be used to improve more “traditional” indices such as NDVI. Future research will attempt to use indices based off this band and the other red-edge bands to derive recovery trajectories and examine its use for postfire vegetation recovery monitoring in other environments.

Acknowledgments

I would like to thank my field team, Brandon Rose and Lucas Chavez, for their assistance and commitment during our field campaign. Funding for the field work in this research was provided by the Texas State Graduate College’s Doctoral Research Support Fellowship and from the Texas State Geography Department’s Ray and Marian Butler Environmental Geography Scholarship.

V. CONCLUSION

The purpose of this research was to explore the pre-fire risk, postfire burn severity and three year out vegetation recovery for the 2016 Berry Fire in Grand Teton National Park (as well as the 2016 Maple Fire in the case of burn severity). By doing so, an in depth analysis of the conditions that led to the Berry Fire, the affects the fire had on the landscape and the recovery of that landscape over the years were all examined. As each of these dynamics influences and impacts the following dynamic, they all combine to create a holistic view of the conditions and effects of the Berry Fire. For each topic, gaps in the literature were identified and studies were created to address these gaps and explore the topic as it relates to the Berry Fire.

For fire risk, the use of fuel datasets in risk assessments based on multicriteria evaluation of GIS and remote sensing datasets was identified as an area which required study. Alongside this gap, the relationship between fire risk values and postfire burn severity levels was little explored and so an experiment was designed to address both of these gaps in conjunction. For burn severity, a lack of research in which spectral indices are used to estimate quantitative fire effects as opposed to CBI field estimates was identified. Additionally, recently the Sentinel-2 satellite constellation was launched by the ESA which possess spectral bands located in the red-edge region of the EMS. These bands were used to generate additional spectral indices to determine their effectiveness at estimating various field measured burn severity metrics. Finally, disagreement between whether SMA or spectral indices works best for post-fire vegetation recovery when estimating FVC has left a gap which required further study. For this section, I also included the red-edge indices as their potential for monitoring and mapping post-fire

vegetation recovery has not been adequately explored.

This research was conducted using recent GIScience techniques that are changing the way fire ecology research is conducted. For the pre-fire risk, a combination of cartographic modeling and multi-criteria evaluation were implemented. This approach entails the use of several cartographic layers which are manipulated using raster algebra to provide an output whose values represent some combination of the input layers. Because this technique was used to map fire risk, the output's values represented the risk of an ignition/spread of wildfire combined with vulnerability based on fuel type, canopy cover, relative moisture content, slope, elevation, aspect and distance to roads, trails and structures. Each of these inputs were ranked according to how they impact fire risk, with higher rankings going to data values which increase risk more. These inputs were then weighted based largely on the weighting scheme in Adab, Kanniah and Solaimani (2013), but with the inclusion of fuel variables.

The output fire risk layer was then used in combination with burn severities measured by the MTBS program to determine if there was a relationship between the level of risk and resulting burn severity. This was accomplished using logistic regression in which the level of burn severity was used as the dependent variable and the generated fire risk as the independent variable. Results indicate that a relationship between fire risk and burn severity is weak overall, with moderately strong relationships only existing in unburned areas and in the broad 'moderate to high' burn severity category. This indicates that while a relationship exists, it is not a strong enough relationship for the proposed fire risk to consistently predict levels of burn severity. Additionally, the proposed fire risk index was evaluated against three other fire risk indices, all of which demonstrated poorer

performance than the proposed model.

The second analysis in this work attempted to estimate quantitative field measured fire effects using a combination of “traditional” and red-edge based indices for the Berry and Maple Fires. Currently, the majority of burn severity studies only attempt to estimate burn severity using the CBI, which is measured optically and so is subjective. Field data collected by Turner et al. (2019) in the summer of 2017 was used as the ground truth data whereas thirty spectral indices were calculated from pre- and post-fire imagery. These indices included burn ratios, red-edge indices, modified red-edge burn ratios and more “traditional” indices (e.g. NDVI, GNDVI). The indices were then used in an all-possible-models multivariate regression to determine the most optimal models for estimating each field measurement. The one, two and three variable models which met the R^2 and VIF criteria were reported as successful models.

The results indicated that a total of six field measurements could be accurately estimated using these spectral indices, three of which achieved R^2 s above 0.7. Interestingly, red-edge bands were included in every acceptable model and appear to have outperformed more “traditional” spectral indices. Specifically, red-edge indices based on Sentinel-2 band five were included in all the best performing models and band five based indices outperformed the indices generated using bands six and seven. This strengthens the findings of other researchers who found band five to be useful for estimating burn severity (Korets et al., 2010; Fernández-Manso, Fernández-Manso and Quintano 2016; Navarro et al. 2017).

The final analysis in this work attempted to estimate the postfire FVC for the Berry Fire in summer 2019 using regression fits for various spectral indices as well as

using MESMA to determine which method performed best. To accomplish this a field campaign was conducted in the summer of 2019 in which sixty plots were collected. Within each plot eight downward and eight upward facing hemispherical photographs were collected for a total of nine-hundred and sixty hemispherical photography. Six-hundred and eighty of these were processed in CAN-EYE to provide field measured FVC which was used for calibrating the spectral indices regression fits and for assessing the performance of all approaches.

Ten spectral indices were calculated using Sentinel-2 imagery acquired directly after the summer 2019 field campaign. Of these indices, two were “traditional” and the remaining eight were red-edge based. MESMA was derived using the process flow within the ERDAS Imagine environment, during which three forest and three herbaceous signatures were used to capture the spectral variability of the scene. The results show that of the regression fitted spectral indices, NDVI_{red} performed the best. Because this band is derived using Sentinel-2 band five, this agrees with other research on the usefulness of band five in multiple remote sensing studies involving vegetation monitoring, land use/land cover change detection and burn severity assessment (Fernández-Manso, Fernández-Manso and Quintano 2016; Navarro et al. 2017; Korhonen et al., 2017; Forkuor et al., 2017; Evangelides and Nobajas, 2020). Because of MESMA not adequately mapping vegetation recovery (failed to achieve significance) the red-edge index NDVI_{red} was identified as the most effective means for mapping FVC for the Berry Fire.

These three studies attempt to examine three different temporal periods in fire ecology: the pre-fire conditions, the immediate postfire alteration of the landscape and

the long-term recovery of a fire afflicted landscape. In doing so, this study provides a picture of the interactions between the landscape and wildfire. Future research will attempt to further explore the relationships between fire risk, burn severity and vegetation recovery. In this work the relationship between fire risk and burn severity was shown to generally be weak. However, more research is required to better establish the strength of this relationship.

Other research has examined the connection between burn severity and vegetation recovery, generally finding the two to be strongly correlated for the first two years with a substantial decrease after this initial period of recovery. Our results appear to agree with this finding as our *in situ* measurements were only moderately correlated with burn severity three years postfire. Future research will attempt to further explore this relationship to determine if a combination of burn severity and pre-fire vegetation cover can be used to accurately project rates of recovery.

Additional future research projects related to the work presented here include fire spread modeling for the Berry Fire, burn severity mapping using CBI data and red-edge bands, and continued monitoring of vegetation recovery. In addition to these research projects, I plan to experiment with alternative assessments of fire risk to improve the relationship between risk and burn severity. If a strong enough relationship can be established between risk and burn severity and a suitable model for predicting vegetation recovery based on pre-fire vegetation cover and burn severity is developed, I believe it will be possible to identify areas most at risk based on recovery lengths from predicted burn severities in addition to chance of ignition/spread and vulnerability. The research presented in this manuscript provides the foundation on which this future research will be

built.

REFERENCES

- Abrahamson, W. G. 1984. Species responses to fire on the Florida Lake Wales Ridge. *American Journal of Botany* 71(1): 35-43.
- Adab, H., Kanniah, K. D., and Solaimani, K. 2013. Modeling forest fire risk in the northeast of Iran using remote sensing and GIS techniques. *Natural hazards* 65(3): 1723-1743.
- Amiro, B. D., Chen, J. M., and Liu, J. 2000. Net primary productivity following forest fire for Canadian ecoregions. *Canadian Journal of Forest Research* 30(6): 939-947.
- Ahlgren I.F., Ahlgren C.E. 1960. Ecological effects of forest fires. *The Botanical Review* 26:483–533.
- Anderson, J. R. 1976. *A land use and land cover classification system for use with remote sensor data* (Vol. 964). US Government Printing Office.
- Arroyo, L. A., Pascual, C., and Manzanera, J. A. 2008. Fire models and methods to map fuel types: the role of remote sensing. *Forest ecology and management* 256(6): 1239-1252.
- Bayle, A., Carlson, B. Z., Thierion, V., Isenmann, M., and Choler, P. 2019. Improved Mapping of Mountain Shrublands Using the Sentinel-2 Red-Edge Band. *Remote Sensing* 11(23): 2807.
- Benavides-Solorio, J., and MacDonald, L. H. 2001. Post-fire runoff and erosion from simulated rainfall on small plots, Colorado Front Range. *Hydrological Processes* 15(15): 2931-2952.

- Beverly J.L., Herd E.P.K., Conner J.C.R. 2009. Modeling fire susceptibility in west central Alberta, Canada. *Forest Ecology and Management* 258:1465–1478.
- Bisson, M., Fornaciai, A., Coli, A., Mazzarini, F., and Pareschi, M. T. 2008. The vegetation resilience after fire (VRAF) index: development, implementation and an illustration from central Italy. *International Journal of Applied Earth Observation and Geoinformation* 10(3): 312-329.
- Boer, M. M., Macfarlane, C., Norris, J., Sadler, R. J., Wallace, J., and Grierson, P. F. 2008. Mapping burned areas and burn severity patterns in SW Australian eucalypt forest using remotely-sensed changes in leaf area index. *Remote Sensing of Environment* 112(12): 4358-4369.
- Bolton, D.K., Coops, N.C. and Wulder, M.A. 2015. Characterizing residual structure and forest recovery following high-severity fire in the western boreal of Canada using Landsat time-series and airborne lidar data. *Remote Sensing of Environment* 163: 48-60.
- Bond, W.J., Keeley, J.E. 2005. Fire as a global ‘herbivore’: the ecology and evolution of flammable ecosystems. *Trends in ecology and evolution*, 20(7):387-394.
- Bourgeau-Chavez, L. L., Kasischke, E. S., Brunzell, S., Mudd, J. P., and Tukman, M. 2002. Mapping fire scars in global boreal forests using imaging radar data. *International Journal of Remote Sensing* 23(20): 4211-4234.
- Brandis, K., and Jacobson, C. 2003. Estimation of vegetative fuel loads using Landsat TM imagery in New South Wales, Australia. *International Journal of Wildland Fire* 12(2): 185-194.

- Burgan, R. E., Andrews, P. L., Bradshaw, L. S., Chase, C. H., Hartford, R. A., and Latham, D. J. 1997. Current status of the wildland fire assessment system (WFAS). *Fire Management Notes*, 57(2), 14-17.
- Butler, B.W., Anderson, W.R., Catchpole, E.A. 2007. Influence of slope on fire spread rate. In *In: Butler, Bret W.; Cook, Wayne, comps. The fire environment--innovations, management, and policy; conference proceedings. 26-30 March 2007; Destin, FL. Proceedings RMRS-P-46CD. Fort Collins, CO: US Department of Agriculture, Forest Service, Rocky Mountain Research Station.* 46:75-82.
- Caetano, M., Mertes, L., Cadete, L., and Pereira, J. 1996. Assessment of AVHRR data for characterizing burned areas and post-fire vegetation recovery. *EARSeL Advances in Remote Sensing* 4: 124-134.
- Chen, X., Vogelmann, J.E., Rollins, M., Ohlen, D., Key, C.H., Yang, L., Huang, C. and Shi, H., 2011. Detecting post-fire burn severity and vegetation recovery using multitemporal remote sensing spectral indices and field-collected composite burn index data in a ponderosa pine forest. *International Journal of Remote Sensing* 32(23): 7905-7927.
- Chuvieco, E. 2009. *Earth observation of wildland fires in Mediterranean ecosystems* (pp. 129-148). Dordrecht, the Netherlands: Springer.
- Chuvieco, E., Aguado, I., Yebra, M., Nieto, H., Salas, J., Martín, M. P., Vilar L., Martínez J., Martín S., Ibarra P., De La Riva, J., Baeza J., Rodríguez F., Molina J.R., Herrera M.A., Zamora R. 2010. Development of a framework for fire risk assessment using remote sensing and geographic information system technologies. *Ecological Modelling* 221(1): 46-58.

- Chuvieco, E., and Congalton, R. G. 1989. Application of remote sensing and geographic information systems to forest fire risk mapping. *Remote sensing of Environment* 29(2): 147-159.
- Chuvieco, E., Riaño, D., Danson, F. M., and Martin, P. 2006. Use of a radiative transfer model to simulate the postfire spectral response to burn severity. *Journal of Geophysical Research: Biogeosciences*, 111(G4).
- Chuvieco, E., and Salas, J. 1996. Mapping the spatial distribution of forest fire danger using GIS. *International Journal of Geographical Information Science* 10(3): 333-345.
- Chuvieco, E., Salas, J., and Vega, C. 1997. Remote sensing and GIS for long-term fire risk mapping. *A review of remote sensing methods for the study of large wildland fires* 91-108.
- Congressional Research Service. 2019. Wildfire Statistics.
<https://crsreports.congress.gov/product/pdf/IF/IF10244>. Last accessed: April 4 2020.
- Davies, G.M., Domenech-Jardi, R., Gray, A., Johnson, P.C.D. 2016. Vegetation structure and fire weather influence variation in burn severity and fuel consumption during peatland wildfires. *Biogeosciences*, 12(18):5737-15762.
- Díaz-Delgado, R., Lloret, F., and Pons, X. 2003. Influence of fire severity on plant regeneration by means of remote sensing imagery. *International Journal of Remote Sensing* 24(8): 1751-1763.

- Epting, J., Verbyla, D., and Sorbel, B. 2005. Evaluation of remotely sensed indices for assessing burn severity in interior Alaska using Landsat TM and ETM+. *Remote Sensing of Environment* 96(3-4): 328-339.
- Erten, E., Kurgun, V., Musaoglu, N. 2004. Forest fire risk zone mapping from satellite imagery and GIS: a case study. In *XXth Congress of the International Society for Photogrammetry and Remote Sensing, Istanbul, Turkey*, 222-230.
- Evangelides, C. and Nobajas, A. 2020. Red-Edge Normalised Difference Vegetation Index (NDVI705) from Sentinel-2 imagery to assess post-fire regeneration. *Remote Sensing Applications: Society and Environment* 17: 100283.
- Falkowski, M. J., Gessler, P. E., Morgan, P., Hudak, A. T., and Smith, A. M. 2005. Characterizing and mapping forest fire fuels using ASTER imagery and gradient modeling. *Forest Ecology and Management* 217(2-3): 129-146.
- Flannigan, M. D., Stocks, B. J., and Wotton, B. M. 2000. Climate change and forest fires. *Science of the total environment* 262(3): 221-229.
- Fernández-Manso, A., Fernández-Manso, O., and Quintano, C. 2016. SENTINEL-2A red-edge spectral indices suitability for discriminating burn severity. *International journal of applied earth observation and geoinformation* 50: 170-175.
- Fernandez-Manso, A., Quintano, C., and Roberts, D. A. 2016. Burn severity influence on post-fire vegetation cover resilience from Landsat MESMA fraction images time series in Mediterranean forest ecosystems. *Remote Sensing of Environment* 184: 112-123.

- Finney, M.A. 1995. FARSITE: a fire area simulator for fire managers. In In: Weise, David R.; Martin, Robert E., technical coordinators. *The Biswell symposium: fire issues and solutions in urban interface and wildland ecosystems*; February 15-17, 1994; Walnut Creek, California. Gen. Tech. Rep. PSW-GTR-158. Albany, CA: Pacific Southwest Research Station, Forest Service, US Department of Agriculture; 158: 55-56.
- Finney M.A., Ryan K.C. 1995. Use of the FARSITE fire growth model for fire prediction in US National Parks. In *The International Emergency Management and Engineering Conference*, 9-12.
- Finney, M.A., 2006. An overview of FlamMap fire modeling capabilities. In In: *Andrews, Patricia L.; Butler, Bret W., comps. 2006. Fuels Management-How to Measure Success: Conference Proceedings. 28-30 March 2006; Portland, OR. Proceedings RMRS-P-41. Fort Collins, CO: US Department of Agriculture, Forest Service, Rocky Mountain Research Station. 41: 213-220.*
- Flannigan, M., Cantin, A.S., de Groot, W.J., Wotton, M., Newbery, A., Gowman L.M. 2013. Global wildland fire season severity in the 21st century. *Forest Ecology and Management* 294:54–61.
- Forkuor, G., Dimobe, K., Serme, I., and Tondoh, J. E. 2018. Landsat-8 vs. Sentinel-2: examining the added value of sentinel-2's red-edge bands to land-use and land-cover mapping in Burkina Faso. *GIScience & Remote Sensing* 55(3): 331-354.

- Frolking, S., Palace, M. W., Clark, D. B., Chambers, J. Q., Shugart, H. H., and Hurtt, G. C. 2009. Forest disturbance and recovery: A general review in the context of spaceborne remote sensing of impacts on aboveground biomass and canopy structure. *Journal of Geophysical Research: Biogeosciences* 114(G2).
- Gao, B. C. 1996. NDWI—A normalized difference water index for remote sensing of vegetation liquid water from space. *Remote sensing of environment* 58(3): 257-266.
- García, M. L., and Caselles, V. 1991. Mapping burns and natural reforestation using Thematic Mapper data. *Geocarto International* 6(1): 31-37.
- García-Llamas, P., Suárez-Seoane, S., Fernández-Guisuraga, J.M., Fernández-García, V., Fernández-Manso, A., Quintano, C., Taboada, A., Marcos, E. and Calvo, L. 2019. Evaluation and comparison of Landsat 8, Sentinel-2 and Deimos-1 remote sensing indices for assessing burn severity in Mediterranean fire-prone ecosystems. *International Journal of Applied Earth Observation and Geoinformation* 80:137-144.
- Gitas, I., Mitri, G., Veraverbeke, S., and Polychronaki, A. 2012. Advances in remote sensing of post-fire vegetation recovery monitoring-a review. In *Remote Sensing of Biomass-Principles and Applications*. InTech.
- Gitelson, A., & Merzlyak, M. N. (1994). Spectral reflectance changes associated with autumn senescence of *Aesculus hippocastanum* L. and *Acer platanoides* L. leaves. Spectral features and relation to chlorophyll estimation. *Journal of plant physiology* 143(3): 286-292.

- Goetz, S. J., Fiske, G. J., and Bunn, A. G. 2006. Using satellite time-series data sets to analyze fire disturbance and forest recovery across Canada. *Remote Sensing of Environment* 101(3): 352-365.
- Gordon, C.E., Price, O.F. and Tasker, E.M. 2017. Mapping and exploring variation in post-fire vegetation recovery following mixed severity wildfire using airborne LiDAR. *Ecological Applications* 27(5):1618-1632.
- Gouveia, C., DaCamara, C. C., and Trigo, R. M. 2010. Post-fire vegetation recovery in Portugal based on spot/vegetation data. *Natural Hazards and Earth System Sciences* 10(4): 673-684.
- de Groot, W.J., Flannigan, M.D., Cantin, A.S. 2013. Climate change impacts on future boreal fire regimes. *Forest Ecology and Management* 294:35–44.
- Haaland, D. M., & Thomas, E. V. (1988). Partial least-squares methods for spectral analyses. 2. Application to simulated and glass spectral data. *Analytical Chemistry* 60(11): 1202-1208.
- Hardy, C.C. 2005. Wildland fire hazard and risk: problems, definitions, and context. *Forest ecology and management* 211(1-2): 73-82.
- Harris, S., Veraverbeke, S., & Hook, S. 2011. Evaluating spectral indices for assessing fire severity in chaparral ecosystems (Southern California) using MODIS/ASTER (MASTER) airborne simulator data. *Remote sensing* 3(11): 2403-2419.
- He, H.S., Shang, B.Z., Crow, T.R., Gustafson, E.J., Shifley, S.R. 2004. Simulating forest fuel and fire risk dynamics across landscapes—LANDIS fuel module design. *Ecological Modelling* 180(1):135-151.

Hernandez-Leal, P.A., Arbelo, M., Gonzalez-Calvo, A. 2006. Fire risk assessment using satellite data. *Advances in Space Research* 37:741–746.

Hexagon Geospatial. 2018. Subpixel classification user's guide. *ERDAS Imagine Help*.

Retrieved on June 18th 2020 from:

file:///C:/Program%20Files/Hexagon/ERDAS%20IMAGINE%202018/help/html/index.htm#SubpixelClassifierStrategyandInterpretation.htm

Hicke, J. A., Asner, G. P., Kasischke, E. S., French, N. H., Randerson, J. T., Collatz, G. J., Stocks, B.J., Tucker, C.J., Los, S.O., and Field, C. B. 2003. Postfire response of North American boreal forest net primary productivity analyzed with satellite observations. *Global Change Biology* 9(8): 1145-1157.

Hoffmann, A. A., Siegert, F., and Hinrichs, A. 1999. *Fire damage in East Kalimantan in 1997/98 related to land use and vegetation classes: satellite radar inventory results and proposals for further actions* (p. 26). IFFM/SFMP.

Hope, A., Tague, C., and Clark, R. 2007. Characterizing post-fire vegetation recovery of California chaparral using TM/ETM+ time-series data. *International Journal of Remote Sensing* 28(6): 1339-1354.

Hopkinson, C. and Chasmer, L., 2009. Testing LiDAR models of fractional cover across multiple forest ecozones. *Remote Sensing of Environment* 113(1): 275-288.

Horler, D.N.H., DOCKRAY, M. and Barber, J., 1983. The red edge of plant leaf reflectance. *International journal of remote sensing* 4(2): 273-288.

- Hudak, A.T., Morgan, P., Bobbitt, M.J., Smith, A.M., Lewis, S.A., Lentile, L.B., Robichaud, P.R., Clark, J.T. and McKinley, R.A. 2007. The relationship of multispectral satellite imagery to immediate fire effects. *Fire Ecology* 3(1): 64-90.
- Hurteau, M. D., Bradford, J. B., Fulé, P. Z., Taylor, A. H., and Martin, K. L. 2014. Climate change, fire management, and ecological services in the southwestern US. *Forest Ecology and Management* 327: 280-289.
- Jaiswal, R. K., Mukherjee, S., Raju, K. D., and Saxena, R. 2002. Forest fire risk zone mapping from satellite imagery and GIS. *International Journal of Applied Earth Observation and Geoinformation* 4(1): 1-10.
- Jia, G. J., Burke, I. C., Goetz, A. F., Kaufmann, M. R., and Kindel, B. C. 2006. Assessing spatial patterns of forest fuel using AVIRIS data. *Remote Sensing of Environment* 102(3-4): 318-327.
- Jin, Y., Randerson, J.T., Goetz, S.J., Beck, P.S., Loranty, M.M. and Goulden, M.L., 2012. The influence of burn severity on postfire vegetation recovery and albedo change during early succession in North American boreal forests. *Journal of Geophysical Research: Biogeosciences* 117(G1).
- Johnstone, J. F., and Chapin, F. S. 2006. Effects of soil burn severity on post-fire tree recruitment in boreal forest. *Ecosystems* 9(1): 14-31.
- Kane, V. R., North, M. P., Lutz, J. A., Churchill, D. J., Roberts, S. L., Smith, D. F., McGaughey R.J., Kane J.T., and Brooks, M. L. 2014. Assessing fire effects on forest spatial structure using a fusion of Landsat and airborne LiDAR data in Yosemite National Park. *Remote Sensing of Environment* 151: 89-101.

- Kasischke, E. S., Turetsky, M. R., Ottmar, R. D., French, N. H., Hoy, E. E., and Kane, E. S. 2008. Evaluation of the composite burn index for assessing fire severity in Alaskan black spruce forests. *International Journal of Wildland Fire* 17(4): 515-526.
- Keane, R. E., Burgan, R., and van Wagtenonk, J. 2001. Mapping wildland fuels for fire management across multiple scales: integrating remote sensing, GIS, and biophysical modeling. *International Journal of Wildland Fire* 10(4): 301-319.
- Keane, R.E., Drury, S.A., Karau, E.C., Hessburg, P.F., Reynolds K.M. 2010. A method for mapping fire hazard and risk across multiple scales and its application in fire management. *Ecological Modelling* 221:2–18.
- Keeley, J. E. 2009. Fire intensity, fire severity and burn severity: a brief review and suggested usage. *International Journal of Wildland Fire* 18(1): 116-126.
- Key, C. H., & Benson, N. C. 2006. Landscape assessment (LA). In: Lutes, Duncan C.; Keane, Robert E.; Caratti, John F.; Key, Carl H.; Benson, Nathan C.; Sutherland, Steve; Gangi, Larry J. 2006. *FIREMON: Fire effects monitoring and inventory system. Gen. Tech. Rep. RMRS-GTR-164-CD. Fort Collins, CO: US Department of Agriculture, Forest Service, Rocky Mountain Research Station.* p. LA-1-55, 164.
- Koetz, B., Morsdorf, F., Van der Linden, S., Curt, T., and Allgöwer, B. 2008. Multi-source land cover classification for forest fire management based on imaging spectrometry and LiDAR data. *Forest Ecology and Management* 256(3): 263-271.

- Korhonen, L., Packalen, P., and Rautiainen, M. 2017. Comparison of Sentinel-2 and Landsat 8 in the estimation of boreal forest canopy cover and leaf area index. *Remote sensing of environment* 195: 259-274.
- Korets, M. A., Ryzhkova, V. A., Danilova, I. V., Sukhinin, A. I., & Bartalev, S. A. 2010. Forest Disturbance Assessment Using Satellite Data of Moderate and Low Resolution. In *Environmental Change in Siberia* (pp. 3-19). Springer, Dordrech.
- Krasnow K., Schoennagel T., Veblen T.T.. 2009. Forest fuel mapping and evaluation of LANDFIRE fuel maps in Boulder County, Colorado, USA. *Forest Ecology and Management* 257(7):1603-1612.
- Lee, R.J. and Chow, T.E. 2015. Post-wildfire assessment of vegetation regeneration in Bastrop, Texas, using Landsat imagery. *GIScience & Remote Sensing* 52(5): 609-626
- Lee, S.W., Lee, M.B., Lee, Y.G., Won, M.S., Kim, J.J., and Hong, S.K. 2009. Relationship between landscape structure and burn severity at the landscape and class levels in Samchuck, South Korea. *Forest Ecology and Management* 258(7):1594-1604.
- Lentile, L. B., Smith, A. M., Hudak, A. T., Morgan, P., Bobbitt, M. J., Lewis, S. A., & Robichaud, P. R. 2009. Remote sensing for prediction of 1-year post-fire ecosystem condition. *International Journal of Wildland Fire*, 18(5), 594-608.
- Lentile, L.B., Smith, F.W., Shepperd, W.D. 2006. Influence of topography and forest structure on patterns of mixed severity fire in ponderosa pine forests of the South Dakota Black Hills, USA. *International Journal of Wildland Fire*, 15(4):557-566.

- Lewis, S. A., Wu, J. Q., and Robichaud, P. R. 2006. Assessing burn severity and comparing soil water repellency, Hayman Fire, Colorado. *Hydrological Processes: An International Journal* 20(1): 1-16.
- Liew, S. C., Kwoh, L. K., Padmanabhan, K., Lim, O. K., and Lim, H. 1999. Delineating land/forest fire burnt scars with ERS interferometric synthetic aperture radar. *Geophysical Research Letters* 26(16): 2409-2412.
- Lippitt, C. L., Stow, D. A., Roberts, D. A., and Coulter, L. L. 2018. Multidate MESMA for monitoring vegetation growth forms in southern California shrublands. *International Journal of Remote Sensing* 39(3): 655-683.
- Loboda, T. V., and Csiszar, I. A. 2007. Reconstruction of fire spread within wildland fire events in Northern Eurasia from the MODIS active fire product. *Global and Planetary Change* 56(3-4): 258-273.
- Loudermilk, E. L., Stanton, A., Scheller, R. M., Dilts, T. E., Weisberg, P. J., Skinner, C., and Yang, J. 2014. Effectiveness of fuel treatments for mitigating wildfire risk and sequestering forest carbon: a case study in the Lake Tahoe Basin. *Forest Ecology and Management* 323: 114-125.
- Maeda, E. E., Arcoverde, G. F., Pellikka, P. K., and Shimabukuro, Y. E. 2011. Fire risk assessment in the Brazilian Amazon using MODIS imagery and change vector analysis. *Applied Geography* 31(1): 76-84.
- Mandanici, E. and Bitelli, G. 2016. Preliminary comparison of sentinel-2 and landsat 8 imagery for a combined use. *Remote Sensing* 8(12): 1014

- Martinez, B., Baret, F., Camacho-de Coca, F., Garcia-Haro, F.J., Verger, A. and Melia, J., 2004, October. Validation of MSG vegetation products: Part I. Field retrieval of LAI and FVC from hemispherical photographs. In *Remote Sensing for Agriculture, Ecosystems, and Hydrology VI* 5568: 57-68). International Society for Optics and Photonics.
- McKenzie, D., Gedalof, Z. E., Peterson, D. L., and Mote, P. 2004. Climatic change, wildfire, and conservation. *Conservation biology* 18(4): 890-902.
- Meng, R., Dennison, P.E., Huang, C., Moritz, M.A. and D'Antonio, C. 2015. Effects of fire severity and post-fire climate on short-term vegetation recovery of mixed-conifer and red fir forests in the Sierra Nevada Mountains of California. *Remote Sensing of Environment* 171: 311-325
- Miller, J. D., Safford, H. D., Crimmins, M., and Thode, A. E. 2009. Quantitative evidence for increasing forest fire severity in the Sierra Nevada and southern Cascade Mountains, California and Nevada, USA. *Ecosystems* 12(1): 16-32.
- Miller, J. D., and Thode, A. E. 2007. Quantifying burn severity in a heterogeneous landscape with a relative version of the delta Normalized Burn Ratio (dNBR). *Remote Sensing of Environment* 109(1): 66-80.
- Mitri, G. H., and Gitas, I. Z. 2008. Mapping the severity of fire using object-based classification of IKONOS imagery. *International Journal of Wildland Fire* 17(3): 431-442.

- Mitri, G. H., and Gitas, I. Z. 2013. Mapping post-fire forest regeneration and vegetation recovery using a combination of very high spatial resolution and hyperspectral satellite imagery. *International Journal of Applied Earth Observation and Geoinformation* 20: 60-66.
- Moody, J. A., and Martin, D. A. 2001. Post-fire, rainfall intensity–peak discharge relations for three mountainous watersheds in the western USA. *Hydrological processes* 15(15): 2981-2993.
- Morgan, P., Keane, R. E., Dillon, G. K., Jain, T. B., Hudak, A. T., Karau, E. C., Sikkink, P.G., Holden Z.A. and Strand, E. K. 2014. Challenges of assessing fire and burn severity using field measures, remote sensing and modelling. *International Journal of Wildland Fire* 23(8): 1045-1060.
- Morsdorf, F., Meier, E., Kötz, B., Itten, K. I., Dobbertin, M., and Allgöwer, B. 2004. LIDAR-based geometric reconstruction of boreal type forest stands at single tree level for forest and wildland fire management. *Remote Sensing of Environment* 92(3): 353-362.
- Mu, X., Huang, S., Ren, H., Yan, G., Song, W. and Ruan, G., 2014. Validating GEOV1 fractional vegetation cover derived from coarse-resolution remote sensing images over croplands. *IEEE Journal of Selected Topics in Applied Earth Observations and Remote Sensing* 8(2): 439-446.
- Murphy, K. A., Reynolds, J. H., and Koltun, J. M. 2008. Evaluating the ability of the differenced Normalized Burn Ratio (dNBR) to predict ecologically significant burn severity in Alaskan boreal forests. *International Journal of Wildland Fire* 17(4): 490-499.

- Mutlu, M., Popescu, S. C., Stripling, C., and Spencer, T. 2008. Mapping surface fuel models using lidar and multispectral data fusion for fire behavior. *Remote Sensing of Environment* 112(1): 274-285.
- National Park Service. 2017. Yellowstone National Park Tatanka Complex and Maple Fire. *2017 BURNED AREA EMERGENCY REHABILITATION REPORTS*.
- Navarro, G., Caballero, I., Silva, G., Parra, P. C., Vázquez, Á., and Caldeira, R. 2017. Evaluation of forest fire on Madeira Island using Sentinel-2A MSI imagery. *International Journal of Applied Earth Observation and Geoinformation* 58: 97-106.
- Ne'eman, G., Lahav, H., and Izhaki, I. 1995. Recovery of vegetation in a natural east Mediterranean pine forest on Mount Carmel, Israel as affected by management strategies. *Forest Ecology and Management* 75(1-3): 17-26.
- Parks, S. A., Dillon, G. K., and Miller, C. 2014. A new metric for quantifying burn severity: the relativized burn ratio. *Remote Sensing* 6(3): 1827-1844.
- Pausas, J. G. 1997. Resprouting of *Quercus suber* in NE Spain after fire. *Journal of Vegetation Science* 8(5): 703-706.
- Pausas, J. G., Ribeiro, E., and Vallejo, R. 2004. Post-fire regeneration variability of *Pinus halepensis* in the eastern Iberian Peninsula. *Forest ecology and management* 203(1-3): 251-259.
- Peng, G. X., Jing, L. I., Chen, Y. H., and Norizan, A. P. 2007. A forest fire risk assessment using ASTER images in Peninsular Malaysia. *Journal of China University of Mining and Technology* 17(2): 232-237.

- Pereira, J. M. 1999. A comparative evaluation of NOAA/AVHRR vegetation indexes for burned surface detection and mapping. *IEEE Transactions on Geoscience and Remote Sensing* 37(1): 217-226.
- Pierson, F. B., Robichaud, P. R., Moffet, C. A., Spaeth, K. E., Hardegree, S. P., Clark, P. E., and Williams, C. J. 2008. Fire effects on rangeland hydrology and erosion in a steep sagebrush-dominated landscape. *Hydrological Processes: An International Journal* 22(16): 2916-2929.
- Polychronaki, A., Gitas, I. Z., and Minchella, A. 2014. Monitoring post-fire vegetation recovery in the Mediterranean using SPOT and ERS imagery. *International Journal of Wildland Fire* 23(5): 631-642
- Pradhan, B., Dini Hairi Bin Suliman, M., and Arshad Bin Awang, M. 2007. Forest fire susceptibility and risk mapping using remote sensing and geographical information systems (GIS). *Disaster Prevention and Management: An International Journal* 16(3): 344-352.
- Prichard SJ, Kennedy MC. 2014. Fuel treatments and landform modify landscape patterns of burn severity in an extreme fire event. *Ecological Applications*, 24(3):571-590.
- Quintano, C., Fernández-Manso, A., Calvo, L., Marcos, E., & Valbuena, L. 2015. Land surface temperature as potential indicator of burn severity in forest Mediterranean ecosystems. *International Journal of Applied Earth Observation and Geoinformation*, 36, 1-12.

- Racine, C. H., Johnson, L. A., and Viereck, L. A. 1987. Patterns of vegetation recovery after tundra fires in northwestern Alaska, USA. *Arctic and Alpine Research* 19(4): 461-469.
- Riaño, D., Chuvieco, E., Ustin, S., Zomer, R., Dennison, P., Roberts, D., and Salas, J. 2002. Assessment of vegetation regeneration after fire through multitemporal analysis of AVIRIS images in the Santa Monica Mountains. *Remote Sensing of Environment* 79(1): 60-71.
- Robichaud, P. R., Lewis, S. A., Laes, D. Y., Hudak, A. T., Kokaly, R. F., and Zamudio, J. A. 2007. Postfire soil burn severity mapping with hyperspectral image unmixing. *Remote Sensing of Environment* 108(4): 467-480
- Saberi, S.J. and Harvey, B.J. Forthcoming. Quantifying burn severity in forests of the interior Pacific Northwest: From field measurements to satellite spectral indices.
- Robichaud, P. R., Wagenbrenner, J. W., Brown, R. E., Wohlgemuth, P. M., and Beyers, J. L. 2008. Evaluating the effectiveness of contour-felled log erosion barriers as a post-fire runoff and erosion mitigation treatment in the western United States. *International Journal of Wildland Fire* 17(2), 255-273.
- Rocca, M. E., Brown, P. M., MacDonald, L. H., and Carrico, C. M. 2014. Climate change impacts on fire regimes and key ecosystem services in Rocky Mountain forests. *Forest Ecology and Management* 327: 290-305.
- Röder, A., Hill, J., Duguay, B., Alloza, J. A., and Vallejo, R. 2008. Using long time series of Landsat data to monitor fire events and post-fire dynamics and identify driving factors. A case study in the Ayora region (eastern Spain). *Remote Sensing of Environment* 112(1): 259-273.

- Roy, D. P., Boschetti, L., and Trigg, S. N. 2006. Remote sensing of fire severity: assessing the performance of the normalized burn ratio. *IEEE Geoscience and Remote Sensing Letters* 3(1): 112-116.
- Ryan, C.M., Williams, M., Hill, T.C., Grace, J. and Woodhouse, I.H. 2013. Assessing the phenology of southern tropical Africa: A comparison of hemispherical photography, scatterometry, and optical/NIR remote sensing. *IEEE transactions on geoscience and remote sensing* 52(1): 519-528
- Sankey, T. T., Moffet, C., and Weber, K. 2008. Postfire recovery of sagebrush communities: assessment using SPOT-5 and very large-scale aerial imagery. *Rangeland ecology & management* 61(6): 598-604
- Schoennagel, T., Veblen, T. T., and Romme, W. H. 2004. The interaction of fire, fuels, and climate across Rocky Mountain forests. *AIBS Bulletin* 54(7): 661-676.
- Scott, D. F. 1993. The hydrological effects of fire in South African mountain catchments. *Journal of Hydrology* 150(2-4): 409-432.
- Scott, J.H., Burgan, R.E. 2005. Standard fire behavior fuel models: a comprehensive set of fuel models for use with Rothermel's surface fire spread model. *USDA Forest Service, Rocky Mountain Research Station*. General Technical Report RMRS-GTR-153. (Fort Collins, CO).
- Smith, D. W. 1970. Concentrations of soil nutrients before and after fire. *Canadian Journal of Soil Science* 50(1): 17-29.
- Sowmya, S. V., and Somashekar, R. K. 2010. Application of remote sensing and geographical information system in mapping forest fire risk zone at Bhadra wildlife sanctuary, India. *Journal of Environmental Biology* 31(6): 969.

- Stetler KM, Venn TJ, Calkin DE. 2010. The effects of wildfire and environmental amenities on property values in northwest Montana, USA. *Ecological Economics* 69:2233–2243.
- Stow, D., Petersen, A., Rogan, J., and Franklin, J. 2007. Mapping burn severity of Mediterranean-type vegetation using satellite multispectral data. *Giscience and Remote Sensing* 44(1): 1-23.
- Stueve, K. M., Cerney, D. L., Rochefort, R. M., and Kurth, L. L. 2009. Post-fire tree establishment patterns at the alpine treeline ecotone: Mount Rainier National Park, Washington, USA. *Journal of vegetation science* 20(1): 107-120.
- Turner, M. G., Braziunas, K. H., Hansen, W. D., & Harvey, B. J. 2019. Short-interval severe fire erodes the resilience of subalpine lodgepole pine forests. *Proceedings of the National Academy of Sciences* 116(23), 11319-11328.
- Turner, M. G., Smithwick, E. A., Metzger, K. L., Tinker, D. B., and Romme, W. H. 2007. Inorganic nitrogen availability after severe stand-replacing fire in the Greater Yellowstone ecosystem. *Proceedings of the National Academy of Sciences* 104(12): 4782-4789.
- Van Leeuwen, W. J. 2008. Monitoring the effects of forest restoration treatments on post-fire vegetation recovery with MODIS multitemporal data. *Sensors* 8(3): 2017-2042.
- Van Leeuwen, W. J., Casady, G. M., Neary, D. G., Bautista, S., Alloza, J. A., Carmel, Y., Wittenberg, L., Malkinson, D., and Orr, B. J. 2010. Monitoring post-wildfire vegetation response with remotely sensed time-series data in Spain, USA and Israel. *International Journal of Wildland Fire* 19(1): 75-93.

- Van Wagtendonk, J. W., Root, R. R., and Key, C. H. 2004. Comparison of AVIRIS and Landsat ETM+ detection capabilities for burn severity. *Remote Sensing of Environment* 92(3): 397-408.
- Veraverbeke, S., Gitas, I., Katagis, T., Polychronaki, A., Somers, B., and Goossens, R. 2012 (a). Assessing post-fire vegetation recovery using red–near infrared vegetation indices: accounting for background and vegetation variability. *ISPRS Journal of Photogrammetry and Remote Sensing* 68: 28-39.
- Veraverbeke, S., & Hook, S. J. 2013. Evaluating spectral indices and spectral mixture analysis for assessing fire severity, combustion completeness and carbon emissions. *International journal of wildland fire*, 22(5), 707-720.
- Veraverbeke, S., Lhermitte, S., Verstraeten, W. W., and Goossens, R. 2010. The temporal dimension of differenced Normalized Burn Ratio (dNBR) fire/burn severity studies: the case of the large 2007 Peloponnese wildfires in Greece. *Remote Sensing of Environment* 114(11): 2548-2563.
- Veraverbeke, S., Lhermitte, S., Verstraeten, W. W., and Goossens, R. 2011. A time-integrated MODIS burn severity assessment using the multi-temporal differenced normalized burn ratio (dNBRMT). *International Journal of Applied Earth Observation and Geoinformation* 13(1): 52-58.
- Veraverbeke, S., Somers, B., Gitas, I., Katagis, T., Polychronaki, A., and Goossens, R. 2012 (b). Spectral mixture analysis to assess post-fire vegetation regeneration using Landsat Thematic Mapper imagery: Accounting for soil brightness variation. *International Journal of Applied Earth Observation and Geoinformation* 14(1): 1-11.

- Verbyla, D., & Lord, R. 2008. Estimating post-fire organic soil depth in the Alaskan boreal forest using the normalized burn ratio. *International Journal of Remote Sensing*, 29(13), 3845-3853.
- Viegas DX. 2004. Slope and wind effects on fire propagation. *International Journal of Wildland Fire* 13:143.
- Vila, J. P. S., and Barbosa, P. 2010. Post-fire vegetation regrowth detection in the Deiva Marina region (Liguria-Italy) using Landsat TM and ETM+ data. *Ecological Modelling* 221(1): 75-84.
- Watts, J.M. 1997. Fire risk assessment using multiattribute evaluation. *Fire Safety Science*, 5:679-690.
- Weaver, J. F., Lindsey, D., Bikos, D., Schmidt, C. C., and Prins, E. 2004. Fire detection using GOES rapid scan imagery. *Weather and Forecasting* 19(3): 496-510.
- Weiss, M. and Baret, F., 2017. CAN_EYE V6. 4.91 user manual.
- Weise, D. R., and Biging, G. S. 1997. A qualitative comparison of fire spread models incorporating wind and slope effects. *Forest Science* 43(2): 170-180.
- Westerling AL, Bryant BP. 2008. Climate change and wildfire in California. *Climatic Change* 87:231–249.
- White, J. D., Ryan, K. C., Key, C. C., and Running, S. W. 1996. Remote sensing of forest fire severity and vegetation recovery. *International Journal of Wildland Fire* 6(3): 125-136.
- Wimberly, M. C., and Liu, Z. 2014. Interactions of climate, fire, and management in future forests of the Pacific Northwest. *Forest Ecology and Management* 327: 270-279.

- Yang, E. S., Christopher, S. A., Kondragunta, S., and Zhang, X. 2011. Use of hourly Geostationary Operational Environmental Satellite (GOES) fire emissions in a Community Multiscale Air Quality (CMAQ) model for improving surface particulate matter predictions. *Journal of Geophysical Research: Atmospheres* 116(D4).
- Yebra, M., Chuvieco, E., and Riaño, D. 2008. Estimation of live fuel moisture content from MODIS images for fire risk assessment. *Agricultural and forest meteorology* 148(4): 523-536.
- Yebra, M., Dennison, P. E., Chuvieco, E., Riaño, D., Zylstra, P., Hunt Jr, E. R., Danson F.M., Qi Y., and Jurdao, S. 2013. A global review of remote sensing of live fuel moisture content for fire danger assessment: Moving towards operational products. *Remote Sensing of Environment* 136: 455-468.
- Yesilnacar E, Topal T. 2005. Landslide susceptibility mapping: a comparison of logistic regression and neural networks methods in a medium scale study, Hendek region (Turkey). *Engineering Geology*, 79(3-4):251-266.
- Yu, B., Chen, F., Li, B., Wang, L., and Wu, M. 2017. Fire Risk Prediction Using Remote Sensed Products: A Case of Cambodia. *Photogrammetric Engineering and Remote Sensing* 83(1): 19-25.
- Zhang, X., and Kondragunta, S. 2008. Temporal and spatial variability in biomass burned areas across the USA derived from the GOES fire product. *Remote Sensing of Environment* 112(6): 2886-2897.

- Zhang, C., Ma, L., Chen, J., Rao, Y., Zhou, Y. and Chen, X., 2019. Assessing the impact of endmember variability on linear Spectral Mixture Analysis (LSMA): A theoretical and simulation analysis. *Remote Sensing of Environment* 235: 111471
- Zhang, H.K., Roy, D.P., Yan, L., Li, Z., Huang, H., Vermote, E., Skakun, S. and Roger, J.C., 2018. Characterization of Sentinel-2A and Landsat-8 top of atmosphere, surface, and nadir BRDF adjusted reflectance and NDVI differences. *Remote sensing of environment* 215: 482-494